Università degli Studi di Firenze
Scuola di Ingegneria
DIEF - Department of Industrial Engineering of Florence

PhD School: *Energetica e Tecnologie Industriali ed Ambientali Innovative*
Scientific Area: ING-IND/09 - *Sistemi per l'Energia e l'Ambiente*

Experimental Investigation on Gas Turbine Burner Operated with Simulated Exhaust Gas Recirculation

PhD Candidate: Ing. Sofia Galeotti

Tutor: Prof. Ing. Bruno Facchini

Co-tutor: Prof. Ing. Antonio Andreini

PhD School Coordinator: Prof. Ing. Giovanni Ferrara

XXXVII PhD School Cycle - 2021-2024

Acknowledgements

These three years have been intense but also incredibly rewarding. Throughout this journey, I have learned so much and grown, both personally and professionally, and I would like to express my deepest gratitude to all the people I had the pleasure and the good fortune to have by my side, even during the most challenging times. Realizing that I could truly rely on them has been one of the most precious gifts of this experience.

I would like to begin by sincerely thanking Professor Facchini and Professor Andreini, who first introduced me to research with enthusiasm and curiosity. Over the years, they have guided, taught, and inspired me through their passion, dedication, and attention to every detail. Their support has been fundamental throughout this journey, and I am deeply grateful for all the opportunities and encouragement they have given me.
A heartfelt thanks goes to the entire HTC group: through countless aperitivi, rinfreschini, HTC-activities and missions, we managed to make these three years of hard work not only productive but also truly enjoyable and full of good memories. I would like to mention all the colleagues at the THT Lab and Santa Marta, all the other guys in Calenzano, and my fellow PhD colleagues from the 37th cycle, with whom I shared this beautiful path. A special thank you goes to the friends I've made along this journey, who have become more than just colleagues. I won't name you all, but I think you know who you are.
An infinite thank goes to the hard core of THT, who welcomed me downstairs in the lab, despite my constant chatter the slow lunches. In between

many dolcini and paninetti, they taught me everything I know, from how to hack the coffee machine to the most advanced "combustion diagnostics" techniques. Ale, the fearful Lab Supervisor, but with a soft side, Ricca, who knows just about everything and seems tough but is a true cat lover, and Tommi, the calm and patient Professor Bacci. There are no words to express my gratitude, this work wouldn't have been possible without your experience and irreplaceable help.
I would also like to thank Giulia and Roberto for their constant support during the experiments and outside of the test cell, and all the partners from the Transition project, whose contributions have greatly enriched this work and offered me the opportunity to meet new and interesting realities. I would like also to express my gratitude to the thesis reviewers, whose valuable and meticulous suggestions significantly contributed to the improvement of this work.

Outside of the university, I want to thank my heart friends who've been putting up with me for quite some time now. Rebe (amo), even though panda-parties are rarer now, we still found a way to psychoanalyze each other remotely. Titta, who's always on the run but never misses time for true friends, Rafa, tough yet caring for those who matter and Fede, who might be in Spain but always makes sure to feel close. To the Castagno crew, who is always there, even without warning. In particular Ale, Eli, and Matti, but also everybody else, just as important, and to all my other friends as well.

Lastly, the biggest and most important thanks go to my family, who have always believed in me and supported me in every possible way. Words are not enough to fully express how grateful I am for all the support, encouragement, and love I received along the way.

This Ph.D thesis was carried out within the research projects TRANSITION, funded by European Union's Horizon Europe Research and Innovation program (G.A. No 101069665), gratefully acknowledged.

Abstract

As the world confronts the urgent challenge of climate change, research plays a pivotal role in driving the transition towards sustainable energy solutions. The increasing energy demand necessitates a shift not only towards renewable sources, but also towards optimizing conventional technologies to minimize their carbon footprint. Integrating Carbon Capture and Storage (CCS) technologies with gas turbine power plants plays a crucial role in reducing greenhouse gas emissions and improving the cost-effectiveness of de-carbonization efforts. Enhanced efficiency of CCS systems can be achieved by increasing CO_2 concentrations in the turbine exhaust, which can be gained with Exhaust Gas Recirculation (EGR). While high EGR rates improve CCS efficiency, they also challenge combustion stability because of the reduced oxygen availability.
The present work fits in this context with the purpose of contributing to the development of advanced combustion technologies for natural gas fired gas turbines to permit engine operations with high EGR rates, allowing a consequent drastic reduction of the CCS costs and units' size. In particular, experimental investigations were conducted at the THT Lab of the University of Florence on a well-established industrial burner design from Baker Hughes. Advanced optical diagnostic techniques, namely Particle Image Velocimetry and OH* chemiluminescence, were employed to analyze the flame behavior, allowing for the understanding of how operating conditions affect dynamics, stability, and pollutant emissions. The large experimental database collected in this work has allowed for a detailed analysis of the burner's behavior, providing key insights into its

performance under various conditions. A detailed characterization of the burner was first conducted under standard conditions before moving to an oxygen-depleted environment caused by EGR. The findings illuminate the crucial role of pilot fuel in maintaining combustion stability, as well as the trade-offs between premix levels and emissions. In simulated EGR conditions results show that CO emissions rise significantly, partly because of the use of CO_2 dilution to simulate the lower oxygen content due to EGR. A dedicated study was performed to assess the consequences of such experimental strategy, underlying the validity of this approximation as a precautionary and robust experimental method, in the perspective of a general preliminary screening.
A key innovation explored in this work is the injection of hydrogen to sustain the natural gas combustion at oxygen depleted conditions caused by EGR. Notably, the addition of hydrogen to the fuel stream emerged as a promising strategy to enhance flame stability under EGR conditions, with positive implications for the dynamic behavior and reductions in CO emissions. Furthermore, different fuel injection modes were tested, in order to assess the impact of the burner geometric features, enlightening how the fuel distribution affects flame stability and emissions.
Ultimately, this research underscores the significance of experimental studies in understanding combustion behavior in unconventional conditions. The insights gained from this work provide valuable guidance for optimizing burner designs for high EGR applications and contribute to the validation of numerical models for predicting combustion phenomena.

The activities of this Ph.D. project have been carried out within the European Project TRANSITION (*fuTure hydRogen Assisted gas turbiNeS for effective carbon capTure IntegratiON*), funded by European Union's Horizon Europe Research and Innovation program (G.A. No 101069665).

Contents

Nomenclature

Symbols

$\%CO_2$	CO_2 dilution mass flow rate fraction	[%]
CS	Combustion mass flow rate split	[–]
D	Pilot holes diameter	$[m]$
d	Diameter	$[m]$
Da	Damköhler number	[–]
$\%EGR$	EGR mass flow rate fraction	[%]
ESR	Extinction Strain Rate	$[1/s]$
f	Frequency	$[Hz]$
f_s	Acquisition frequency	$[Hz]$
LFS	Laminar Flame Speed	$[m/s]$
m	Mass flow rate	$[kg/s]$
$\%N_2$	N_2 dilution mass flow rate fraction	[%]
N	Number of pilot holes	[–]
OH^*	OH* intensity	$[a.u.]$
p	Pressure	$[Pa]$
P"	Pressure fluctuation amplitude	$[Pa]$
$\%PMX$	Premix fuel line thermal power fraction	[%]
St	Stokes number	[–]
T	Temperature	$[K]$
T_{flame}	Adiabatic flame temperature	$[K]$
TP	Thermal power	$[kW]$
$TP(H_2)$	Hydrogen thermal power fraction	[–]

U	Axial velocity component	$[m/s]$
V	Radial velocity component	$[m/s]$
UV	Velocity magnitude on xy plane	$[m/s]$
x	Axial coordinate	$[m]$
y	Radial coordinate	$[m]$
Y	Mass fraction	$[\%]$

Greeks

α	Thermal diffusivity	$[m^2/s]$
β	Fuel-air ratio	$[-]$
γ	Specific heat ratio	$[-]$
δ	Boundary layer thickness	$[m]$
ε	Emissivity	$[-]$
λ	Wavelength	$[m\ ]$
μ	Dynamic viscosity	$[Pa \cdot s]$
ν	Kinematic viscosity	$[m^2/s]$
ρ	Density	$[kg/m^3]$
τ	Characteristic time	$[s]$
ϕ	Equivalence ratio	$[-]$

Subscripts

avg	Average
CC	Combustion chamber
$comb$	Combustion
$cond$	Condenser
Dil	Diluent species
dw	Downstream
$Inlet$	Inlet condition
MAX	Maximum value
MIN	Minimum value
$Oxid$	Oxidizer
p	PIV particles
REF	Reference conditions
TOT	Total

Acronyms and Abbreviations

BH	Baker Hughes
CB	Center-body fuel line
CCD	Charge Coupled Device sensor
CCS	Carbon Capture and Storage
CCU	Carbon Capture and Utilization
CPU	Compression and Purification Unit
CWL	Central Wave Length
DFT	Discrete Fourier Transform
DIL	Diluent species
DLN	Dry Low NO_x
EGR	Exhaust Gas Recirculation
EXP	Experimental data
FoV	Field of View
FWHM	Full Width at Half Maximum
HRSG	Heat Recovery Steam Generator
IA	PIV Interrogation Area
M	Mirror
LA	Laser Arm
LBO	Lean Blow Out
LC	Cylindrical Lens
LS	Spherical Lens
NG	Natural Gas
NGCC	Natural Gas Combine Cycle
NR	Non-Reactive conditions
OX	Oxidizer flow
PFR	Plug-Flow Reactor
PID	Proportional-Integral-Derivative
PIV	Particle Image Velocimetry
PLT	Pilot fuel line
PMX	Premix fuel line
POD	Proper Orthogonal Decomposition

PSR	Perfectly Stirred Reactor
PTU	Programmable Time Unit
R	Reactive conditions
RMS	Root Mean Square
RN	Reactor Network
TRL	Technology Readiness Level
UV	Ultraviolet

Chapter 1

Introduction and Background

Exhaust Gas Recirculation (EGR) is a well-established technique in internal combustion engines, employed to limit NO_x emissions thanks to the reduction of the flame temperature. Implementing EGR in those systems is relatively straightforward and does not introduce significant difficulties. The consequent reduction in nitrogen oxides (NO_x) emissions is significant, and outweighs the associated negative consequences, such as increased particulate matter and unburned hydrocarbons [1].
In principle, the operational concept of EGR could also be applied to gas turbines systems to lower pollutant emissions. However, the implementation involves considerable plant complications and high costs, limiting the current applications. Indeed, modern Dry Low NO_x (DLN) combustion systems can already achieve near-single-digit NO_x emissions [2], and the complexities associated to EGR are not justified by the related emission reduction. Instead, the most promising application of EGR in gas turbines lies in the possibility to increase CO_2 content in exhaust gases, which can be exploited to improve the efficiency of carbon capture systems [3]. Such technologies are indeed gaining significant importance and popularity in the last years, as the energy demand continues to rise and the shift towards more sustainable energy solutions becomes inevitable. In this perspective the energy sector must not only expand the contribution of

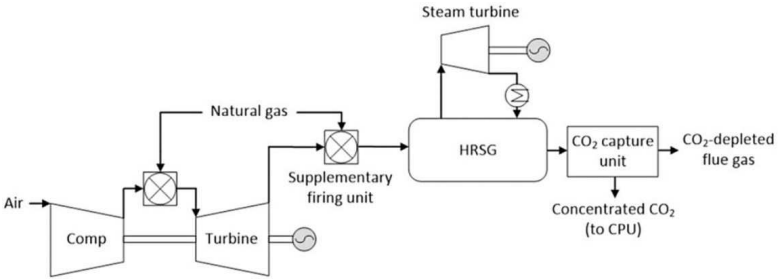

Figure 1.1: Standard scheme of Natural Gas Combined Cycle (NGCC) system integrated with advanced EGR combustion and carbon capture systems. (Compr=compressor, HRSG=Heat Recovery Steam Generator, CPU=Compression and Purification Unit)

renewable energies but also focus on reducing the carbon footprint of conventional technologies. In advanced economies, electricity generation is dominated by natural gas applications, and this trend is expected to continue over the next decade, thanks to the high flexibility that can be exploited to complement the variability of renewable energy [4]. In this context Carbon Capture and Storage systems become a crucial technology for meeting future climate goals and minimize the impact of greenhouse gas emissions.

The main factor restraining an efficient coupling between gas turbine power plants and CCS systems is the low CO_2 concentration in the turbine exhaust, due to lean equivalence ratios and intense dilution with secondary air. This limits the efficiency of capture processes, which rises with the CO_2 content in incoming flow [5]. The implementation of EGR to the gas turbine offers the possibility to mitigate this issue, allowing to increase the CO_2 content in the exhaust, with beneficial effects on the system efficiency [3, 6].

Figure 1.1 illustrates a schematic of a standard Natural Gas Combined Cycle (NGCC) system integrated with advanced EGR combustion and a carbon capture system. The direct application of EGR to gas turbines presents significant challenges due to the large specific volumes of flows

involved. However, this coupling allows to reach higher CO_2 content in the flue gases, along with a reduced flow volume, involving a substantial decrease in CCU/CCS costs and unit size. Nevertheless, the resulting operating conditions become challenging for traditional combustion systems, as the oxygen available for the combustion process diminishes. This generally affects the combustor's operational range, with consequences on the combustion efficiency and pollutant emissions [7].
The next section provides an overview of the existing research on EGR applied to gas turbines, examining benefits and limitations of current technologies. The present work seeks to address the existing gaps and contribute with novel insights, by investigating the effects of EGR on the combustion process in an industrial gas turbine burner. In particular, the research aims to add meaningful advancements in the application of EGR in gas turbine systems, offering findings that may have implications for emissions reduction and combustion stability in future implementations.

1.1 Exhaust Gas Recirculation in gas turbines

In one of the earliest studies, Røkke and Hustad [8] studied the impact of EGR in a 65 kW combustor, operated both in diffusion mode with a pilot burner and in premixed mode, adding separately the diluent gas composing EGR gases in the air and fuel flows. The results highlight how the oxygen content in exhaust gases directly affected NO_x formation, and EGR can be effectively used to manage emissions in conventional applications, in addition to the intent of enhancing the CO_2 concentration for capture purposes.
ElKady and Evulet [7, 9–12] explored the effects of EGR on a General Electric F-Class Dry Low NO_x (DLN) combustor at engine conditions. Their results revealed substantial shifts in flame dynamics when EGR was introduced, illustrating how the re-circulated exhaust gases could alter combustion stability. Furthermore, a notable increase in CO and UHC emissions was observed, limiting achievable EGR levels.
Further investigations on full scale engines by Burdet et al. [13] involved

experimental tests on an EV burner, revealing that stable operation was achievable even under high EGR ratios, with oxygen concentrations reduced to 2-5% by volume in the exhaust gases. The results also pointed out that unmixed zones in the fuel-air mixture became less problematic for NO_x formation under these high EGR conditions, suggesting that EGR could mitigate some traditional concerns regarding unburned pollutants. Yu et al. [14] investigated NO_x emissions in a methane-air non-premixed flame with EGR, highlighting that optimized NO_x reduction could be achieved with an EGR ratio of 25% without compromising flame stability. In a more recent work Bellas et al. [15] evaluated the effects of EGR in a pilot-scale study on a Turbec T100 microturbine, concluding that CO and unburned hydrocarbons (UHC) emissions sharply increased during partial load operation, and indicating that combustion chamber designs might require specific adaptations to effectively perform with EGR.
A novel research by Rosec et al. [16] on an EGR-configured gas turbine combustor fueled with oxygen-enriched mixtures demonstrated that an appropriate EGR level could allow substantial reductions in NO_x, CO, and soot emissions.
In parallel with these studies, advancements in optical diagnostic techniques have allowed for more detailed insights into flame dynamics under these unconventional conditions. In one of the first studies Konishi et al. [17] utilized C_2 radical imaging to investigate the effects of air preheat and low oxygen concentration on the flame temperature and fluctuations. Despite the limited temporal resolution available at the time, time-resolved temperature profiles were derived in a concentric diffusion flame with propane as fuel.
Later work by Kobayashi et al. [18] used OH-Planar Laser-Induced Fluorescence (PLIF) at high pressure on a simplified configuration, highlighting that CO_2 dilution decreased the smallest scale of flame wrinkling in methane-air turbulent flames, overall resulting in lower turbulent burning velocities.

Coh\'e et al. [19] captured instantaneous flame fronts under various pressures using laser-induced Mie scattering of olive oil seed, observing that flame surface density remained consistent regardless of CO_2 dilution, though combustion intensity increased with higher CO_2 levels.
Askari et al. [20] applied the Schlieren technique to study syngas flames in a cylindrical chamber, finding that higher selective EGR concentrations promoted flame stability in lean mixtures, which is significant for reducing pollutant formation.
Further extending this line of research, Lipardi et al. [21] used NO-LIF imaging to investigate NO_x formation and flame reactivity in premixed flames under EGR conditions at ambient pressure. Results showed that EGR dilution resulted in increased NO concentrations within the flame front, while post-flame reaction rates decreased.
In one of the latest studies Shen et al. [22] investigated experimentally the influence of EGR on the spatial and temporal distribution of heat release in a micro-gas turbine, concluding that mixing assumes less importance under these conditions, coherently with previous studies.
Lastly, Rodriguez Camacho et al. [23] in a recent research employed CH* chemiluminescence to study the flame dynamic response with different oxidizer compositions. The outcomes indicate that at extremely low oxygen levels not only the lack of oxygen but also the different concentrations of diluent gas can affect the flame behavior.
Further insights into the effects of EGR and the presence of various diluents on the flame emission spectrum will be presented in section 3.2.2, dedicated to chemiluminescence.

Many of these findings collectively highlight a positive effect of EGR in reducing NO_x emissions. However, they also reveal an associated increase in CO levels due to the lower flame stability caused by the lower oxygen content. To address the challenges posed by these adverse effects, various solutions can be implemented to enhance the combustor operation under such demanding conditions. In the present study, the innovative approach introduced is the addition of a small amount of hydrogen, both

injected pure and blended with natural gas. This approach aims to improve combustion characteristics in order to benefit from the advantages of EGR technology for carbon capture applications.

1.2 Hydrogen addition

The addition of hydrogen introduces non-negligible complications in a natural gas fired power plant; however, it has the potential to provide significant advantages in stabilizing the flame. By leveraging hydrogen's unique combustion properties, it is possible to enhance the stability of the flame, particularly in conditions where traditional fuels may struggle. Numerous studies have explored the effects of hydrogen blending into methane and natural gas, examining various aspects such as kinetic reactions [24, 25], flame propagation rates [26, 27]. Hydrogen's laminar flame speed is almost 7 times higher than that of methane, resulting in a much faster combustion process, which significantly alters the flame behavior. These differences in flame speed are crucial, as they persist under operating conditions found in gas turbine combustors, influencing both flame holding and static stability. The increase in flame speed associated with hydrogen blending directly affects the flame shape and location, and dynamic stability of the system which can either improve or worsen, depending on the combustor design and operational conditions.
Anderson [28] in one of the earliest studies noted that in a perforated-plate flame holder configuration hydrogen injection would stabilize the flame and make it quieter.
More recently Oztarlik et al. [29] proved that the injection of a small hydrogen amount is able to stabilize a thermo-acoustically unstable flame, but with a negative impact on NO_x levels. Similar results were found also by Barbosa et al. [30] for a lean propane-air premixed flame, with reduced oscillations with swirled hydrogen injection, associated with limited NO_x emissions but with a significant increase in CO.
Cheng et al. [31] investigated the impact of different hydrogen fractions on NO_x emissions in methane-air low-swirl flames at engine conditions,

showing a linear dependence on adiabatic flame temperature concluding that low swirl injection is able to operate with significant hydrogen fractions without important modifications.
The studies of Shanbhogue et al. [32] on swirl-stabilized flames revealed that the introduction of hydrogen into the fuel mixture led to significant changes in both flame holding and thermoacoustic stability limits. These changes were attributed to the increased extinction strain rate, which is a measure of the flame's sensitivity to stretching and thinning. As the hydrogen concentration in the fuel mixture increased, the extinction strain rate rises, leading to altered flame dynamics and a narrowing of the stability margins.
The relationship between hydrogen concentration and flame stability has been explored by Aguilar et al. [33], Terhaar et al. [34], highlighting the importance of balancing the benefits of hydrogen's faster combustion with the potential risks to combustion stability.

While this discussion does not aim to provide a comprehensive review of hydrogen's effects, it serves to contextualize the existing literature and helps clarify the work that has been conducted in this area. A comprehensive review on the effect of hydrogen addition focused on flame dynamics and thermoacoustic instabilities for gas turbine application was presented recently by Beita et al. [35].

The literature contains several studies on hydrogen with diluents, typically within syngas applications where hydrogen constitutes only a minor component of the fuel blend [36, 37].
Hydrogen applications within EGR systems can be found for internal combustion engine applications [38–40], while this approach remains largely unexplored for gas turbines. The most recent work from Rodriguez Camacho et al. [41] represents one of the first studies in this context. In particular the focus was on the effect on the flame dynamic behavior visualized with CH* chemiluminescence imaging, and other aspects such emissions were not addressed.

Studying the application of EGR in gas turbines is of significant importance, given that the existing literature on this subject remains relatively limited. The integration of hydrogen into this system further enhances the novelty of the topic, as it represents an area that has not been extensively explored in previous research.

1.3 CO_2 dilution to simulate EGR

For the purpose of the study, in the experiments it was necessary to reproduce in a laboratory test rig the combustion conditions generated by EGR on a gas turbine. Implementing the actual recirculation of exhaust gases in the experimental setup would have required major plant modifications, with significantly higher costs and long delays, which were not justified by the objectives of the present investigation. A more practical approach consists in diluting the combustion air with appropriate gases to emulate the oxidizer composition associated with EGR operation. The exact oxidizer composition resulting from EGR in a gas turbine depends on several parameters, primarily the amount of recirculated gases and the engine load, which determine the thermal power output and the equivalence ratio. In general, the addition of CO_2 and N_2 to air is sufficient to approximate the oxidizer mixture resulting from the recirculation of natural gas combustion products. In the present work, CO_2 was preferentially used for air dilution, mainly due to its lower specific volume compared to N_2, which makes handling and storage more practical during extensive experimental campaigns. The considered application focuses on dry EGR, where the water content is removed from the exhaust gases before recirculation. Therefore, the effect of H_2O presence in the oxidizer was not investigated.
The oxygen mass fraction in the oxidizer was selected as the main similarity parameter to relate experimental conditions to real EGR scenarios. Indeed, the reduction in oxygen availability is the dominant effect of EGR on combustion, even though other secondary effects, such as changes in thermodynamic and kinetic properties, also play a role. During the

experimental tests, a certain inlet oxygen mass fraction was targeted, resulting in an oxidizer composition with higher CO_2 and lower N_2 content compared to actual EGR mixtures.

Relevant studies in the literature provide insights into the role of CO_2 addition on combustion processes. Fackler et al. [42], through their work on a recirculation-stabilized combustor, highlighted the chemical effects of CO_2 dilution, showing that the preferential scavenging of free radicals by CO_2 can significantly suppress NO_x formation. Experimental and numerical investigations on the effect of CO_2 enrichment on laminar flame speed demonstrated a strong impact on flame reactivity [43–45], confirming that CO_2 cannot be considered an inert species from a kinetic standpoint [46]. Although focused on oxy-fuel combustion rather than EGR, additional studies offer valuable observations regarding CO_2 effects. In particular, OH* chemiluminescence imaging showed that CO_2-enriched flames exhibit an extended reaction zone compared to traditional air-stabilized swirl flames, leading to the suppression of NO_x emissions and relatively low CO emissions, demonstrating the potential of distributed combustion strategies in CO_2-rich environments [47]. Other research indicated that CO emissions during CO_2-diluted oxy-fuel combustion remain low near stoichiometric conditions, but increase rapidly when moving towards lean combustion. No data was available for oxygen concentrations below 22% at an equivalence ratio of 0.95, suggesting possible instability issues at lower oxygen contents [48]. Investigations on oxy-fuel flames in a swirl combustor showed that the higher specific heat capacity of CO_2 significantly modifies the flame structure compared to air combustion [49].

Finally, it is important to consider that at the high temperatures typically reached in gas turbine combustors, CO_2 not only acts through its thermodynamic properties (such as increasing the heat capacity of the mixture), but also participates directly in chemical reactions. When the concentration of CO_2 in the reactants is high, the carbon dioxide molecule dissociates in CO, primarily through the reaction $CO_2 + H \rightarrow CO + OH$. This reaction inhibits the reactivity because it consumes H radicals, and directly produces CO [50, 51]. The process becomes significant at high

temperatures [52], and is influenced by several other factors, including CO_2 partial pressure and the presence of catalysts. This mechanism provides an additional pathway for CO formation, influencing combustion kinetics and emissions, and must be taken into account when assessing the effects of CO_2 dilution as a strategy to reproduce EGR. The implications of this approach were evaluated in the present work through a dedicated investigation, presented in chapter 5.

1.4 TRANSITION project

The present work is part of the European project TRANSITION (fuTure hydRogen Assisted gas turbiNeS for effective carbon capTure IntegratiON), which aims to pave the way for the carbon-neutral energy generation from natural gas-fired power plants. The efficient integration of gas turbine systems with CO_2 capture and sequestration processes is the path chosen to achieve this objective in this project context. The key to maximizing this efficiency, while significantly reducing costs, lies in the use of very high levels of Exhaust Gas Recirculation (EGR), which can increase the CO_2 concentration at the inlet of the carbon capture unit [53].

These operating conditions present challenges for conventional combustion systems, as reduced oxygen levels in the combustor narrow the engine's operability window [7]. The project's primary aim is to identify and design technical solutions that extend the operational limits of gas turbines when EGR is pushed to high levels. The proposed concepts will try to ensure high flame stability while maintaining low emissions of NO_x, CO, and Unburnt Hydrocarbons (UHC). Among the many possible strategies the role of hydrogen, a novel approach, has been explored as critical in achieving these objectives, along with other technical strategies aimed at supporting combustion across a broad range of operating loads and environmental conditions.

In particular, two scenarios are examined in the TRANSITION project, each with distinct goals. The first focuses on retrofitting existing gas

turbine units, with strategies such as the ones explored in the present work. During the preliminary study phase it was estimated that at ISO base load conditions the current technology is expected to achieve an EGR rate of 35%. The innovative solutions developed in this project aim to push that rate to 50% by using localized injections of hydrogen in the flame stabilization region. This approach appears well-suited for retrofitting existing units, as it requires minimal modifications to the plant layout. Furthermore, at part load conditions, the properties of hydrogen addition could be even more beneficial to enhance the flame stability and balance the adverse effects of the lower temperature and pressure of the oxidizer.

The second scenario explores technologies capable of sustaining combustion even with minimal oxygen availability in the primary combustion zone, with oxygen injection in the flame stabilization region, but such approach is not part of this investigation.

The project involves a first experimental campaign at ambient pressure to support the design phase of GT-EGR burners. This preliminary screening has been performed in the single cup tubular rig at the THT-Lab of UNIFI, with optical access to allow flame visualization, which will be the work presented in this thesis. The targeted TRL (Technology Readiness Level), which is used to estimate the maturity of technologies in research programs, for this phase of the investigation is TRL3, (Experimental/analytical proof of concept), where the key characteristics are demonstrated in a single nozzle rig at reduced conditions (ambient pressure). Real hardware is employed, testing different configurations of an established burner design from Baker Hughes, with the results that will be illustrated in this study. The most promising geometries and novel configurations will be finally tested at high pressure in a second experimental campaign that will take place at the DLR (Deutsches Zentrum für Luft- und Raumfahrt) in Stuttgart. Tests in a single sector optical test rig at close to engine conditions will increase the level of advancement of the research up to TRL4, expanding the knowledge on this technology with the final aim of implementing it in real systems.

Beyond the experimental campaigns, the TRANSITION project integrates a comprehensive numerical modeling effort aimed at significantly improving the predictive capability of combustion simulations with real hardware burners operated under highly unconventional EGR-rich conditions. Dedicated high-fidelity turbulent combustion models are developed and validated against the experimental data, allowing for the exploration of a broader range of operating conditions and burner configurations, including solutions for extreme oxygen-deficient scenarios. Moreover, the project adopts an integrated approach, encompassing system-level analyses that extend beyond burner design to address the entire power plant context. Energy management and economic assessments are conducted to quantify the impact of GT-EGR integration on overall plant performance, cost-effectiveness, and operational flexibility, while sustainability evaluations aim to ensure that the proposed technologies align with the broader goals of decarbonization and the energy transition. In this way, the TRANSITION project not only advances combustion science at the component level but also contributes to shaping viable pathways toward a low-carbon energy future.

1.5 Aim of the work

The research carried out within this Ph.D. thesis falls inside the TRANSITION project framework, aiming to contribute to the development of new burner concepts, able to efficiently operate in unconventional operating conditions such as exhaust gas recirculation.
Despite the significant improvements in terms of reliability of computational models, certain aspects of the combustion process remain particularly difficult to be simulated numerically. The dynamic behavior and pollutant emissions estimation are certainly among them, and specifically transient phenomena such as lean blow out require great computational effort to be accurately reproduced. Moreover, models that have been developed and validated for standard configurations may not work properly under unconventional conditions such as the ones covered in this work.

Therefore, dedicated experimental investigations are essential throughout the burner design process.
This work aims to address the research gap identified in the literature, where there is a limited number of studies, particularly those using optical diagnostic techniques, focused on technically relevant solutions. Although combustion modeling and diagnostics have advanced, many studies still concentrate on simplified configurations, leaving a significant gap in the understanding of complex combustion behaviors under unconventional conditions, which have gained attention only in recent years. By integrating advanced optical diagnostics, this study provides valuable experimental data, revealing underexplored aspects of flame dynamics and stabilization mechanisms while offering deeper insights into the practical challenges of burner design. Testing at ambient pressure allows for the exploration of a wide range of solutions with limited effort. Specifically, this research employs optical diagnostics, along with conventional techniques such as emission measurements and pressure oscillation detection, to investigate the behavior of an industrial burner under conditions simulating the low oxygen levels caused by EGR. In particular, the vitiation of the combustion air with CO_2 has been adopted to reproduce the low inlet oxygen content caused by EGR. This approach was chosen as it is convenient for storage purposes, and once the implications of such choice have been made clear, it was considered a good compromise for this stage of the research.
In the perspective of retrofitting existing gas turbine units, the burner selected for the investigation is a well established design employed by Baker Hughes in industrial gas turbines, involving the complexities encountered in the operation of real hardware components. The investigated burner architecture is designed to operate in conventional conditions, with standard air as oxidizer. Detailed measurements have been performed under EGR-like conditions, with the purpose to evaluate the consequences of such challenging conditions on the burner performance. The collected results allow to identify critical issues and limitations of the current technologies.

Among the possible strategies that can be adopted to improve flame stability in order to limit the detrimental consequences of EGR presented earlier, the present study explores the use of pilot hydrogen flames, which is the main novelty of this work. The amount of hydrogen that can be used is limited by the reduction in the CO_2 content at the exhaust, which is intended to be maximized to improve the efficiency of CCS. Nevertheless, even in small amounts, beneficial effects are encountered.
The last aspect investigated in this work is the effect of the fuel injection mode. Indeed, the fuel distribution in the primary zone of the combustor plays a vital role in the flame stabilization process, and comparing the results obtained with different injection systems allows to understand the impact of geometric parameters on the flame behavior.
The outcomes of this PhD work can be leveraged to enhance burner performance under challenging conditions associated with exhaust gas recirculation. By investigating various fuel mixtures and injection strategies, this research provides valuable insights into flame stabilization mechanisms and the consequences on pollutant emissions and dynamics. The findings contribute to a deeper understanding of the combustion process under oxygen depleted conditions, which are essential in the perspective of implementing EGR in gas turbine systems. Furthermore, these results can contribute to the development and optimization of numerical models, providing valuable data collected under unconventional conditions, where limited information is available in the literature. In particular, well-defined boundary conditions are essential for CFD validation, and are typically not accessible in real technical (i.e., industrial) cases. Overall, the significance of these outcomes lies in their potential application to real-case scenarios where EGR is exploited to optimize the coupling between gas turbine engines and carbon capture units, with the consequent reduction of CO_2 emissions into the atmosphere.

1.6 Thesis outline

After this introductory chapter, the dissertation is organized in the following chapters:

- **Chapter 2** reports a detailed description of the experimental apparatus used for the investigation. The hardware employed for the experiments is presented, starting with the test cell facility, followed by description of the optical rig for reactive tests, which was designed in a previous Ph.D project [54]. The investigated burner is then presented, highlighting the main features and all tested configurations. The chapter concludes with an overview of the tested operating conditions,

- **Chapter 3** covers the measurement techniques employed for the investigations. Particle Image Velocimetry (PIV) and OH* chemiluminescence will be introduced, with their experimental set up and data reduction procedure. In addition to optical techniques used to investigate the flame structure and behavior, burner performance has been characterized in terms of pollutant emissions and pressure oscillations.

- **Chapter 4** reports the first part of the experimental campaign, with the characterization of the burner operated in standard conditions. The analysis starts from the burner design condition, with only natural gas as fuel, before introducing the effect of a limited amount of hydrogen. PIV and OH* measurements will be presented in order to investigate the flow field and flame structure. The collected information allows to better interpret the effects of the different operating conditions on the burner performance, which is quantified in terms of pollutant emission and stability limits.

- **Chapter 5** covers the effect of the experimental strategy chosen to reproduce EGR-like conditions. It includes a preliminary numerical study and a dedicated experimental investigation, comparing the employed method of CO_2 dilution with the use of nitrogen.

- **Chapter 6** presents the flame study under simulated EGR conditions, investigating the behavior of the burner in terms of flame shape, emissions and dynamic stability. Following the same approach as chapter 4, initially the burner is fueled with natural gas and the consequences of EGR are evaluated in this condition. In the second part, the effect of hydrogen injection is introduced, in order to see if it enhances flame stability, allowing to mitigate the impact of the challenging conditions created by EGR. In contrast to the previous chapter, where only a limited set of operating points was examined to evaluate the effect of oxidizer composition, this chapter presents a comprehensive exploration of a broad range of operating conditions. The objective was to identify the most significant operating points and to analyze the influence of various parameters, with particular emphasis on the effect of hydrogen.

- **Chapter 7** is dedicated to the effect of the fuel injection mode on the burner performance. In particular, the results obtained with seven different configurations including the baseline case will be presented, enlightening the variations in flame shape, emissions, stability limits and dynamic behavior. The effect of different injection systems will be detailed, in order to understand how the geometric features can be leveraged to improve the burner performance.

In the last chapter, an overview of the main achievements of this research is given together with conclusions and recommendations for future works.

Chapter 2

Experimental apparatus

The experimental campaign took place at the THT Lab of the University of Florence. This chapter is dedicated to the description of the experimental apparatus adopted for the investigation. First the hardware employed for the reactive test campaign will be presented, starting with the facility of the combustion test cell, followed by the test rig with the associated instrumentation. The investigated burner concept is then detailed, presenting the burner architecture and the fuel lines arrangement, with all different configurations tested to assess the impact of the fuel injection mode.
The chapter concludes with the definition of the operating conditions, which are unconventional with respect to standard tests on gas turbines combustors. In fact, some considerations about the strategy used to reproduce EGR in the test rig are necessary, and a dedicated study will be presented in chapter 5.

2.1 Facility: combustion test cell

Starting with a global overview, Figure 2.1 presents a schematic layout of the combustion test cell, in which the optical test rig is installed.

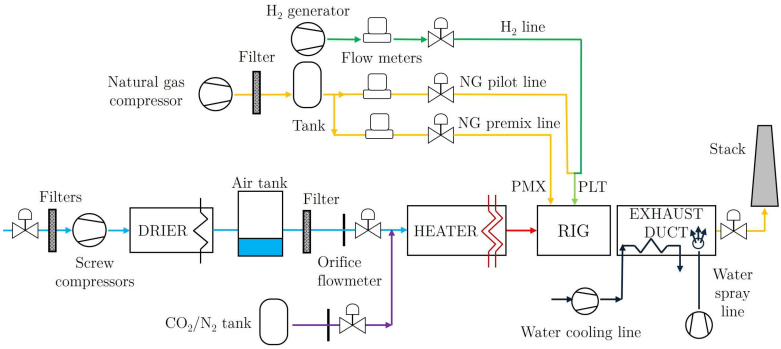

Figure 2.1: Schematic of the test cell facility layout

2.1.1 Air line and auxiliaries

Following the blue marks representing the air line, the combustion air flow is supplied to the test rig by two screw compressors, able to provide up to 1 kg/s of air at a maximum pressure of 10 barA. The system includes a modulating valve that maintains a constant delivery pressure. Following compression, the air passes through several filters and an air dryer set to a dew point of -20°C (253 K), ensuring the elimination of impurities and moisture before reaching the test cell. Subsequently, an electric heater up to 600 kW, increases the air temperature to a maximum of 400°C (673 K). A Proportional-Integral-Derivative (PID) control system automatically adjusts the power input of the electric heater to maintain a consistent delivery temperature.

The mass flow rate of the air is regulated by a globe valve positioned upstream of the electric heater, while the downstream pressure in the rig is controlled by a high-temperature control disk valve. During the present experimental campaign the back-pressure valve has been kept open since the rig was operated at ambient pressure. A water jacket exhaust duct is located directly after the rig to prevent any potential interference from the back-pressure valve on the combustion process. The water jacket consists of a 1-meter-long straight duct, where water flows in an annular

channel around the air duct, cooling it down. The duct is equipped with four water sprayers, which are used to cool the hot gases and regulate the exit temperature to remain within the allowable operating range of the valve. The water system is managed by dedicated pumps, with the flow rate adjusted based on feedback from the exhaust gas temperature and the water temperature at the sprayers' exit.
As anticipated, EGR conditions have been reproduced by diluting the combustion air with inert gases in order to lower the oxygen level. CO_2 or N_2 are stored in a pressurized tank with a capacity of approximately 6000 liters and injected upstream of the electric heater, as shown in Figure 2.1, in order to deliver a homogeneous mixture to the test section in terms of temperature and composition.
The air and CO_2/N_2 mass flow rates are measured with calibrated orifice flow meters (compliant with standard EN ISO 5167-1), which have an absolute uncertainty of 1%, calculated using the Kline and McClintock method [55].

2.1.2 Fuel lines

The test rig is supplied by two natural gas lines that deliver a maximum flow rate of about 90 Nm^3/h, represented by yellow lines in Figure 2.1. Natural gas is taken from the local gas network (20 mbar) and compressed to 16 bar. The screw compressor is equipped with several filters (micron rating up to 0.1 μm) to remove contaminants from the gas flow, and a 200 liters tank is installed on the delivery line to smooth out pressure fluctuations. In order to maintain a constant delivery pressure, the compression system automatically adjusts the electric motor rotational speed and the bypass valve aperture. The mass flow rate of each line is measured with orifice flow meters (compliant with standard EN ISO 5167-1), with an absolute uncertainty of 1% according to the Kline and McClintock method [55]). Fuel mass flow rates are controlled with globe valves and shut off valves are installed on all the fuel lines for safety reasons.
The supply of natural gas on the domestic line varies throughout the

day in terms of chemical composition, and for this reason a fuel sample is taken and analyzed after each test. The gas composition measured on a test day is reported in Table 2.1 as a representative sample. In addition to a small percentage of inert (1% of CO_2 and nitrogen), a non-negligible amount of ethane is present, which has a certain effect on the fuel chemical properties. In particular, the lower reactivity of ethane compared to methane slightly lowers the adiabatic flame temperature, but increases the laminar flame speed, because its dissociation produces additional radicals [56]. Pollutant emissions are consequently also affected by the exact fuel composition [57].

Chemical species	**Concentration (%)**
Methane	89.704
Ethane	6.862
Carbon dioxide	1.131
Nitrogen	1.009
Propane	0.917
N-butane	0.166
I-butane	0.113
Helium	0.035
N-pentane	0.034
I-pentane	0.024
Oxygen	0.004

Table 2.1: Gas composition measured on 01/17/2024

Regarding the hydrogen supply, H_2 (green line in Fig. 2.1) is not stored and only produced on demand with an electrolyzer, which can deliver up to 14000 Nl/h of hydrogen at 8 bar, with a purity of 99.5 $\pm$ 0.2%. The hydrogen mass flow rate is measured with a dedicated Coriolis mass flow meter, with an accuracy of 0.25%.

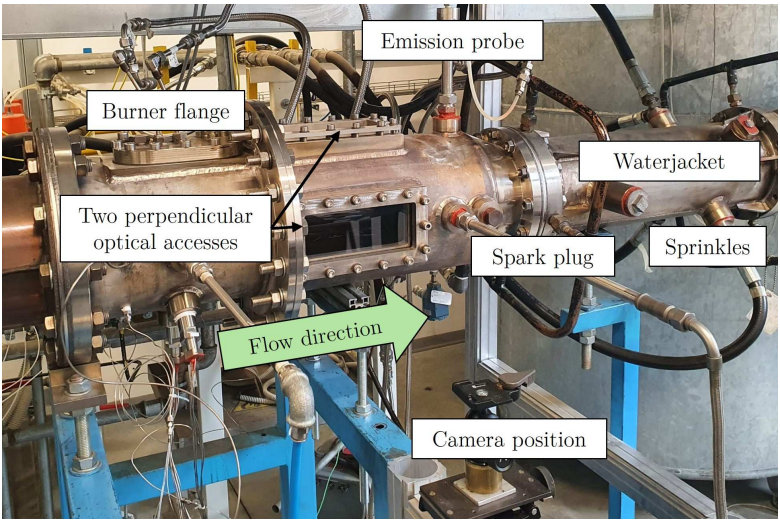

Figure 2.2: Picture of the test rig for experiments under reactive conditions

2.2 Optical test rig

Figure 2.2 shows a picture of the optical test rig employed for the reactive test campaign. It was designed during a previous PhD thesis, and the detailed description of the design process can be found in [54]. This section provides a description of the key features for the sake of completeness.

The test rig is characterized by a modular design to accommodate different burner concepts with minimal component replacement. Figure 2.3 shows a cross section parallel (a) and normal (b) to the chamber axis, highlighting the different components.

The outer casing is composed of an upstream and downstream vessel made of AISI 304 stainless steel. The upstream vessel connects the test article to the lab air supply system and accommodates the burner connection flange with the fuel inlets. The downstream vessel houses the combustor chamber and includes the two optical accesses and additional ports for

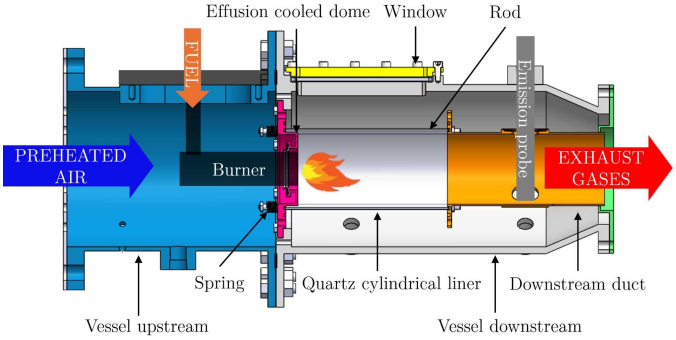

(a)

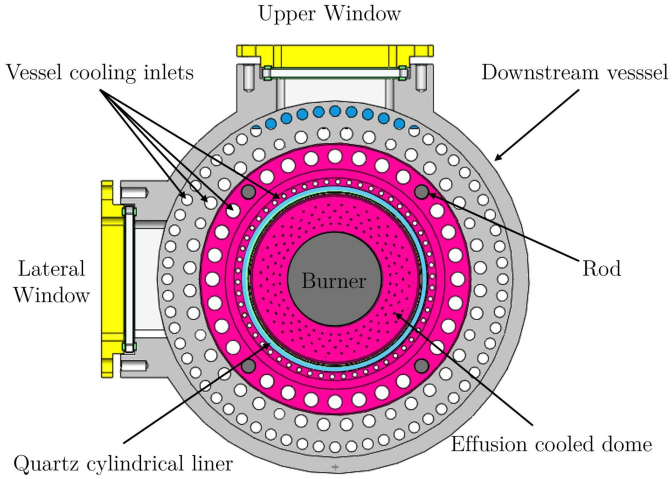

(b)

Figure 2.3: Cross section parallel (a) and normal (b) to burner axis of the test rig

measuring probes. It is connected downstream to the exhaust quenching system. Optical accesses on the outer vessel consist of two rectangular 5 mm thick quartz windows arranged perpendicularly, as shown in Figure 2.3b. Graphite gaskets are used to avoid leakage and to prevent the contact between quartz and the metallic frames connected to the outer vessel with bolted joints.

The combustion chamber consists of a dome, liner and a downstream duct. The so-called dome is both the actual dome of the combustion chamber and the component which connects the chamber to the outer vessel with bolted junctions. A mobile ferrule is used to hold the burner, in order to allow thermal deformations without raising stresses, limiting at the same time the air leakage inside the combustion chamber. The dome is subjected to high thermal loads because of the flame proximity, and Inconel 718 has been employed for the manufacturing. Effusion cooling is also implemented to limit the temperature of this component, with 4 rings of 0.7 mm holes inclined at 30° with respect to the dome surface.

The liner is a 2.5 mm thick quartz cylinder. It is held in place by four tie rods and four springs connecting the dome to the plate located downstream. The springs are preloaded with nuts to secure the liner and accommodate thermal expansion without leakage. Graphite gaskets are employed to avoid direct contact with the metal surfaces and to ensure an effective sealing.

The downstream duct directs exhaust gases to the test rig exhaust system, and is held up by a support, with some clearance to avoid stresses. It includes ports for measuring probes, equipped with ferrules to allow different thermal deformation of the outer vessel and the combustion chamber. The downstream duct and the associated support are made of AISI 304 stainless steel.

The combustion chamber is cooled by forced convection of a fraction of the incoming air that flows in the annulus between the liner and the confining vessel, not used in the combustion process. Dedicated flow checks were performed to evaluate the flow-split between liner and dome cooling and the combustion air. Approximately only 14% of the air flows

inside the burner, and additional 1% enters the combustion chamber with the effusion cooling holes, leaving 85% of the total air mass flow rate for the external cooling. The high temperature combustion exhaust mix with the cooling air downstream of the metallic liner duct, lowering the temperature of the flow that arrives at the rig quenching system.
A spark plug is used for ignition, located downstream of the optical liner, facing the inside of the downstream duct. It is shown in the picture of Figure 2.2 and in Figure 2.4, with the exact position reported in Table 2.2 with all sensor positions. When the burner is ignited, the spark plug releases a 16 joule spark 2 times per second. In case of ignition failure, after 15 seconds a shut-off valve cuts off the fuel flow and the procedure is repeated from the start.

2.2.1 Rig instrumentation

The test rig is equipped with several sensors, used to monitor operating conditions during test execution and to acquire quantities of interest for the investigation.
Figure 2.4 shows the position of the instrumentation installed on the test rig, summarized in Table 2.2.

The static pressure is acquired at 1 Hz with a NetScannerTM System 9116 pressure scanner with temperature compensated piezo-resistive relative pressure sensors. It has a measuring range of 0-100 PSI (0-690000 Pa) with an uncertainty of 345 Pa (±0.05% Full Scale). The static pressure is measured across the calibrated orifices to retrieve mass flow rates, according to standard EN ISO 5167-1, and in different locations inside the test article. Specifically, two static pressure taps are installed in the upstream vessel to monitor the inlet pressure (section A of Fig. 2.4), one is located on the casing to measure the annulus pressure (section C), and two in the downstream duct (section F).
K-type thermocouples are used to measure the temperature of both flow and metal components, acquired with an HP/Agilent switch unit con-

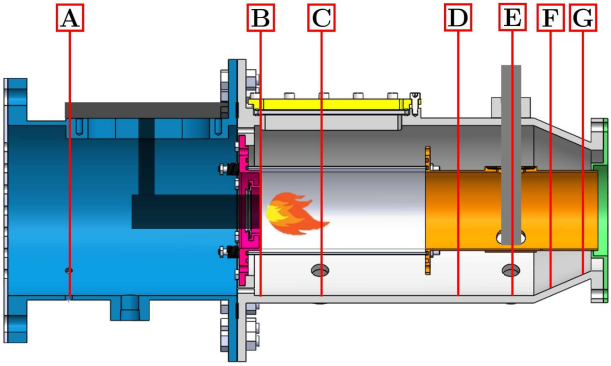

Figure 2.4: Schematic of sensor positions

Section	x [mm]	Component	Number	Sensor	Measured quantity
A	-252	Upstream vessel	2	Static pressure tap	p_{inlet}
		Upstream vessel	1	K-thermocouple	T_{inlet}
B	0	Dome cold side	2	K-thermocouple	$T_{dome\ 1-2}$
		Dome annulus	2	K-thermocouple	$T_{dome\ 3-4}$
C	77	Downstream vessel	1	Static pressure tap	$p_{annulus}$
D	271	Downstream duct	3	K-thermocouple	$T_{dw\ D\ 1-2-3}$
		Downstream duct	1	Spark plug	[-]
E	327	Downstream duct	3	K-thermocouple	$T_{dw\ E\ 1-2-3}$
		Downstream duct	1	PCB	P''
		Downstream duct	1	Gas analyzer probe	CO, CO_2, O_2, NO_x
F	367	Downstream duct	2	Static pressure tap	p_{CC}
G	398	Downstream duct	3	K-thermocouple	$T_{dw\ G\ 1-2-3}$

Table 2.2: Sensor positions

nected to an external reference junction, with an accuracy of ±0.5 K. The dome temperature is measured on the cold side and on the downstream surface in the annulus between the liner and the outer vessel (section B of Fig. 2.4). Nine K-thermocouples are installed on the downstream duct at three different axial locations and three distinct circumferential positions (sections D-F-G). The inlet flow temperature is measured in the upstream vessel (section A), and the exhaust temperature is monitored downstream

of the quenching system.
The downstream duct is also equipped with ports for the dynamic pressure sensor (PCB) and the exhaust gas sampling probe (both located in section E), which will be described in more detail in the next chapter dedicated to the measurement techniques.
Real-time monitoring of all rig parameters is managed with an in-house LabVIEW software tool. Once stationary conditions are achieved, data collected at each test point are averaged over 30 seconds.

2.3 Burner concept

The burner concept investigated in this work is a well-established design employed by Baker Hughes for industrial gas turbine applications. Different configurations were tested, starting with the baseline case which was thoroughly characterized.
The concept is a lean premixed burner, derived from an aero-derivative design, whose main characteristic is the versatility to operate stably under widely varying conditions [58]. A schematic of the burner cross section is reported in Figure 2.5. It is composed of two counter-rotating axial swirlers, a center-body and a converging nozzle.
The burner was designed to satisfy the restraints of flashback and auto-ignition, and a reduced combustor size [59]. The converging duct is conceived to continuously accelerate the air flow, reducing the boundary layer thickness to prevent flashback in the boundary layers [58]. Furthermore, the exit velocity is set by design to be significantly greater than the turbulent flame speed of natural gas lean mixtures, preventing flame flashback.

2.3.1 Burner fuel lines

A total of three independent fuel lines is present, in order to control pollutant emissions and at the same time ensure a stable combustion process also at partial load.

- Premix line (PMX): injects the fuel at the tip of one of the two

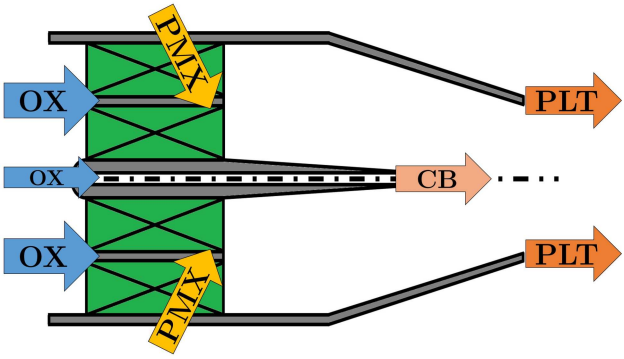

Figure 2.5: Burner concept schematic

swirlers in a jet-in-crossflow configuration. Strong mixing is ensured thanks to the intense turbulence created by the shear layer generated between the two swirlers in the converging nozzle, which follows the swirler before entering the combustion chamber [60].

- Pilot line (PLT): injects the fuel directly into the combustion chamber through circumferentially equally spaced holes. Pilot fuel jets give rise to a diffusive flame front, helping the flame stabilization and allowing safe and stable operation at different engine loads, while keeping an adequate margin for NO_x emission requirements [61].

- Center-body line (CB): injects the fuel along the burner axis in co-flow with the incoming combustion air. The injection point is located upstream of the burner outlet, therefore ensuring a certain degree of premixing, although less than that achieved at the premix line. In certain applications the conical center-body is used to supply liquid fuel to an atomizer at its tip. When it is not fed with fuel the center-body is cooled by small amounts of purge air channeled through a hole along the burner axis.

The burner is 3D printed, allowing the realization of complex geome-

tries such as the hollow vanes of the external swirler through which the premix line fuel flows.

During the experimental campaign only two fuel lines were fed at the same time. The center-body third line has been employed only with one configuration (B5), and has not been fed for the baseline case. The premix and center body fuel lines have been fed only with natural gas, while hydrogen injection has been tested on the pilot line, which is normally fueled with natural gas. In certain conditions a blend of natural gas and hydrogen has been introduced through the pilot line, in order to limit the hydrogen amount while operating at high piloting fraction. The blend was realized immediately upstream of the connection flange which holds the burner in place on the upstream vessel, with the arrangement shown in Figure 2.6.

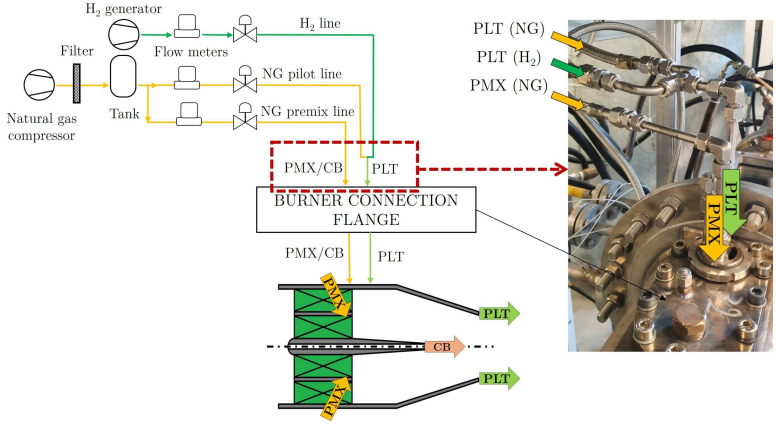

Figure 2.6: Fuel lines layout and picture of the burner connecting flange with fuel inlets

2.3.2 Investigated configurations

The fuel distribution in the combustor primary zone is crucial in the flame stabilization process. Indeed, different injection strategies have been

tested, with particular focus on the pilot holes geometry. The pilot line is in fact the primarily responsible for flame anchoring, which is crucial under challenging conditions such as those encountered with EGR.
A total of 7 test articles has been printed for the experimental campaign. The baseline configuration derives from a well-establish design, and was thoroughly characterized in the first part of the study. A restricted number of test points was selected for the other layouts.
The main flow field has been kept essentially unaltered among the different configurations, and only the fuel injection system has been varied. Different geometries of the pilot holes were tested, modifying the interaction between pilot jets and the main-flow leaving the burner, with consequences on the mixing process and the fuel distribution inside the flow field.
In particular, the pilot injection system for the baseline case (B0) consists of N holes, each with an equal diameter D, arranged in a non-axisymmetric pattern around the burner: 1/4 N are positioned on a smaller radius on the dome with inward injection angles, while the remaining holes are directed outward and positioned at slightly larger radius. For the other configurations pilot holes are arranged in an axisymmetric pattern, and different inclinations have been tested in order to assess the impact of the hole orientation on the flame behavior. The number of holes was also increased (B2), maintaining the jet exit velocity by decreasing the hole diameter in order to match the same total area. This configuration allows to achieve a less scattered fuel distribution in the tangential direction, thus improving the mixing process. Despite the same exit velocity, jet penetration is reduced because of the lower fuel mass flow rate, that rapidly mixes with the main-flow.
The pilot jet exit velocity is another parameter strongly affecting the flame anchoring process. In engine operation the pilot jet velocity changes with pilot mass flow rate, therefore both varying the premix split with constant total thermal output or adjusting the total thermal power during load regulation. However, in this way it is not possible to discern the variation in the pilot speed from the change in equivalence ratio of premixed main flow due to the premix fuel flow rate. The effect of increasing the pilot

jets' velocity has been investigated testing a smaller hole exit cross section in configuration B4, with N holes of equal diameter 0.7*D, obtaining half the total exit cross section. This leads to higher jet penetration, and for this configuration pilot jets are straight, with null radial component. Lower jet velocity is instead tested with configuration B1 (N holes of equal diameter 1.2*D), with the addition of a tangential component.
Finally different premixing systems have been adopted, changing the mixture distribution of the main-flow entering the combustion chamber. This was done by varying the injection location of the premix fuel, which for the baseline case is the tip of the inner swirler. For the other variants premix fuel is injected in cross-flow at the tip of the outer swirler, placing the premix fuel closer to the burner walls, therefore promoting the interaction with the pilot fuel. For another design variant, the center-body fuel line is employed (B5-CB), generating lower premix level because of the reduced length available before entering the combustion chamber.
All investigated burner layouts are summarized below:

- Baseline (B0)
  - PLT: N holes of equal diameter D, 1/4 N oriented inwardly and positioned at smaller radius, 3/4 N oriented in outward direction
  - PMX on inner swirler
- Configuration 1 (B1)
  - PLT: N axisymmetric holes of equal diameter 1.2*D, outward and with tangential component
  - PMX on outer swirler
- Configuration 2 (B2)
  - PLT: 2N axisymmetric holes of equal diameter 0.7*D, outward direction
  - PMX on outer swirler

- Configuration 4 (B4)
  - PLT: N axisymmetric holes of equal diameter 0.7*D, straight direction
  - PMX on outer swirler
- Configuration 5-PMX (B5-PMX)
  - PLT: N axisymmetric holes of equal diameter D, outward direction
  - PMX on outer swirler
- Configuration 5-CB (B5-CB)
  - PLT: N axisymmetric holes of equal diameter D, outward direction
  - CB[1]: Center-body line
  - No PMX line
- Configuration 6 (B6)
  - PLT: N axisymmetric holes of equal diameter D, positioned at the same radial coordinate, with twice outward angle direction
  - PMX on outer swirler

2.4 Operating conditions

The purpose of the present investigation is to study the behavior of gas turbines burners operated in challenging conditions caused by high EGR rates.
As anticipated, the experimental campaign has been performed at ambient pressure, therefore the inlet pressure p_{inlet} is slightly over atmospheric value due to the induced burner pressure drop. The latter is defined as:

[1]For configuration B5-CB %PMX means %CB

$$\frac{\Delta P}{P} = \frac{p_{inlet} - p_{CC}}{p_{inlet}} \tag{2.1}$$

with the static pressure measured in the position reported in Table 2.2. The upstream pressure p_{inlet} is measured in a large plenum, therefore the total pressure can be considered to be equal to the measured static pressure.
The burner pressure drop has been kept at the design value of the burner during the whole measurement campaign. Slight variations were measured for the test with simulated EGR, as the total mass flow rate of the oxidant was kept constant, while the composition of the mixture and thus the molecular weight varied. The inlet temperature of the oxidizer T_{inlet} has been kept constant at 300°C.

2.4.1 Simulating EGR conditions

Implementing recirculation of exhaust gas at lab scale is quite challenging because of the associated costs and the volumes involved; similar complications arise when employing nitrogen enriched mixtures, because of the low density of nitrogen. Therefore, CO_2 dilution of the combustion air has been selected as a good trade-off for this primary investigation phase, since it offers the opportunity to manage storage better than mixtures with nitrogen, while preserving the purpose of the investigation. The validity of this approach was investigated both numerically with a chemical kinetics study and experimentally by replicating a restricted set of test points with nitrogen instead of CO_2, with the results that will be shown in a dedicated section in chapter 5.
During test execution, the EGR condition is represented by the inlet oxygen mass fraction Y_{O2}, which is a key similarity parameter between real EGR and simulated conditions, since one of the main challenges of EGR is the reduction of inlet oxygen levels.

2.4.2 Fuel split and hydrogen limit

The burner is usually operated with natural gas as fuel, but the present work aims to investigate the effect of adding a limited amount of hydrogen through the pilot fuel line. Because of this dual fuel configuration, fuel splits are defined with thermal power:

- PMX% is the thermal fraction of the premix line (always fully natural gas) over the total thermal power.
- TP(H_2) is the fraction of hydrogen thermal power over the burner total thermal power, which indeed comprehends both the premix and pilot contributions regardless of the type of fuel employed. The hydrogen fraction is limited by the reduction of CO_2 content in the exhaust, and it is kept belowe 10% of the total thermal power, as detailed above.

The total thermal power TP_{TOT} has been varied in the first part of the investigation, dedicated to the characterization of the baseline configuration of the burner with natural gas, in order to see the influence of this parameter on the flame behavior. For the other burner configurations and for the dual fuel operation the total thermal power has been kept constant at TP_{REF}. This leads to slight differences in terms of adiabatic flame temperatures T_{flame} when the fuel or the oxidizer composition varies, because of the different composition of the combustion products and the resulting average specific heat of the mixture. For the investigated conditions this effect is however very limited.
The premix fuel fraction is limited by the insurgence of strong thermoacoustic instabilities that have been observed during the experimental campaign, which will be presented in the results chapters.

The primary goal of achieving stable combustion with high EGR rates is the increase in the CO_2 content at the exhaust, in order to maximize the efficiency of CCS systems. The adoption of hydrogen to boost flame stability goes in the opposite direction, as it reduces carbon conversion,

and it is necessary to quantify how the exhaust gas composition changes. Numerical tools have been exploited for such purpose, in order to estimate an upper limit on the fraction of hydrogen that can be used to improve flame stability. In particular a Python-Cantera script has been employed, which will be described in detail in chapter 5. Briefly, it simulates the implementation of dry EGR on a real gas turbine, and has been exploited to compute the composition of both the mixture entering the combustion chamber and the exhaust.
With hydrogen representing 5% of the total thermal power it is necessary to increase the EGR rate by 3% in order to achieve the same CO_2 content at the turbine exhaust as in the case with the burner fueled entirely by natural gas. By increasing the hydrogen fraction to 10% of the total thermal power, the required increment of EGR rate rises to 6%. This last value has been considered a reasonable compromise for the burner operability, representing a good trade-off between higher achievable EGR and a limited reduction of CO_2 at the exhaust.

2.4.3 Test matrix

Summarizing, the investigated operating conditions are reported in Table 2.3, determined through the following main control parameters:

- T_{inlet} is the combustor inlet temperature, set to 300 °C (573 K) to simulate typical gas turbine compressor discharge temperatures.

- p_{CC} is the combustor chamber pressure, slightly above the ambient pressure.

- $\Delta P/P$ is the pressure drop across the combustion chamber, which was held constant at the burner design value.

- TP_{TOT} is the total thermal power. The reference value used for scaling the results is denoted as TP_{REF}. For the investigated conditions thermal power modifications are consistent with variations in the adiabatic flame temperature T_{flame}, calculated assuming a

Parameter	Value	Unit
p_{CC}	101325	[Pa]
T_{inlet}	573	[K]
$\Delta P/P$	Const*	[%]
TP_{TOT}	TP_{REF}	[kW]
PMX%	0-95	[%TP]
$TP(H_2)$	0-10	[%TP]
Y_{O2}	23.2-15.0	[%mass]

Table 2.3: Tested operating conditions.
**Detailed value is confidential*

perfect mixing between the burner combustion air and the total amount of fuel injected.

- %PMX, the fuel split between the premix (CB for B5-CB) and the pilot fuel lines, which is expressed as percentage of the total thermal power TP_{TOT}.
- $TP(H_2)$ is the hydrogen thermal power fraction over the total thermal power
- The air vitiation in EGR-like conditions is expressed as oxygen mass concentration (Y_{O2} %), reached after the addition of a certain amount of CO_2/N_2 into the main air flow entering the test rig (Y_{O2} = 23.2% for standard air)

Throughout the different chapters, various conditions are employed for the experimental tests, in terms of fuel and oxidizer mixture composition. Table 2.4 provides a summary of these conditions, concluding the overview of the operating parameters and offering a quick reference guide for the rest of the discussion.

Chapter	Description	Fuel	Oxidizer
Chapter 4	Burner characterization in standard conditions	Pure NG NG+H_2	Air
Chapter 5	Impact of CO_2 addition to reproduce EGR conditions	Pure NG	Air+CO_2 Air+N_2
Chapter 6	Effect of simulated EGR	Pure NG NG+H_2	Air+CO_2
Chapter 7	Effect of fuel injection mode	Pure NG NG+H_2	Air
		Pure NG NG+H_2	Air+CO_2

Table 2.4: Summary of experimental conditions across chapters

Chapter 3

Measurement techniques

This chapter is dedicated to the description of the measurement techniques employed for the investigation. In particular, optical diagnostic techniques have been exploited to characterize the combustion process with high spatial resolution. 2D-PIV has been used to characterize the velocity field on the burner symmetry plane, and OH* chemiluminescence has been used to investigate the flame structure. Combining the information collected with these techniques, it is possible to understand in detail the mechanisms of flame stabilization, with the purpose to enhance the burner performance in the challenging conditions created by EGR. The next sections will present the basic theory and working principle of these techniques, followed be the description of how they have been implemented in the present experimental campaign, and the data reduction procedures. In addition to optical techniques used to investigate the flame structure and behavior, exhaust gas analysis has been performed in order to assess the impact of the different operating conditions on NO_x and CO levels, with particular focus on the effects due to EGR. Lastly, another aspect that was investigated is the rise of strong pressure fluctuations recorded during the reactive tests, which have been monitored with a high frequency pressure sensor. The chapter concludes with section dedicated to clarifying the way of presenting the results, that will be followed for the

next chapters.

3.1 Particle Image Velocimetry

Particle Image Velocimetry (PIV) is an optical technique that allows to instantaneously measure the flow velocity in an extended region. This section provides a brief overview of the key features of the technique, in order to present its basic principles. For a detailed and comprehensive description, reference is made to dedicated works [62–64].
The working principle is shown in Figure 3.1 and it is based on the introduction of seeding particles in the flow and tracking of their movement. A dual-pulse laser sheet is usually used to illuminate the particles, and the scattered light is recorded by a CCD (Charge-Coupled Device) camera in two different instants. The velocity field is retrieved by evaluating the particle displacement between the two images, which are acquired with a known time interval. In order to track the particles movement, images are divided into smaller Interrogation Areas (IA), within which particles are assumed to have rigid motion, and statistic approaches based on 2D cross correlation methods are exploited to compute the displacement vector on the measuring plane. The time delay between the two laser pulses is a key parameter and must be selected accurately: if it is too long the computed velocity cannot be assimilated to an instantaneous value but it is the average one and the assignment of particle pairs between both instances deteriorates; on the other hand if it is too short the particle displacement will be small, thus reducing the measurement gain.

The *scale factor* allows to convert pixels into physical distances, and it is retrieved through spatial calibration. The measurement signal is amplified with a laser system that generates monochromatic light with high density of energy, producing a thin light sheet with a series of optical lenses and inserting it inside the investigation area.
PIV is not a totally non-intrusive technique, as it requires the introduction

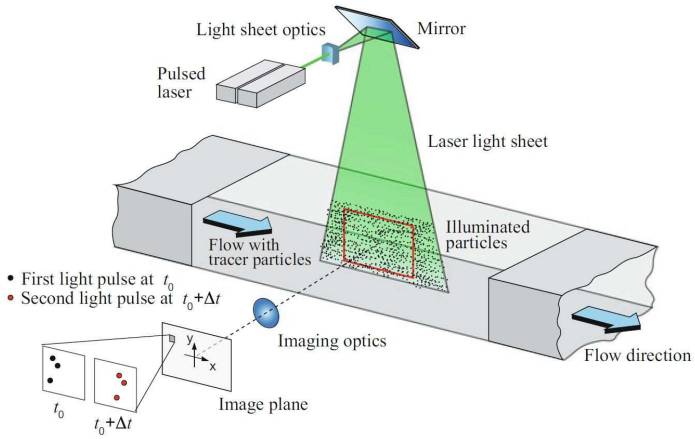

Figure 3.1: Schematic of experimental arrangement for planar 2D PIV [62]

of seeding particles. The latter must be able to follow the flow, to avoid significant discrepancies between the measured velocity, i.e. the particles velocity, and the actual velocity of the flow. Therefore, fluid-mechanical properties of these particles must be accurately checked in relation to the nature of the flow under investigation. The Stokes number is a dimensionless number used to describe the capability of particles to follow the mean flow, defined as:

$$St = \frac{\tau U}{d_p} \tag{3.1}$$

where U is the local drag flow velocity, d_p is the particle diameter, and τ is the response time of the particle, which is the time constant in the exponential decay of the particle velocity due to drag. When the seeding particle density is much greater than the fluid density the characteristic time can be expressed as:

$$\tau = d_p^2 \frac{\rho_p}{18\mu} \tag{3.2}$$

In order to faithfully follow the streamlines, particles must have a limited value of the Stokes number; from a practical point of view it can be stated

that the condition $St < 0.1$ returns an acceptable flow tracing accuracy with errors below 1% [62]. Additionally, seeding particles must have appropriate light reflection properties in order to maximize the scattered light and the measurement sensitivity. In general, either solid, liquid or gaseous seedings can be used. For low temperature or non-reacting applications, one of the most reliable substances that can be used as seeding is mineral oil, while for reactive cases metal oxide powders are generally used.
As commonly known, the PIV measurements are subject to several sources of error, making rigorous uncertainty quantification particularly challenging. Some errors are related to the optical setup, such as imperfect calibration, slight misalignment between the camera sensor and the measurement plane, or image distortion due to lens aberrations. Others are linked to the laser system, including fluctuations in laser power and imperfect laser sheet alignment. Seeding issues, such as non-uniform particle distribution or particle agglomeration, can also degrade measurement quality. In reactive flows, additional disturbances arise from flame luminosity interfering with particle imaging. While all these factors can introduce uncertainties, careful experimental design and validation ensure that the measurements remain reliable and provide an accurate representation of the flow field.

3.1.1 PIV measurement set-up

PIV measurements have been carried out in the present test campaign with a Dantec Dynamics PIV system. The Dantec-FlowManager© software has been employed for data acquisition and post processing. During acquisition, the software controls the instrumentation settings, and a Programmable Timing Unit (PTU) is used to provide the trigger signals to camera and laser system for synchronization.
The laser employed for the investigation is the Litron LDY303, an Nd:YLF pulsed laser at a wavelength of 527 nm with a sample rate range between 0.2 and 20 kHz and a power range of 0-20 mJ per pulse. Images were recorded with a Phantom MIRO M340 camera, equipped with a 2560x1600

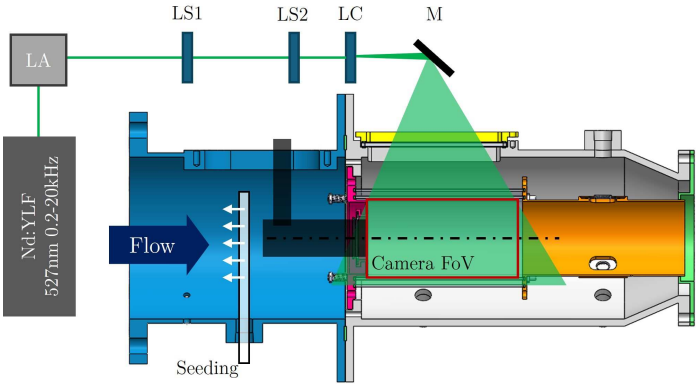

(a)

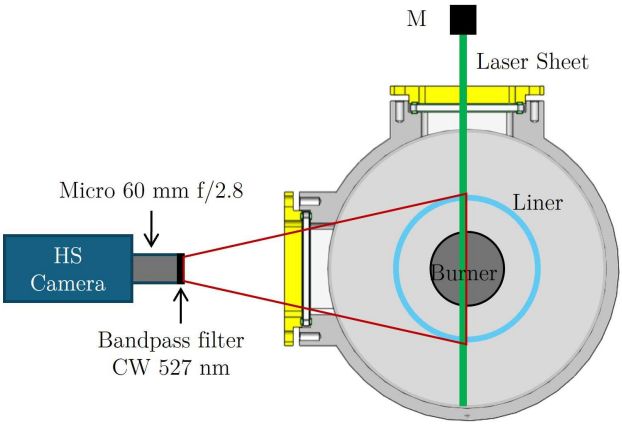

(b)

Figure 3.2: Schematic of PIV measurement set-up

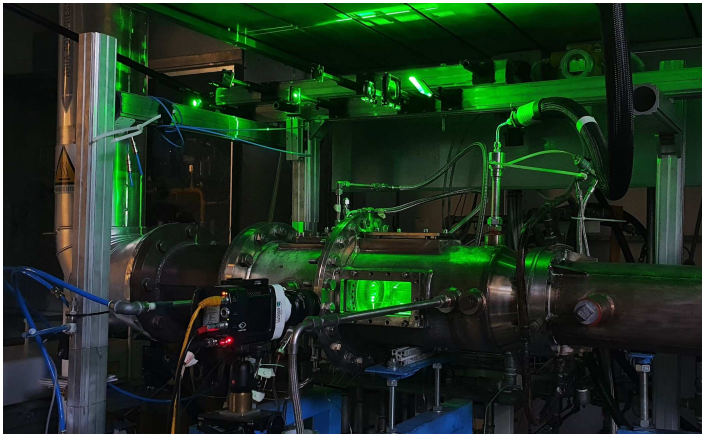

(a)

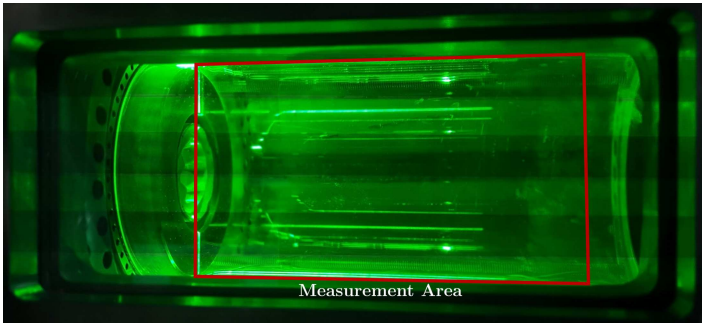

(b)

Figure 3.3: Picture of PIV measurement set-up (a) and measurement area (b)

pixel CMOS sensor with 12 bit sensor depth and 10 μm pixel size. The camera acquisition frequency is 800 fps at full resolution and it can be increased up to 50 kHz with lower resolution. The camera was coupled with a Micro NIKKOR 60mm f/2.8 lens and a narrow band pass filter (Central Wave Length (CWL) of 527 nm and Full Width at Half Maximum (FWHM) of 5 nm) to cut out all the incoming light except for the laser light scattered by the seeding particles.

A time delay of 12 μs has been used for both non-reactive and reactive conditions. For PIV measurements, the camera was operated with an acquisition frequency of 400 fps in double frame mode.

Measurements were performed on the burner vertical symmetry plane. The two perpendicular optical accesses on the external vessel allow the implementation of the PIV technique with the optical set-up shown in Figures 3.2-3.3. The laser beam is brought into an optical trail through a laser arm (LA) connected to the laser outlet. The optical trail consists of two planispheric lenses (LS), with a first concave one (LS1) and a convex one (LS2), followed by a cylindrical concave lens (LC) for the laser sheet generation. A final silver mirror (M) mounted on an adjustable system projects and aligns the laser sheet into the desired part of the test rig. The focal lengths of the lenses and their relative distance have been selected to obtain the desired focal line, with a laser sheet thickness of about 1 mm inside the combustion chamber, as shown in Figure 3.3b with the measurement area. Thanks to the rig's wide optical access and the camera lens opening angle, a single Field of View (FoV) is sufficient to capture the whole area of interest, that extends axially for more than two chamber diameters from the burner outlet. The camera was installed on a structure attached to the test rig to limit any possible effect of thermal expansion on calibration and measurements.

The inner surface of the external vessel was coated with a high-temperature resistant black paint to minimize reflections and keep the Signal-to-Noise ratio within acceptable limits. The cylindrical quartz liner could not be painted, resulting in strong reflections disturbing the measurement outcome in certain limited areas.

Flow field measurements have been performed in both isothermal and reactive conditions, in order to assess the effect of the flame presence on the air pattern. Titanium dioxide particles with submicron mean size were used as seeding, because of the reactive conditions. A Lavision Particle Blaster 110 was used to separate the particles and avoid the formation of agglomerations. It is made of a swirling bed generator consisting of a magnetic stirrer and a magnetic bar housed in a cylinder container. The air flow at the inlet of the seeder can be controlled by adjusting the pressure control valve to increase or decrease the particles' density depending on the tested conditions. An in-house built device was used to insert the particles upstream of the burner, injecting them with a multi-hole distribution pipe in counter-flow configuration, as shown in Figure 3.3a in order to maximize the particle spreading and ensure uniform seeding.

3.1.2 PIV data post processing

For each investigated condition, 800 image pairs of 1920x1080 pixel have been acquired at 400 fps in order to reconstruct the mean flow field. Spatial calibration was performed with a calibration dot pattern to calculate the $scalefactor$, which results in 0.11 (1 mm=9 pixels).
The Dantec-FlowManager © software was used to retrieve the velocity fields from the image pairs. The first step of post-processing is background noise removal, implemented through the subtraction of the averaged single pixel intensity from each acquired image. The PIV standard cross-correlation procedure divides each pair of images in several interrogation areas and the 2D cross correlation is applied to find the particle movement. If particles leave the interrogation zone in the time interval between the two laser pulses, with a phenomenon called *"in-plane drop out"*, the signal strength is consequently reduced. Adaptive PIV is an iterative approach based on grid adaptivity, which allow to limit this issue. The algorithm iteratively adjusts the size and shape of the individual interrogation areas (IA) in order to adapt to local flow gradients [65]. Standard cross-correlation is employed for the first attempt to compute the displacement vector. Then the result is used as a new estimation for

the window shift of the second iteration, with a refinement of the size and shape of the interrogation area. Interrogation area refinement starts from a 128x128 pixel initial window size to a final size of 32x32, with 50% overlap.
Once the vectors have been computed, validation is applied to prevent outliers from disturbing the iterations and thus the velocity measurements. Peak height ratio validation evaluates the ratio between the two highest correlation peaks for each IA at every iteration, and if this value is below the selected threshold (1.5 for the present set-up) the computed vector is rejected. The universal outlier detection algorithm is used to replace the rejected vector with the median of the neighboring vectors.
Instantaneous velocity maps obtained with the Dantec software are further post processed with Matlab © user-defined routines.

3.2 OH* chemiluminescence

Optical diagnostic techniques allow to gain a detailed understanding of the combustion process, providing crucial information for improving modern combustion systems. These methods, although they are not easy to implement, allow for direct monitoring of chemical species and thermodynamic conditions within the reactive flow with high spatial resolution. Among the various combustion diagnostic techniques, chemiluminescence stands out for its accessibility and cost-effectiveness, as it exploits the flame natural emission. The main advantage is that it does not require external excitation like other optical measurements, that imply the use of expensive lasers. The required hardware is only an optical sensor to collect the light emission, and appropriate filters to capture the desired wavelengths. Optical access can be limited to a small opening for a spectroscope, although compromising the measurement resolution. Spatially resolved measurements instead allow to gain detailed information on the combustion process, also profitable to validate computational models, at the price of needing wider optical access. Overall, it is a relatively cheap and simple technique to implement, which can be exploited also

in the early design stages of innovative combustion systems and for the optimization of existing technologies.
In the present work, OH* chemiluminescence imaging has been employed to investigate the flame shape and position under various operating conditions. Coupled with the complementary PIV measurements, which provide detailed information on the flow field, this approach allows for an in-depth study of the flame behavior. While PIV offers planar measurements of the velocity field, enabling the investigation of flow structures and the role of fluid dynamics in flame stabilization, OH* chemiluminescence provides a line-of-sight integrated signal related to the presence of emitting radicals. This makes it particularly useful for identifying the overall shape of the reaction zone and studying global flame dynamics. By combining these techniques, a more comprehensive understanding of combustion processes can be achieved, where PIV reveals the development and influence of the flow field on the flame anchoring and movement, and OH* imaging highlights the concentration of reaction activity. This synergy is especially valuable for analyzing stabilization mechanisms in complex configurations, where both flow features and chemical reactions must be considered together to fully characterize the system behavior.
The next section presents a brief overview of the fundamentals of OH* chemiluminescence technique, followed by some combustion diagnostic applications, with a particular emphasis on the effects of the operating conditions caused by CO_2 dilution. For a comprehensive theoretical analysis reference is made to dedicated works [66–69].

3.2.1 Theoretical background

The term *'chemiluminescence'* refers to the light emitted by atoms, molecules, or radicals as they transition from an excited electronic state back to the ground state. This emission comes directly from chemical reactions, and can be found in processes with unstable and intermediate species, such as combustion. Analyzing the light emission from combustion reactions allows to monitor flame position and its variations, making this method valuable for diagnostic purposes.

The chemiluminescence phenomenon is explained with the spectral lines observed in molecular spectroscopy associated with the absorption, emission, and scattering of photons that occur when a molecule's energy changes [70]. These energy states correspond to variations in electronic configurations, as well as vibrational or rotational motion of the nuclei of a molecule. In particular, a molecule's energy can be expressed as the sum of the electronic, vibrational, and rotational energy. Transitions involving changes in rotational energy levels typically occur in the far-infrared and microwave regions of the spectrum. Vibrational transitions fall within the infrared region, while transitions between electronic energy levels appear in the visible or ultraviolet spectrum. Vibrational transitions usually lead to changes in rotational modes, while electronic transitions cause changes in both rotational and vibrational modes.
The lowest electronic state, known as the ground electronic state, is referred to as the X-state, while higher-energy states are labeled A-state, B-state, and so on. Each electronic state is characterized by a vibrational quantum number (ν): ν" denotes the vibrational quantum number of the ground electronic state, and ν' corresponds to the upper excited electronic state. As mentioned earlier, molecules also undergo rotational changes, and the rotational energy associated with each vibrational state is defined by the rotational quantum number J: J" refers to the ground electronic state's rotational quantum number, and J' represents the rotational quantum number in the excited state. Various transitions are possible, governed by selection rules that determine whether a transition is allowed.

Chemiluminescence implies the formation (R1) and the radiative transition (R2) of excited-state radicals:

$$\mathrm{R1}: \quad \mathrm{P1} + \mathrm{P2} \rightarrow \mathrm{R}* + \text{others} \tag{3.3}$$

$$\mathrm{R2}: \quad \mathrm{R}* \rightarrow \mathrm{R} + \mathrm{h}\nu \tag{3.4}$$

$$\text{R3}: \quad \text{R}* + \text{M} \rightarrow \text{R} + \text{M} \tag{3.5}$$

In these reactions, P1, P2, and R represent different ground-state radicals, (R$*$) is the excited-state radical, and M denotes a third-body species not participating in the transformation of chemical bonds but rather acting as collision partner. As indicated in reaction R3, not all excited-state radicals contribute to chemiluminescence generation, but some may collide or react with other species [71].
In hydrocarbon flames, the primary chemiluminescent emitter species are OH*, CH*, C_2^*, and CO_2^* [70]. The flame spectra observed in the visible and ultraviolet (UV) range are generally the result of electronic transitions in molecules from excited states to ground states. Figure 3.4 shows a typical chemiluminescence spectrum of a premixed turbulent methane-air flame at atmospheric pressure. The spectrum is a superposition of the narrow band peaks from OH*, CH*, and C_2^*, and the broadband emission from CO_2^*.

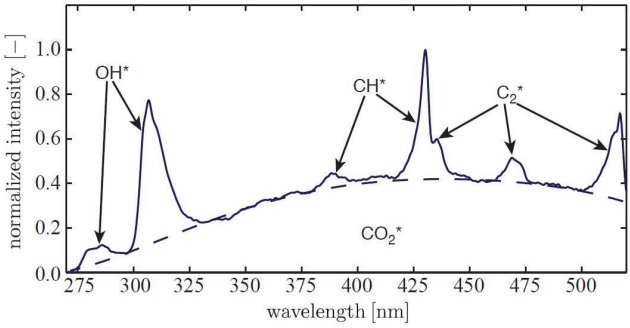

Figure 3.4: Typical chemiluminescence spectrum of a methane-air flame at atmospheric pressure [69]

In hydrogen combustion with air, OH* is the only chemiluminescence emitter, as shown by the emission spectrum reported in Figure 3.5.

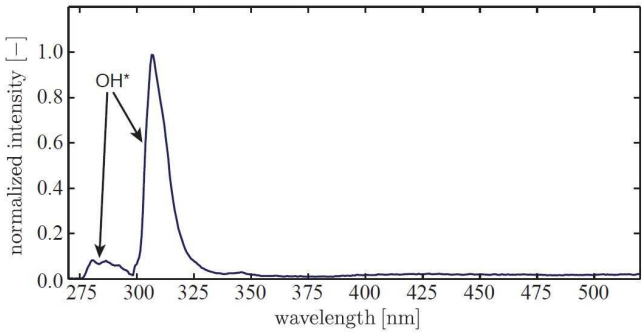

Figure 3.5: Typical chemiluminescence spectrum of an atmospheric hydrogen-air flame [69]

Among the various chemiluminescent species, OH* is often used in combustion research as a marker for the heat release rate [72]. The electronically excited OH* radical is produced through several pathways, mainly in the following reactions:

$$CH + O_2 \rightarrow OH^* + CO \tag{3.6}$$

$$CHO + O \rightarrow OH^* + CO \tag{3.7}$$

$$H + O + M \rightarrow OH^* + M \tag{3.8}$$

In hydrocarbon combustion the primary mechanism for OH* formation is reaction 3.6 [73], while 3.8 is the only one possible for hydrogen flames [74].

Figure 3.6 presents a simplified diagram of the OH radical's energy levels, including the potential curves for the ground and first excited electronic states. The potential curves depict the radical's energy as a function of nuclear distance: the energy is high when the nuclei are close, decreases as the distance increases, and eventually leads to dissociation into O and H

atoms. The vibrational potential curves are reported for both electronic states, and the rotational energy levels for the electronic ground state only, with notation explained earlier. The OH ground electronic state is typically denoted as $X^2\Pi_i$, while the electronic configuration of the first excited state OH* is $A^2\Sigma^+$ [75].

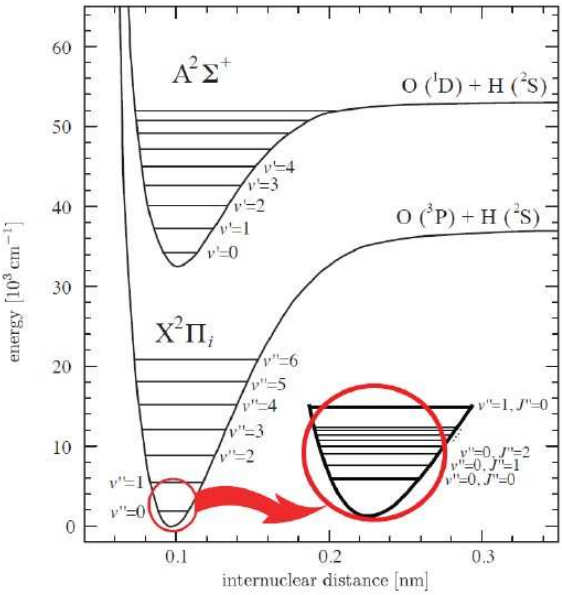

Figure 3.6: Simplified schematic of OH radical energy levels [75]

Once reached the electronically excited state, the OH* radical can return to its stable ground state OH through fluorescence, by emitting a photon which carries the energy difference between the two states:

$$\mathrm{OH}^* \rightarrow \mathrm{OH} + \frac{hc}{\lambda} \tag{3.9}$$

Not all energy transitions lead to photon emission, and only certain transitions result in fluorescence. The more common process is collisional

quenching, a deactivation mechanism that transfers energy via collisions with a third body, potentially leading to transitions to either higher or lower energy levels.

$$OH^* + M \rightarrow OH + M \tag{3.10}$$

The equilibrium distribution of excited radicals depends on the balance between upward and downward transitions, which is temperature-dependent. The emission spectrum is determined by the equilibrium distribution of ro-vibronic states, along with the Einstein coefficients for spontaneous emission, which act as proportionality factors between the number of excited radicals and the intensity of chemiluminescence emission. The OH* spectrum shows distinct bands corresponding to different ro-vibronic transitions and their relative intensities. Specifically, the peak intensity near 309 nm, depicted in Figure 3.4, represents the strongest OH* emission band, originating from a transition with $\Delta\mu = 0$, denoted as $X^2\Pi_i(\nu'' = 0) \leftarrow A^2\Sigma^+(\nu'' = 0)$.
Chemiluminescence is a line-of-sight technique, meaning that the the sensor collects the emission intensity coming from all molecules present along the optical path between the measurement point and the sensor itself. Typically, in time-averaged measurements, the intensity on the flame mid-plane is reconstructed using assumptions of axial symmetry and deconvolution methods such as the inverse Abel transform [76].

3.2.2 Application of OH* chemiluminescence with EGR

In the present work, OH* chemiluminescence has been employed to qualitatively mark the reaction zone, in order to study the flame behavior and understand the stabilization mechanism under different operating conditions. Some comparisons between emission intensities will be presented, attempting to remain consistent by comparing similar conditions. The resulting discussions aim only to provide general indications about relative variations and are not intended to be used to measure thermo-

dynamic quantities. Nevertheless, specially because of the innovative and unconventional conditions analyzed in this study, some additional considerations are necessary to correctly interpret the obtained results.

As anticipated, in the present investigation EGR conditions have been reproduced with CO_2 dilution of the combustion air. This leads to high CO_2 content, with consequences on the flame emission characteristics. Recalling the emission spectrum of natural gas flames shown in Figure 3.4, the OH* peak is superimposed on the CO_2* broadband emission. The intensified camera with band-pass filter centered on the OH* peak therefore collects the emission from both the OH* peak and the part of the broadband emission of CO_2* with wavelengths within the transmissivity range of the filter. In general, it is assumed that the OH* peak remains dominant over the CO_2* contribution, but the high CO_2 concentration in the flow could affect this aspect. In the present test campaign the flame emission spectrum has not been measured, therefore this assumption could not be verified directly.
In the literature, numerous studies have demonstrated how OH* can effectively be used to identify the reaction zone in both hydrocarbon and hydrogen flames [71, 77, 78], and exploited for diagnostic purposes [79]. Nevertheless, extracting detailed information about the combustion process is not straightforward. Several studies highlight that OH* emissions are influenced by local flow conditions, such as strain and turbulence [80–82]. As a result, while OH* serves as a useful indicator for visualizing flame behavior, additional considerations and corrections are often necessary to gain quantitative information in turbulent combustion scenarios. In particular, in order to accurately estimate heat release and equivalence ratio distributions in turbulent combustion environments, the OH* and CH* intensities should be corrected removing the CO_2* broadband emission [69, 83–86].
Most studies in the literature focus on conventional combustion systems where the oxidant is pure air. Limited research is available instead for the unconventional scenario examined in this study, because of the novel

and specific application. Several studies on biogas examine the effects of diluting natural gas with CO_2 or N_2. However, in these instances the overall concentration of the diluting gas in the reactants remains considerably lower than the levels investigated in this study. García-Armingol and Ballester [37] reported that increasing CO_2 levels in CH_4/CO_2 mixtures reduces the intensity of emission spectra in the near UV and visible ranges, without altering their overall shape. Hossain and Nakamura [87] numerically examined how N_2 and CO_2 dilution affects chemiluminescence intensity in laminar counter-flow diffusion flames, focusing on the CH* radical, concluding that increasing the concentration of diluents led to a decrease in CH intensity. In a more recent work, Guiberti et al. [88] investigated flame chemiluminescence from N_2 and CO_2 diluted laminar methane-air premixed flames with experiments and simulations. Their findings highlight that CO_2 dilution modifies chemiluminescence intensity ratios, which can be leveraged to infer the CO_2 concentration in the mixture. Furthermore Oh et al. [89] examined the influence of diluent gas composition, specifically N_2 and CO_2, on the flame emission spectroscopy, concluding that the C_2* spectral band could not serve as a reliable measurement indicator in CO_2-rich EGR environments due to strong background emissions.

An additional aspect to be taken into account is that the optical properties of the flow can vary with high CO_2 concentration. The carbon dioxide molecule at ambient temperature is transparent in the ultraviolet (UV) at wavelengths longer than 205 nm. In the studies of Jeffries et al. [90], it was observed that at high temperatures (over 1000 K) the absorption cross-section becomes significant between 200 and 320 nm, in correspondence of the OH* chemiluminescence peak at 310 nm. Similar results were found by Joutsenoja et al. [91], focusing on the CO_2 absorption in the UV range between 200 and 270 nm. Such range is not included in the bandpass frequency of the filter employed to detect OH* signal in the current study, but the results still provide meaningful indications. Overall, the studies confirm an increase in optical absorption of the reactive mixture due to higher CO_2 content, lowering the portion attributed to OH*.

In addition to the unconventional oxidizer composition, in the present work the addition of a limited amount of hydrogen was introduced in a natural gas flame. This dual fuel configuration was implemented both using pure hydrogen jets and with a hydrogen-natural gas blend. García-Armingol and Ballester [37] explored the possibility of using chemiluminescence to estimate the equivalence ratio in flames with different hydrogen content. A similar approach was proposed by Reyes et al. [92], who employed OH* and CH* chemiluminescence emissions to characterize the combustion of blends of methane and hydrogen in air in a constant volume combustion bomb.

3.2.3 OH* imaging measurement set-up

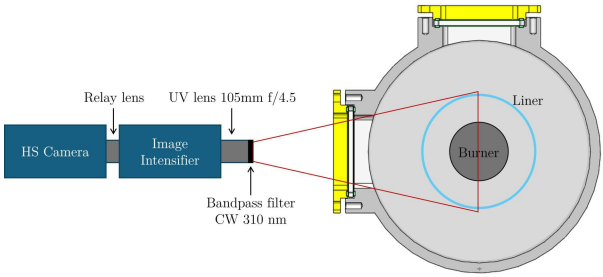

Figure 3.7: OH chemiluminescence measurement set-up*

In the present test campaign spatially resolved OH* chemiluminescence was implemented with a high speed camera coupled to an image intensifier. In particular, the same camera as for the PIV measurements was used, the Phantom Miro M340, coupled through a relay lens with the Hamamatsu C16031-311-Ax image intensifier. The UV lens (Nikon UV 10 5mm f/4.5 lens) was mounted on the image intensifier with a band-pass filter

(CWL=310 nm and FWHM=5 nm) to capture only the wavelengths near the OH* peak, which is located at 309 nm.
Camera and intensifier are synchronized with a Programmable Timing Unit (PTU), which is used to trigger the image acquisition. The acquisition frequency f_s is 1000 Hz for all presented data. The intensifier gate was kept constant at 0.5 ms all stable test points. In some conditions, for example near the lean blow out, where the flame emission intensity is very low, the intensifier gate was increased up to 0.8 ms.
The camera field of view is the same as for the PIV measurements, i.e. the burner vertical symmetry plane, obtained with the measurement set up reported in Figure 3.7.

3.2.4 Data reduction

For each investigated condition, 1000 image pairs (1920 x 1080 pixel) have been acquired at 1000 fps. Image post processing was performed with Matlab © with user-defined routines. As for PIV measurements, spatial calibration was performed with a calibration dot pattern, and a single camera position has been used to capture the whole area of interest. In order to study the flames' steady structure, images are averaged over time, after background subtraction and spatial calibration. Further image post processing has been performed with Matlab © user-defined routines, in order to gain further insights into the combustion process. Axial profiles of OH* intensity have been computed averaging the collected emission along the combustion chamber radius, and global averaged values will also be reported.
As anticipated, chemiluminescence is a line-of-sight technique, but with some assumptions, the flame shape on the mid-plane can be reconstructed thanks to mathematical tools, through the application of an inverse Abel transformation. Briefly, ignoring the flames' self-absorption contribution and assuming an axial symmetry of the image, the OH* intensity distribution on the burner mid-plane can be retrieved. A detailed description of the method can be found in [93].
To match the symmetry requirement, Abel deconvolution has been ap-

plied only on time averaged images, but as the experimental description shows, the pilot fuel is injected in discrete jets, and asymmetric structures arise. For a first evaluation, however, it was considered useful for the investigation to neglect deviations from axisymmetry and to also examine the Abel deconvoluted images, since they provide additional information to complement the line-of-sight images.

3.3 Exhaust gas analysis

The main pollutant emissions produced by a natural gas flame, also with the addition of a limited amount of hydrogen, are NO_x and CO [94]. Exhaust gas analysis has been performed during the reactive tests in order to asses the impact of the different operating conditions, with particular focus on the effect of EGR.
A portable gas analyzer has been used for the measurements, model HORIBA PG350. The analyzer measures the concentration of CO, CO_2, O_2, NO_x in the exhaust gases, but only the results for CO and NO_x will be presented. CO_2 and O_2 levels were monitored during the tests to ensure proper operating conditions, but values are not reported.
The measurement principle for NO_x detection is based on chemiluminescence, while a paramagnetic analyzer is employed for oxygen. CO and CO_2 measurements exploit infrared adsorption [95].
The emission probe is plugged into the flame tube to extract the exhaust gases, in correspondence of section E of Fig. 2.4, with the arrangement shown in Figure 3.8. The probe is water-cooled, and is made of several radially spaced holes, in order to average the exhaust gas composition over the combustion chamber diameter. After being extracted, the gases flow through a thermally insulated pipe kept at 150°C. An inter-cooler is used to remove the vapor content in the exhaust gas before it reaches the analyzer, model HORIBA PSS-5H refrigerator, with a dew point set at 5°C.
The gas analyzer is properly calibrated right before each test employing a rack of calibrated gas mixture tanks. The measurement uncertainty

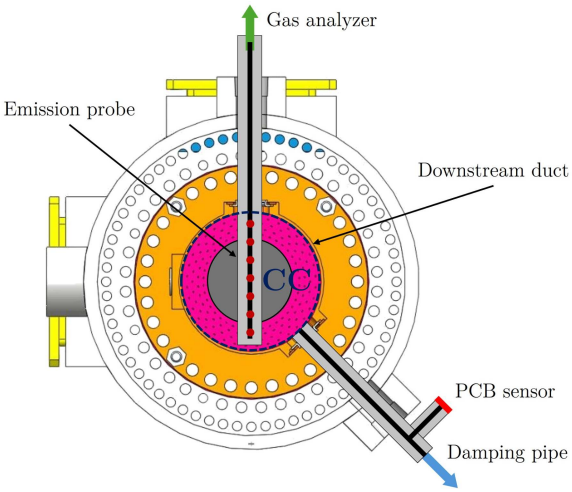

Figure 3.8: Schematic of the high frequency pressure sensor (PCB) and emission probe installation and positioning relative to the combustion chamber (holes for extracting the exhaust gases are in counter-flow with combustion main flow, facing the flame)

on NO_x and CO values has been estimated for a reference condition to be around 2 ppm, and is only marginally affected by the investigated operating conditions. This value considers the entire measurement chain, which includes the uncertainty of the calibration tanks and of the gas analyzer.

3.4 High frequency pressure measurements

A high-frequency pressure sensor has been used to monitor pressure oscillations, with the aim of investigating the flame dynamic behavior and detecting possible thermoacoustic instabilities. Assessing pressure-driven oscillations is fundamental for evaluating burner performance, as such instabilities severely restrict the operational range and, in real gas turbines, can lead to major mechanical damage. For this reason, the dynamic response of the system must be carefully analyzed during

experimental investigations supporting burner development.
The amplitude of pressure oscillations will be reported in terms of their Root Mean Square (RMS) value, denoted as $P"_{RMS}$, being

$$P"_{RMS} = \sqrt{\frac{1}{N}\sum_{i=0}^{N-1} p_i'^2} = \sqrt{\frac{1}{N}\sum_{i=0}^{N-1}(p_i - \bar{p})^2} \tag{3.11}$$

$$\text{where} \quad \bar{p} = \frac{1}{N}\sum_{i=0}^{N-1} p_i$$

The frequency spectrum will also be presented, computed with the Discrete Fourier Transformation (DFT), which transforms samples of signals from the time domain into the frequency domain.
The DFT of a time-based signal with N samples x_i, acquired with an acquisition frequency f_s, produces a frequency range representation X_k with N values.

$$X_n = \sum_{i=0}^{N-1} x_i e^{\frac{-j2\Pi ik}{N}} \quad \text{with } k = 0, 1, 2.., N-1 \tag{3.12}$$

Analogous to the time interval $\Delta t = 1/f_s$ between the samples of x in the time domain, the frequency resolution Δf between the components of X in the frequency domain is:

$$\Delta f = \frac{f_s}{N} = \frac{1}{N\Delta t} \tag{3.13}$$

For the high frequency pressure measurements, a PCB © sensor (model 102M206) has been employed, featuring a piezoelectric sensitive element. The acquisition frequency f_s employed for the investigation is 12.8 kHz and the RMS is evaluated over 0.64 s (N=8200), acquiring the signal with a National Instruments chassis cDAQ-9181.
The sensor is installed in the second part of the combustion chamber downstream of the quartz liner, in correspondence of section E of Figure 2.4, with the arrangement shown in Figure 3.8. The sensitive element is not flash mounted on the chamber surface but is instead located downstream

of a dedicated port surfacing on the inside of the downstream duct, that transmits the pressure signal from the chamber to the outside of confining vessel. At one end, the tube is connected to a very long copper pipe that acts as a damping device, to shield the sensor from the reflected pressure waves. This arrangement, although necessary to limit the sensor's exposure to high temperatures, prevents the synchronization of the high-frequency pressure signal with the chemiluminescence imaging.

3.5 Results presentation

This last section on the experimental set up is dedicated to the description of the results presentation mode for all presented data.

The coordinate system used for the investigation is centered on the burner outlet, with the axial coordinate x and the radial coordinate y. The camera field of view (FoV) for both PIV and OH* chemiluminescence imaging is highlighted in Figure 3.9 with a red rectangle, together with the coordinate system that is used to present the results.

OH* chemilumenescence images are displayed both in terms of absolute and normalized intensity, with arbitrary units (a.u.), as the emission intensity depend on the optical set-up. Normalized intensity values are scaled with the maximum intensity for each case if not specified otherwise.

2D PIV is able to retrieve the velocity components in the laser sheet plane (xy plane). Axial (x) and radial velocity (y) are denoted as 'U' and 'V', respectively, and 'UV' is the velocity magnitude in the xy plane.

Regarding pollutant emissions, because of the wide variation in operating conditions in terms of fuel and oxidant composition, values were not corrected to 15%O_2, as is commonly done in gas turbines. In a recent study, Breer et al. [96] investigated NO emission from a premixed natural gas-hydrogen flame, highlighting that comparisons with volume

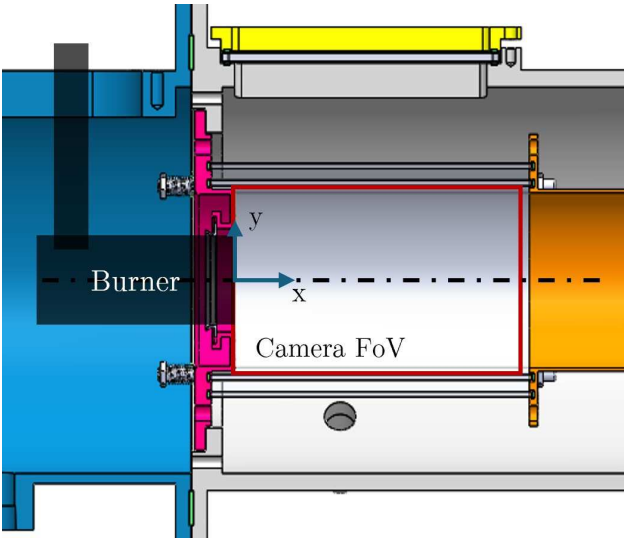

Figure 3.9: PIV and OH camera field of view and coordinate system*

concentration-based values can lead to erroneous conclusions, when H_2 fraction is varied. Possible corrective expressions have been proposed [97], but in the present study it was chosen to present NO_x as raw ppm measured by the gas analyzer on dry flue gas, with the same approach adopted in [13].

Mass flow rate values and adiabatic flame temperatures will not be presented for proprietary reasons. Scaled quantities will be displayed instead. The total thermal power has been kept constant for most of the study at a value indicated as TP_{REF}, which will be used to scale the results at different conditions.

The amplitude of pressure oscillations is reported in terms of their RMS value, denoted as P''_{RMS}, and the frequency spectrum of the oscillations computed with DFT will also be presented, all scaled with a reference value.

Chapter 4

Burner characterization in standard conditions

The first part of the work was focused on the characterization of the baseline configuration of the burner (B0) in standard conditions, which is reported in this chapter. The purpose of this stage is to understand the starting point of the investigation, defining the baseline performance.
In addition to standard diagnostic measurements, such as exhaust gas analysis, used to quantify the burner performance, optical techniques can be exploited to provide a better understanding of the flame stabilization mechanism. With such purpose the flow field was measured with PIV, and the structure and position of the flame were analyzed with OH* chemiluminescence imaging. To provide a comprehensive evaluation, NO_x and CO emissions were recorded, and the burner was also examined for stability through lean blowout (LBO) measurements.
The analysis starts detailing the burner behavior with natural gas as fuel, as it is commonly operated in gas turbines. In the final part of this chapter the effect of hydrogen injection with the pilot line will be illustrated. Some beneficial effects have been observed without EGR, with hydrogen addition expanding the range of stable operation, with positive results on emissions that can also be exploited for conventional operation.

	$\mathbf{T_{inlet}}$ [°C]	ΔP/P [%]	%PMX [%]	$\mathbf{TP_{TOT}}$ [kW]
NR-COLD	30	dP_{REF}	-	-
NR-HOT	300	dP_{REF}	-	-
R-0%PMX	300	dP_{REF}	0	TP_{REF}
R-70%PMX	300	dP_{REF}	70	TP_{REF}

Table 4.1: Operating conditions for PIV measurements in standard conditions

4.1 Flow field measurements

The flow field that develops inside the combustion chamber plays a crucial role in the flame stabilization mechanism. In technical applications various types of airflow patterns are employed within the combustor, but many aerodynamic characteristics are common among these systems. In general, the focus is on achieving large-scale flow recirculation to anchor the reaction process. The formation of a reversal toroidal flow that recirculates some of the hot combustion products to mix with the incoming air and fuel allows the flame to stabilize. Furthermore, effective mixing is vital for achieving high burning rates and reducing soot and nitric oxide emissions [94].

An effective and widely used strategy for inducing flow recirculation in the primary zone is the use of a swirler through which the combustion air passes. When the tangential component imparted to the flow is significant, vortex breakdown leads to recirculation in the core area. This form of recirculation yields better mixing compared to other methods, such as using bluff bodies, because the swirling motion creates strong shear regions, increased turbulence, and high mixing rates [98]. The results presented in this section show that a different strategy has been implemented on the present burner, prioritizing resistance to flash-back and auto-ignition. In the perspective of improving the burner performance at high EGR rates the characterization of the flow field is fundamental. PIV measurements of the velocity field have been performed in the burner symmetry plane

with the purpose to address this aspect.
The operating conditions presented in this section are summarized in Table 4.1, including both non-reactive (NR) and reactive conditions (R).

4.1.1 Non-reactive PIV velocity field

The analysis starts with non-reactive conditions, to examine the velocity field generated by the burner without the influence of combustion. These isothermal measurements equally apply to all studied burner configurations, as the layouts only differ by the fuel injection, and the fuel flow rate can be neglected in cold flow conditions, while differences occur for reacting conditions due to modified location of reaction zones.
Figure 4.1 presents the time-averaged velocity fields measured for isothermal flow, comparing the case at ambient temperature (NR-COLD) with the case with air preheating (NR-HOT) at the same pressure drop.
The typical swirl-stabilized velocity field characterized by the inner recirculation zone is not present, and instead a jet flame velocity field is established. The flow structure is thus a jet that flows out of the burner outlet and enters the combustion chamber. The jet expansion generates recirculation zones in the corner of the chamber, visible as negative axial velocity values. Negative values are very low, and under these conditions the corners of the chamber are practically a stagnation area, with almost null velocity. Assuming that the flow is approximately axisymmetric, the external recirculation zone in the tubular chamber has a toroidal form and is located in the corner between the walls of the cylindrical liner and the dome.
Despite the presence of the double swirler, the counter-rotating configuration leads to a low swirl number (not reported for confidentiality), not sufficiently high to give rise to vortex breakdown. Furthermore, the strong acceleration inside the converging duct is such that the jet remains coherent as it leaves the burner and enters the combustion chamber. With the present experimental set-up, it is not possible to measure the tangential component of the velocity, therefore it is not possible to evaluate the swirl

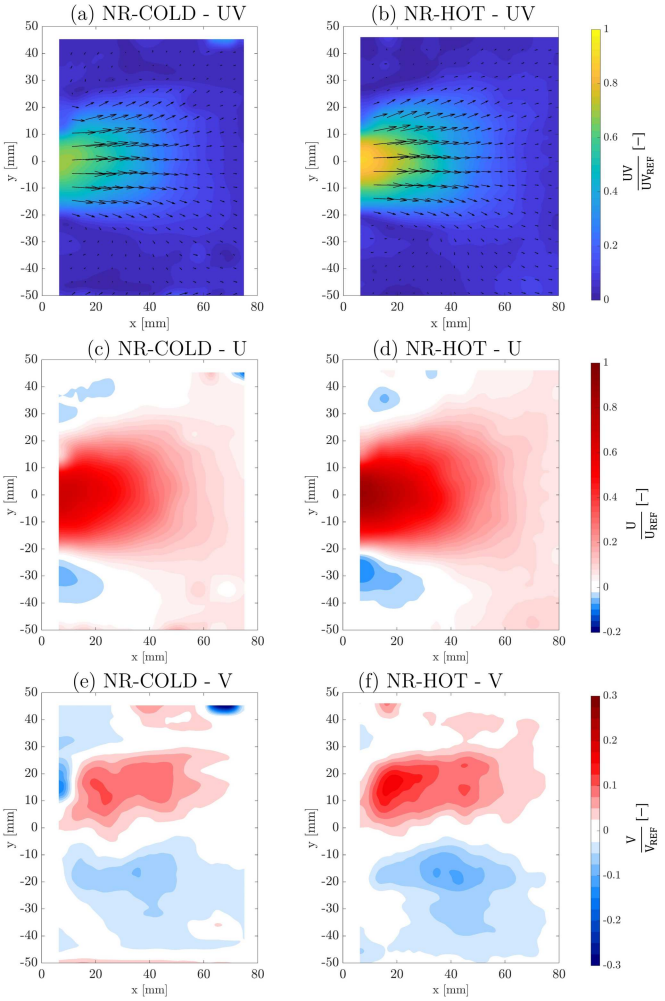

Figure 4.1: Time-averaged non-reactive velocity field: ambient conditions (a-d-e) and with flow preheating at 300°C (b-d-f)

number.

The jet does not open much in radial direction, but remains compact, as

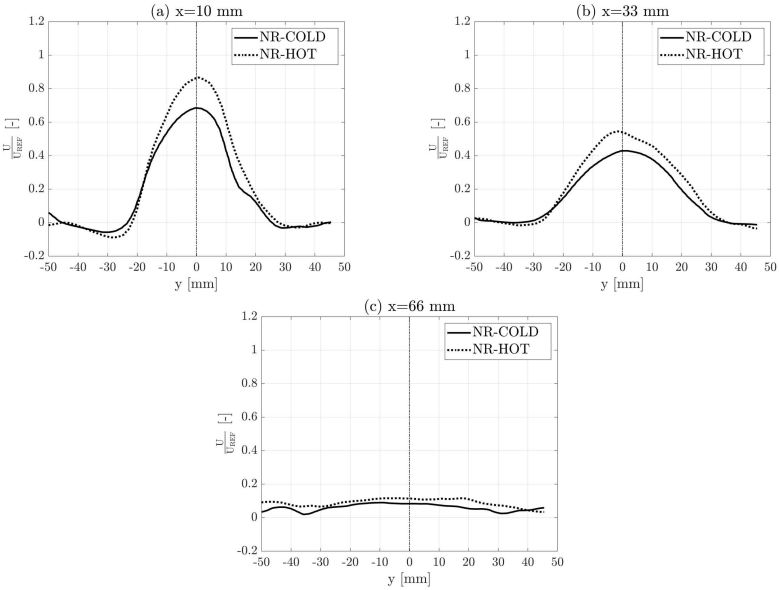

Figure 4.2: Radial profiles of axial velocity U

shown by the very low radial components of the velocity (Figures 4.1-f-e). Comparing the ambient and preheated case, according to the expected behavior, the flow structure does not change significantly. With higher inlet temperature the flow density decreases, and the jet velocity consequently increases. For both conditions, the flow field is not perfectly symmetrical, showing a more intense recirculation in the lower corner, as clearly visible from both velocity component distributions. The geometry of the object and the combustion chamber is nominally axisymmetric, therefore, the highlighted behavior in non-reactive conditions is attributed to possible imperfections in the 3D printing process of the burner, as there is no influence from the flame that could locally alter the flow. Mild asymmetries are to be expected in real hardware systems, given the complex geometry and the highly turbulent flow conditions, where even minimal geometric variations can have a non-negligible effect.

Radial profiles of the axial velocity U have been extracted at different locations to provide a quantitative comparison, shown in Figure 4.2. As seen from the maps, the outer recirculation zone is not very intense, with almost null velocity also at the first radial section. The effect of air preheating is higher near the burner outlet, and the difference between the two cases decreases moving downstream, where the profiles become almost constant.

4.1.2 Effect of reactive conditions and fuel split

Moving to reactive conditions, two different fuel splits have been tested, with the results shown in Figure 4.3. The pressure drop and inlet temperature are the same in the NR-HOT and reactive cases, therefore the air mass flow-rate is also the same except for very small variations of the burner effective area due to the presence of the flame.

The jet flow field is maintained also in reactive conditions, but the lower density due to the high gas temperature leads to higher velocity values with respect to the isothermal case. Beside higher velocity magnitude, the main consequence of the flame presence is a wider opening of the jet, that can be seen from the significant increase in the radial component. Indeed, the strong heat release caused by the combustion process results in thermal expansion of the flow, increases the jet opening in the radial direction. The extension of the outer recirculation zone is therefore reduced, but the recirculation is more intense, as shown by higher negative velocity values with respect to the non-reactive cases.
Radial profiles of axial velocity are reported in Figure 4.4 for the two reactive cases and the isothermal one with preheating. The profiles show again the higher velocity values in reactive conditions, and the wider radial opening of the jet due to thermal expansion. Differences between non-reactive and reactive conditions increase moving downstream from the burner outlet. Indeed, the OH* images presented in the next section will show how especially for the fully diffusive case (0%PMX) the reaction process takes place once the mixing between fuel and main-flow has

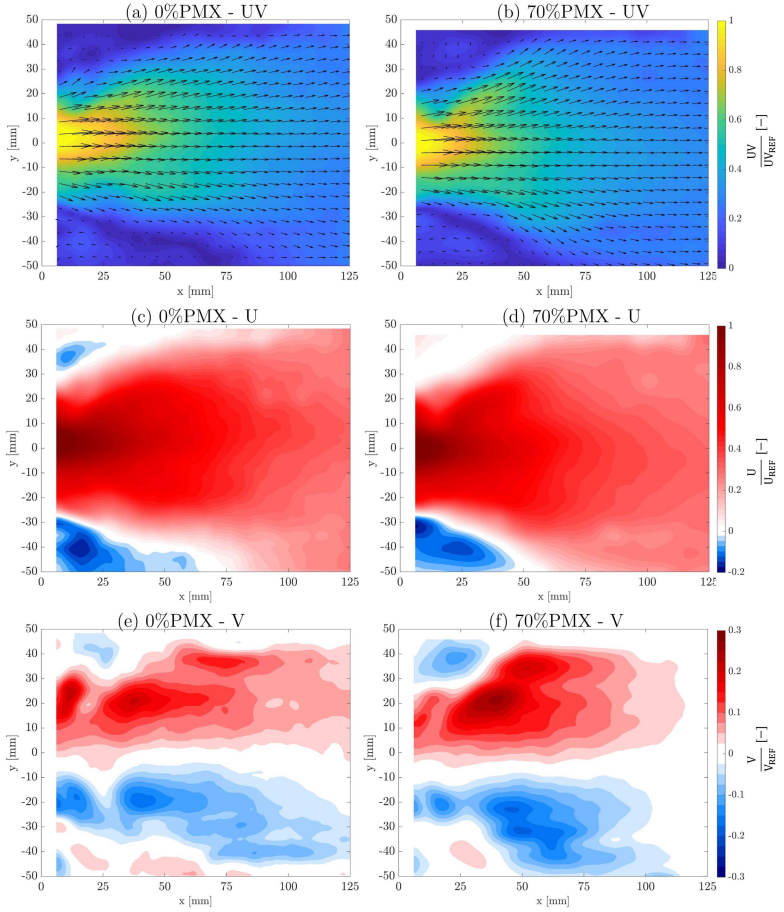

Figure 4.3: Time-averaged velocity field with 100%NG at 0%PMX (a-c-e) and 70%PMX (b-d-f)

occurred, and immediately at the burner outlet the gas temperature has not risen significantly yet. At x=66 mm instead, the flow temperature is greatly increased by the reaction process, and since the mass flow rate is about the same between non reactive and reactive conditions, the flow

velocity increases for the latter.
The effect of fuel split on the velocity field is limited, and only a slight increase in the jet opening can be observed with higher premix fuel fraction. The length of the outer recirculation zone is consequently slightly reduced, as shown by the axial velocity maps. Indeed, the zone with null velocity (white streak) encounters the combustion chamber walls at lower axial distance from the burner outlet in the case with higher premix fuel fraction. The non-perfect symmetry observed under non-reactive conditions persists and is possibly amplified by the presence of the reaction, visible in the more intense recirculation zone in the lower corner. The isothermal flow field is already slightly unbalanced, and the presence of the flame introduces additional sources of asymmetry due to localized heat release zones and the pilot jets, which, besides being discrete, are not perfectly axisymmetric by design (see section 2.3.2).

The main outcome of the characterization of the velocity field is the absence of an inner recirculation zone. Indeed, the low swirl component generated by the counter-rotating swirlers combined with the flow acceleration in the converging duct prevents the occurrence of vortex break-down that would generate an inner recirculation. This heavily affects the flame stabilization process, which can rely on less recirculation of active radicals and faces locally higher flow velocities, but is less influenced by the different operating conditions. This burner design was selected for the present investigation because of its versatility, as it is widely used in different gas turbines models, which is a great advantage in the retrofitting perspective. The burner is characterized by a very strong flashback resistance, a feature that is actually not crucial in the present study. Indeed, EGR generates challenging conditions for the reaction process because of the lower oxygen content, consequently reducing the risk of flashback. In principle the addition of hydrogen increases the chances of this danger again [99], but for this study hydrogen is injected directly into the chamber with the pilot line, which is intrinsically flashback safe due to its diffusive character.
Further insights on flame stabilization mechanism and the impact of the

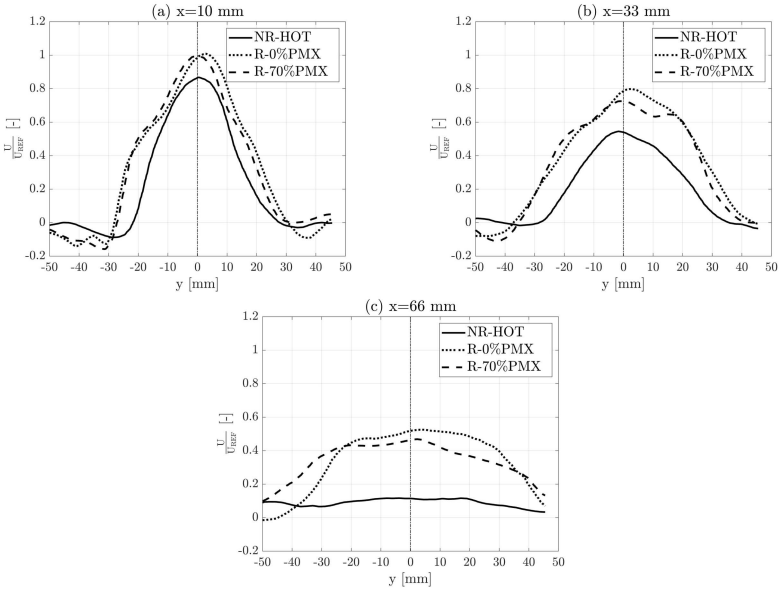

Figure 4.4: Radial profiles of axial velocity U

flowfield will be given in the next section, thanks to OH* chemiluminescence measurements.

4.2 Flame structure

The steady structure of the reaction zone has been investigated with OH* chemiluminescence imaging, in order to detail the flame stabilization process. Figure 4.5 shows the time-averaged distribution of OH* chemiluminescence for the fully diffusive (0%PMX) case, together with the burner schematic. Line-of-sight OH* emission is presented, as detected with the intensified camera. In this condition, the reaction zone is detached from the burner outlet, with a lifted flame configuration. The pilot jets are clearly distinguishable near the burner exit, and the flame slightly opens radially because of the high momentum of the pilot fuel jets which are

oriented in the outward direction.

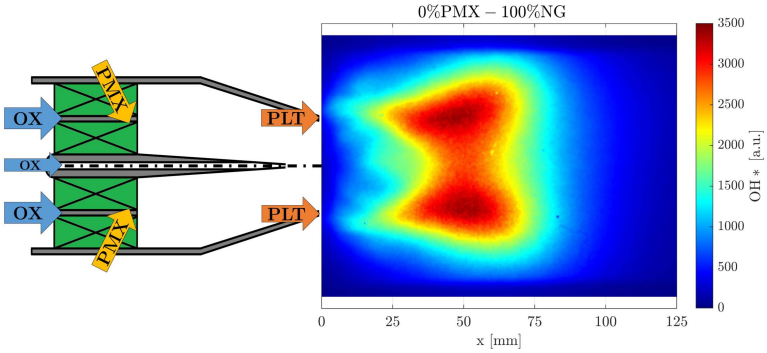

Figure 4.5: Time-averaged OH chemiluminescence for 0%PMX*

In order to spatially correlate reaction zone and flow field and understand how the flame stabilizes, Figure 4.6 shows the inverse Abel transform of normalized OH* images together with the velocity fields measured in the same reactive conditions in the burner symmetry plane, corresponding to the maps reported in Figure 4.3. The inverse Abel transform is referred to the lower half of the image (negative y values, mirrored) in order to be consistent with the corresponding velocity field. Among all control parameters of the engine, it was chosen to analyze the effect of the fuel split between pilot line and premix line, and two different cases are presented.

By definition, Abel transform assumes axisymmetry, but in the investigated configuration, pilot fuel is injected with discrete holes, which give rise to separate reaction zones near the burner exit. Therefore, it is not entirely correct to assume axisymmetry, but since PIV is a planar measurement, this approximation allows us to be congruent and combine the information collected with the two techniques. A Fourier-based algorithm has been employed for Abel deconvolution, with the methodology

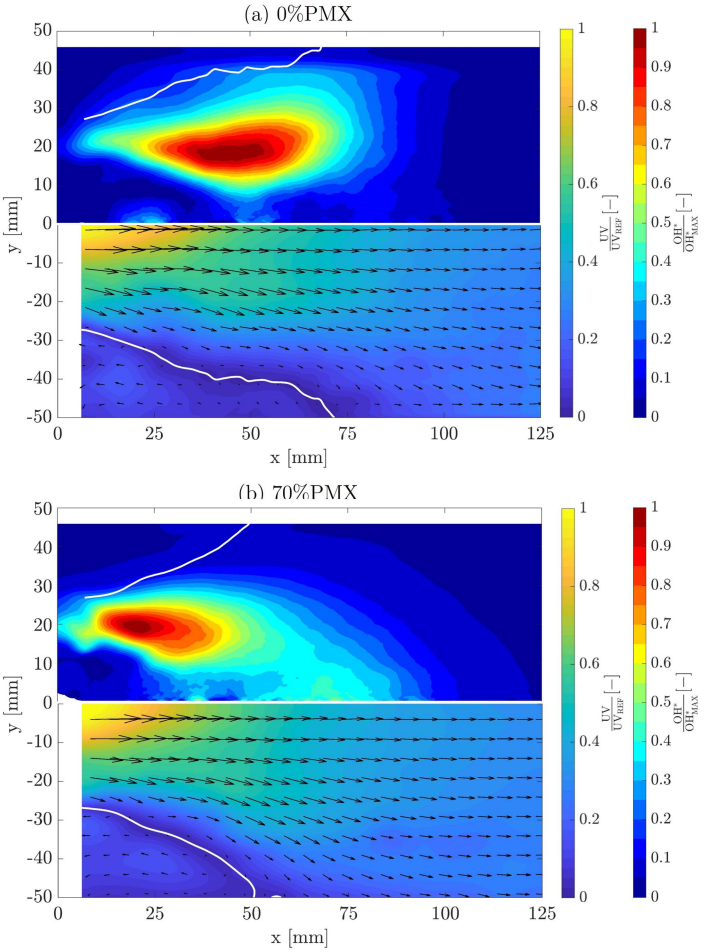

Figure 4.6: Inverse Abel transform of normalized time averaged OH chemiluminescence images (upper half) and time averaged UV velocity magnitude (lower half) for 0%PMX (a) and 70%PMX (b). White lines correspond to UV=0 m/s isolines*

described in [93]. The isoline of null velocity is visualized as a white line in both velocity and OH* distributions, indicating the boundary of the outer recirculation zone.
The jet exit velocity from the burner is such that it does not allow the flame to anchor in the core region, and for both fuel split conditions the flame stabilizes in the vicinity of the outer shear layer, where pilot fuel is injected. In this region, the main flow velocity is low and strong velocity gradients generate intense turbulence, promoting mixing between air and pilot fuel. The outer recirculation zone helps the flame stabilization as it continuously supplies heat and activated radicals from the hot combustion products towards the fresh mixture.
For the fully diffusive condition, the pilot jet velocity is very high, and the flame lifts off and stabilizes at a certain distance from the burner lip. A hollow configuration is present since the whole fuel mass flow rate is injected in the combustion chamber with the pilot jets, and the core jet leaving the burner is pure air. The outward orientation of the pilot jets and the sudden expansion of the cross section makes the reaction zone to open radially toward the combustion chamber walls.

With higher premix fuel fraction, the velocity field does not change substantially, but the reaction zone closes toward the burner axis and approaches the burner exit. Despite the fact that the fuel split is more premixed, the flame still anchors in the vicinity of the pilot jets, which seem to contribute most to the stabilization process, resulting in a predominantly diffusive flame. The total fuel mass flow rate is kept constant between the two cases, therefore the pilot jets' momentum decreases at 70%PMX, and the jet penetration is reduced, allowing the flame to attach closer to the burner exit, and limiting the radial opening. The fuel injected with the premix line reacts along the burner axis where the jet velocity decreases, around 60 mm downstream of the burner exit. The length of the outer recirculation zone is reduced with higher premix split, as the thermal expansion due to the reaction zone near the burner axis pushes the flow toward the combustion chamber walls. A greater jet open-

ing in the radial direction is indeed seen in the PIV maps of Figure 4.3, which show higher values of the radial component for the high-premix case.

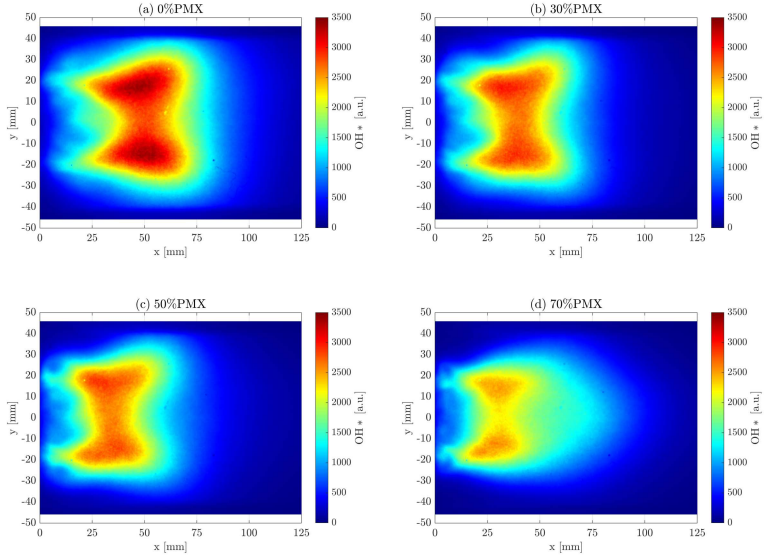

Figure 4.7: Effect of premix fraction on the flame structure

OH* chemiluminescence images of intermediate fuel splits are reported in Figure 4.7, with constant total thermal power. As the premix fuel fraction increases, the reaction zone shortens and approaches the burner outlet, since the pilot jet velocity decreases. The structure of the reaction zone remains similar to the fully diffusive case, with lifted flames anchored near the pilot jets, until the fuel fraction of the premixed line exceeds the pilot one (PMX $>$ 50%), when the flame structure changes substantially and closes toward the burner axis. Maximum OH* intensity decreases with lower pilot spit, as the fully diffusive case gives rise to locally richer spots. Since the measurement is line-of-sight, the slight asymmetries observed in the flow field are compensated by the integrated signal and

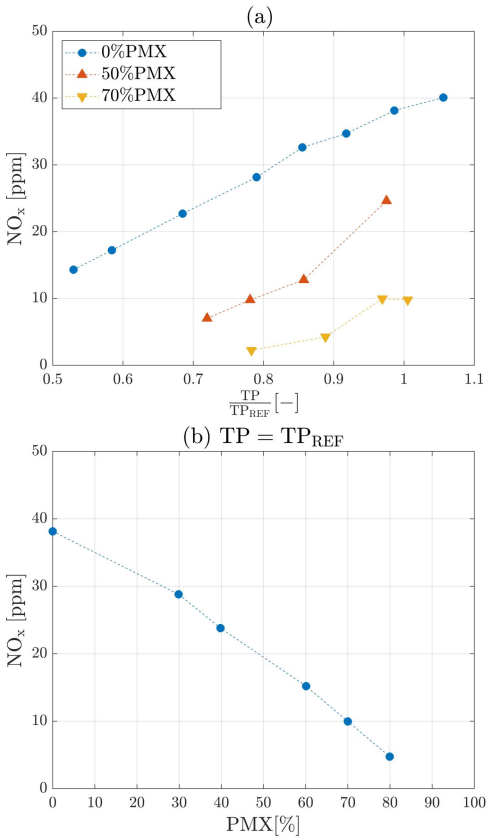

Figure 4.8: NO_x emissions: (a) effect of total thermal power and (b) effect of premix fraction

are not visible, resulting in reaction zones that are practically perfectly symmetrical for all splits under these conditions.

4.3 Emission measurements

Exhaust gas analysis was performed in order to assess the impact of the operating conditions on pollutant emissions.

Figure 4.8 presents NO_x emission as a function of the scaled thermal power and premix fuel fraction respectively, in order to highlight the effect of each variable. In complement to the so far compared cases at identical thermal power, this section presents sweeps of this parameter. Since the burner pressure drop is kept constant and consequently so is the air flow rate, the change in the thermal power due to fuel mass flow rate variation relates to a change in overall equivalence ratio. As expected, NO_x values rise with progressively richer conditions, as the adiabatic flame temperature increases. For the fully diffusive case the increasing slope progressively diminishes moving toward richer conditions. For higher premix splits, the relative increase is larger. A possible explanation for this behavior stays in the fact that, for the fully diffusive case near stoichiometric conditions are locally approached where the flame stabilizes, and consequently NO_x formation reaches a maximum, and a further increase in the global equivalence ratio has a limited effect. On the other hand, for a perfectly premixed natural gas flame, NO_x emissions increase exponentially with the equivalence ratio [94]. With a substantial premix fuel fraction, the global equivalence ratio directly affects the mixture composition near the reaction zone, and when moving to richer conditions, NO_x values continue to increase.

Looking at the effect of fuel split (Figure 4.8b), NO_x emissions decrease with an almost linear trend with the increasing premixed fuel fraction. Indeed, the higher premixing level limits the presence of hot richer spots where thermal NO_x formation is very high. Recalling the chemiluminescence images of Figure 4.7, when increasing the premix fuel fraction the maximum OH* intensity decreases. For a natural gas-air flame, the OH* emission can be correlated to local heat release [100], therefore lower temperatures are locally reached with higher premix fraction, reducing NO_x production. The Abel transformed OH* image of Figure 4.6b shows that the flame still stabilizes near the pilot jets also at higher premix fuel fraction. However, the region near the burner exit becomes leaner since the total fuel mass flow rate is kept constant, with beneficial effect on NO_x emissions. The flowfield measured in reactive conditions reveals the

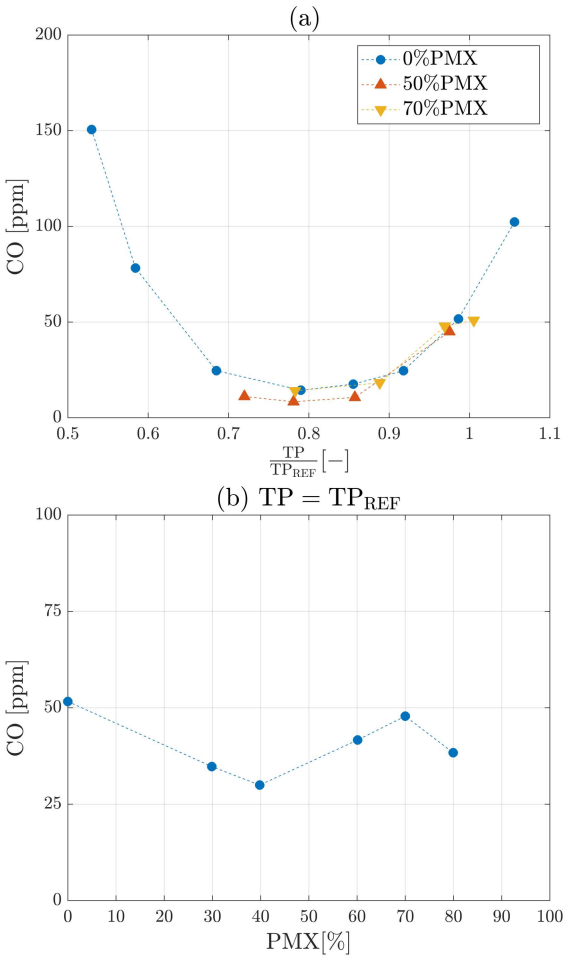

Figure 4.9: CO emissions: (a) effect of total thermal power and (b) effect of premix fraction

absence of an inner recirculation zone. This leads to a low residence time, which helps in controlling NO_x levels. Indeed, the measured values are limited also in the fully diffusive case.

Moving to CO emission, values measured for the same operating conditions are reported in Figure 4.9. Starting with the effect of the thermal power or equivalence ratio (a), all profiles show a non-monotonic trend, with a minimum around 80% of the reference thermal power. For a perfectly premixed natural gas flame, CO emissions have this same trend with equivalence ratio, with the minimum at conditions slightly leaner than stoichiometric, around $\phi = 0.9$. The presence of pilot diffusive jets moves the minimum to lower equivalence ratio, as locally richer conditions are present in the primary zone. High CO levels in very lean conditions are due to the low reaction rates of oxidation associated with low combustion temperatures. An increase in the equivalence ratio corresponds to higher flame temperatures, accelerating the reaction rate and allowing to complete the CO oxidation to CO_2. Over a certain equivalence ratio, the production of CO by chemical dissociation of CO_2 starts to become significant, as less oxygen is available and the equilibrium shifts toward CO.

Figure 4.9b illustrates the effect of the fuel split, showing a non-monotonic trend, with a limited impact on CO values at the considered thermal power. The overall equivalence ratio is lean for all tested configurations, but as recalled before, the diffusive pilot flames give rise to locally rich conditions, where CO oxidation remains incomplete. Starting from the fully diffusive condition (0%PMX), and increasing the premixed fuel fraction, CO emissions are slightly lower because of the enhanced mixing. Indeed, at the burner outlet a high level of premixing between fuel and oxidant is reached. A further increase in the premix fraction causes CO values to rise again. This last condition corresponds to the OH* image of Figure 4.6b where the flame is still anchored near of the pilot jets. Near the burner axis, where the premixed fuel mixture is present, the OH* intensity is quite low, and the high CO emissions measured for this case suggest that the oxidation of the premixed fuel is not completed. With further increase of the premix fuel fraction (80%PMX), CO decreases again, as the premixed fuel mass flow rate increases and the mixture which exits from the burner becomes richer, accelerating CO oxidation.

4.4 Stability limits

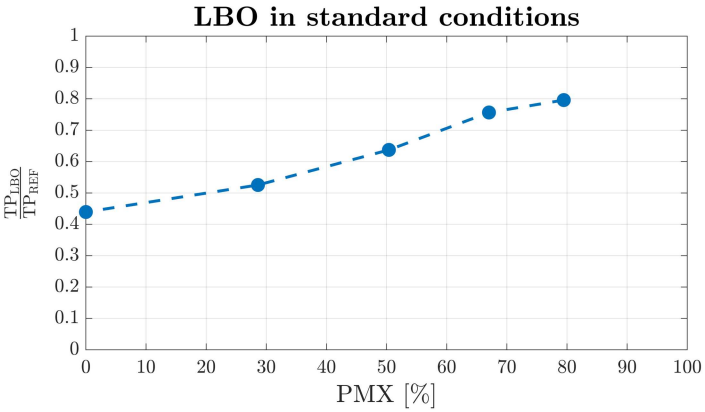

Figure 4.10: Lean blow out margin as a function of the premix split

A key factor in burner design is its ability to maintain stable combustion, which becomes even more critical in the perspective of operation with high EGR rates. In normal operation (without EGR), wider stability limits enable the combustor to operate with leaner equivalence ratio, which lowers the adiabatic flame temperature and subsequently reduces NO_x emissions.

In order to conclude the burner characterization at standard conditions, lean blow tests were conducted to establish stability limits for different fuel splits. In each case, starting from stable conditions, the fuel mass flow rate was gradually decreased while keeping constant the pressure drop across the combustion chamber and therefore the air mass flow rate, until the flame extinguished. The blow-out event was identified by observing the flame, and looking at the pressure oscillations detected with the high frequency pressor sensor, which drop sharply when blow

out is reached. The flame extinguishing is confirmed also by a sharp temperature drop recorded by the thermocouples installed in the second part of the combustion chamber, downstream of the quartz liner, but the pressure signal is more prompt. The flow conditions corresponding to the sudden fluctuation drop were recorded for the lean blow out detection. The procedure was repeated 3 times for each fuel split, showing great repeatability of the results.
Figure 4.10 shows the burner stability limits in terms of scaled thermal power at lean blow out as a function of the premix fuel split. A clear monotonic trend can be observed, with lean blow out occurring at richer conditions as the premix fuel fraction increases.
The critical role of the pilot jets in the flame stabilization process has been demonstrated by OH* chemiluminescence images in the previous section. Indeed, the flame stabilizes near the pilot jets even with high premix fuel fraction (see Fig. 4.6), closer to the outer recirculation zone, helping to stably anchor the reaction zone. Consistently, the blow out margin decreases (since the thermal power corresponding to the lean blow out event increases) with lower pilot fuel fraction and the burner moves to a more unstable condition.
Higher premix fuel fraction is beneficial for emission, because the associated enhanced mixing results in a more uniform fuel distribution, avoiding the formation of richer spots where NO_x form. However, this can negatively affect flame stability, as locally richer conditions are essential for stabilization.

4.5 Effect of hydrogen addition

Hydrogen injection has been introduced in the present study with the final purpose to allow higher levels of EGR to be stably achieved. In this first part of the work, the burner is operated in standard conditions with pure air as oxidizer, and the effect of hydrogen addition has been investigated. Positive consequences were observed in terms of improved

stability, with promising results for the ultimate aim of the study.
This section presents results obtained with hydrogen injection through the pilot line, either pure or blended with natural gas, across various fuel splits. For each condition, a comparison is made with the corresponding results obtained with pure natural gas at the same total thermal power. Typically, the hydrogen contribution is below 10% of the total thermal power. However, in specific cases, where indicated, this threshold was intentionally exceeded to investigate the behavior of pure hydrogen jets, which have a pronounced effect on flame stabilization.

4.5.1 Flame structure

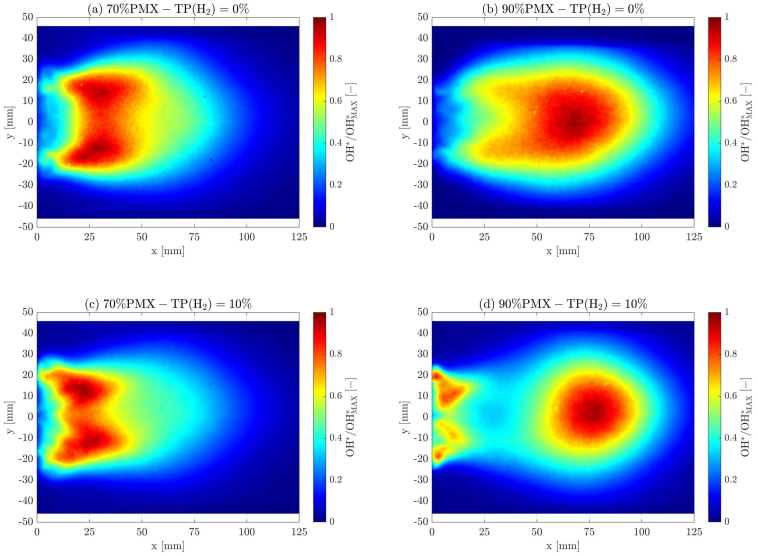

Figure 4.11: Effect of hydrogen addition on the flame structure

The effect of hydrogen addition on the flame steady structure has been studied with OH* chemiluminescence imaging. The comparison of the reaction zone with and without hydrogen addition to the pilot fuel is

presented in Figure 4.11 for two different premix splits. The first row of images shows the pure natural gas case, while the second row of images, the hydrogen fraction of the total thermal power is 10%. On the lower left (c-70%PMX), a blend of natural gas and hydrogen has been made on the pilot fuel line, while on the right (d-90%PMX), pure hydrogen is injected with the pilot jets.

Starting with the 70%PMX condition, despite the limited amount of hydrogen fraction in the total thermal power, the effect on the flame shape is clearly visible, since it constitutes a large share of the thermal power on the pilot fuel, which is responsible for the flame front definition by anchoring the combustion process, as seen above in section 4.2. The higher laminar flame speed of hydrogen takes the zone with high OH* intensity closer to the burner exit, and the flame is well attached. The reaction zone is overall shorter and its radial extension is also slightly reduced, because the pilot fuel burns immediately at the burner exit, limiting the opening of the pilot jets and giving rise to a more compact flame.

Moving to the higher premix fuel split (Fig. 4.11b-d), when pilot jets are 100% hydrogen, the variation of the flame structure is much more evident. For the case with natural gas this highly premixed condition is unstable, and the time-averaged reaction zone is very long and detached from the burner exit. This condition is associated to intense pressure oscillations, as it will be detailed in the next section, recorded as the flame is subject to intense longitudinal fluctuations. The apparent length is due to the temporal averaging of more localized instantaneous spots at different axial position. The pilot jets are detectable near the burner exit, but the main reaction zone is shifted downstream on the burner center line. For the case with hydrogen pilot jets (Fig. 4.11d), an interesting distribution appears, with two separate, clearly distinguishable reaction zones. Hydrogen jet diffusion flames are attached at the burner exit, and the premixed natural gas burns downstream on the burner axis. The two reaction zones are linked with an area with low OH* intensity, indicating a certain interaction, albeit weak.

As expected, the introduction of hydrogen seems to better anchor the flame near the dome, a behavior that may help stability in the perspective of the challenging EGR conditions. As a drawback, the burner itself and the dome are subjected to higher thermal loads, given the proximity of the flame. This aspect is aggravated and can become critical in engine conditions at high pressure, even to the point of affecting the structural integrity of the burner. Nevertheless, for the tested conditions, no damage has been detected on the burner outlet, and the dome temperature stayed within controlled and safe values.

4.5.2 Dynamic behavior

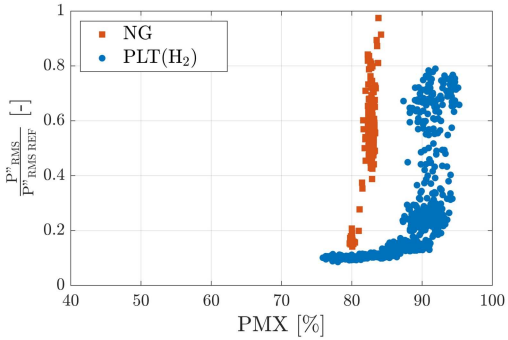

Figure 4.12: Effect of hydrogen addition on pressure oscillations amplitude at high premix fraction

One of the great advantages of doping natural gas with a small percentage of hydrogen was seen in the reduction of thermoacoustic instabilities that arise when the burner is operated with natural gas for very high premix fractions.

Figure 4.12 shows the amplitude of pressure oscillations recorded with the dynamic pressure sensor (PCB) positioned downstream of the quartz liner, as a function of premix thermal power fraction. This time, the pilot fuel line is fed with 100% hydrogen, even though the hydrogen fraction

of the total thermal power is higher than 10%, in order to investigate this particular aspect. Therefore, the hydrogen thermal power fraction coincides with the pilot thermal power fraction.
In the case without hydrogen addition, the amplitude of pressure oscillation grows suddenly and significantly as the premix fraction exceeds 80%. When hydrogen is injected with the pilot fuel line, the pressure oscillation amplitude starts to increase around 85%, and escalates only when the premix fuel fraction is more than 88%.
These results are consistent with previous studies, as recalled in the introduction, where the beneficial role of the injection of a small amount of hydrogen to reduce instabilities has been observed in simplified configurations [28–30].
The widening of the range of stable operating conditions allows safe operation at very high premix levels, with beneficial effects on NO_x emissions, as it will be detailed in the next section.

4.5.3 Pollutant emissions

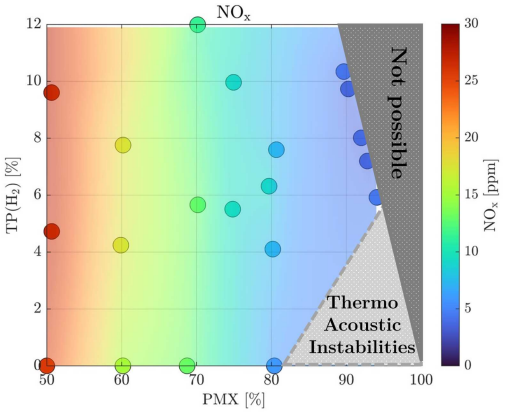

Figure 4.13: Impact of hydrogen and premix thermal power fraction on NO_x emission

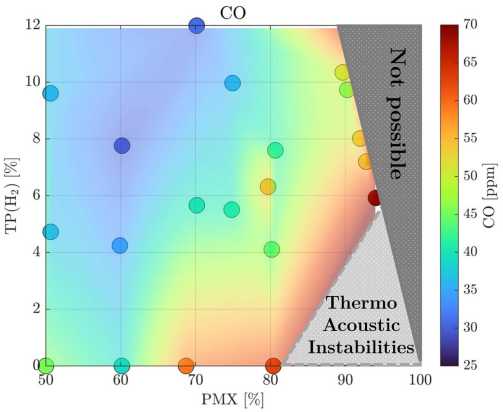

Figure 4.14: Impact of hydrogen and premix thermal power fraction on CO emission

Figure 4.13 reports NO_x as a function of both premix thermal power fraction and hydrogen fraction. No hydrogen is injected with the premix line, therefore there is a "not possible" region in top right where the sum of premix split and hydrogen exceeds 100%.
With 100% natural gas ($TP(H_2)$=0%), NO_x levels decrease linearly as the premix fuel fraction is increased, but the emergence of pressure oscillations limits this parameter variation at 80% for the investigated configuration with the burner operated in this tubular flame tube without air dilution. With hydrogen addition, it is possible to obtain very low NO_x emission thanks to a higher degree of premixing, as very low values on the right upper part of the map show. With constant premix thermal power fraction, increasing the hydrogen content only slightly increases NO_x levels, but the reduction that can be achieved by increasing premix is much greater than the increase due to a higher hydrogen fraction. It has to be kept in mind that the present application with EGR and CCS severely limits the hydrogen fraction that can be added, and this last aspect of lower carbon content is consequently restrained. The OH* chemiluminescence images presented in the previous section (Fig. 4.11) show that the reaction zone

is shorter with hydrogen addition, lowering the already reduced residence time in high temperature zones where thermal NO_x forms. This results in NO_x emissions not rising significantly even with higher hydrogen fraction. CO emissions are reported for completeness in Figure 4.14, but the effect of hydrogen injection is limited. It is hard to identify a distinct trend and values are scattered. In general, increasing the hydrogen fraction with constant premix reduces CO emissions, partly as a consequence of the lower amount of carbon in the fuel. Furthermore, when moving to high premix fractions CO values tend to rise.

4.5.4 Stability limits

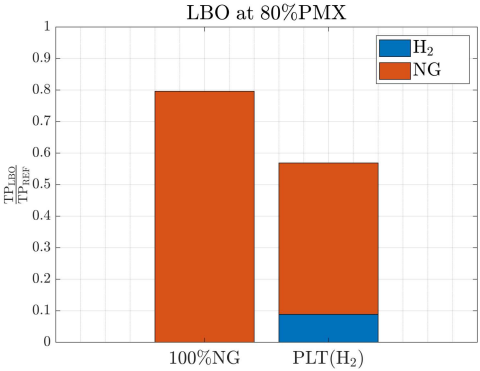

Figure 4.15: Effect of hydrogen addition on LBO margin

Since the main role of hydrogen is to improve the flame stability, lean blow out tests were repeated with hydrogen injection through the pilot line.
Only a single case was investigated, with pure hydrogen pilot jets. The hydrogen mass flow rate was kept constant, and lean blow out was approached by lowering the natural gas mass flow rate of the premix line. Therefore both premix fraction and total thermal power varied at the same time, but the purpose of such test was to investigate how much the

flame stability is improved by a small hydrogen amount. The hydrogen mass flow rate was fixed at 9% of the thermal power adopted for the rest of the investigation (TP_{REF}).

Lean blow out was reached at 80%PMX, with a total thermal power 30% lower than the case with pure natural gas with the same premix fraction. Figure 4.15 reports the comparison, emphasizing the small hydrogen thermal power fraction required. This significant improvement in the lean blow out margin is promising in the perspective of exploiting hydrogen reactivity to enhance the burner performance at high EGR rates.

Chapter 5

Impact of CO_2 addition to reproduce EGR conditions

As anticipated, from the experimental standpoint the effect of EGR is simulated through the dilution of the combustion air with CO_2, targeting a certain oxygen mass fraction Y_{O2}. While this strategy greatly simplifies the experimental setup, it requires a careful evaluation of its implications, as it does not fully replicate the complex gas composition of real dry EGR. The present chapter is dedicated to assessing the validity and limitations of the experimental approach adopted to reproduce EGR conditions at lab scale. To this end, a dedicated test campaign was carried out, including reactive tests where the combustion air was diluted with nitrogen instead of CO_2. Although N_2 addition does not replicate actual EGR composition either, it offers a useful comparison between two different diluents: one rich in CO_2 and the other rich in N_2 but free of CO_2. Additionally, a preliminary numerical study was performed to further support the experimental findings, focusing on how the different diluents affect key thermokinetic parameters. Together, the experimental and numerical analyses aim to provide a deeper understanding of the role of the diluent composition on combustion behavior under EGR-like conditions.

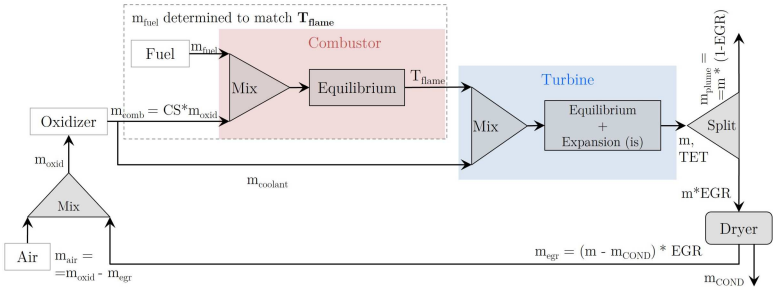

(a) Real EGR scheme

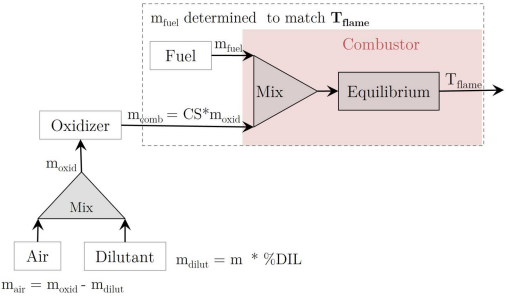

(b) CO_2/N_2 dilution

Figure 5.1: Cantera function schemes for calculating the oxidizer composition

5.1 Oxidizer composition

To realistically investigate the EGR impact on the combustion process in a gas turbine, it is crucial to compute the composition of the mixture entering the combustion chamber. This section presents the tool employed to estimate the oxidizer composition, which in the case of real EGR is not straightforward.

When EGR is implemented on a gas turbine, the inlet composition depends on the recirculating products, which are, in turn, the outcome of the combustion of an unknown mixture composition, and therefore solving

this problem requires an iterative approach. For this purpose, an in-house algorithm written in Python 3.9 with the Cantera library 2.5.1 was developed [101].

Figure 5.1 depicts the block diagrams of the algorithm developed to solve the problem and to evaluate the oxidizer composition: (a) is the scheme of dry EGR implemented on a real gas turbine, while (b) represents the experimental test rig with CO_2/N_2 dilution.

Starting with the real gas turbine plant, EGR is implemented with a closed loop, which implies an iterative solution. In gas turbines, not the entire airflow enters the combustion chamber, but part of the air is used for cooling and injected downstream. Therefore, a certain dilution rate is present between the air entering the combustion chamber and the turbine exhaust. Combustion split (CS) is defined as the ratio between the oxidizer mass flow rate entering the combustor and the total oxidizer mass flow rate, which includes cooling air for the combustor and early turbine stages, and other secondary flows.

$$CS = \frac{m_{comb}}{m_{oxid}} \tag{5.1}$$

The value is highly dependent on the turbine class and, in the case of variable/adaptive geometry, also on the operating conditions.

The combustion process is modeled by assuming adiabatic, isobaric thermochemical equilibrium (with detailed species) of the reactants and products. The function determines the composition of the overall mixture at equilibrium, given the temperature, pressure, and initial composition of the mixture.

Subsequently,the products are mixed with the oxidizer portion that did not take part in the reaction and is brought to equilibrium conditions through the introduction of an isoentropic expansion, simulating the flow thermodynamic behavior within the turbine. Most of the water content of the exhaust gas is then removed with a dryer, which considers a vapor saturation temperature of 5°C (278 K), and finally the loop is closed with the dried exhaust gas recirculated and mixed with fresh air.

The CO_2/N_2 dilution layout is much simpler, since there is no need for

an iterative approach and the mixture composition is defined a-priori by the concentration of each chemical species.
The control parameters are %EGR and $\%CO_2$ or $\%N_2$, defined respectively with the recirculated or the diluent mass flow rates over the total one.

$$\%EGR = \frac{m_{EGR}}{m_{tot}}; \quad \%CO_2 = \frac{m_{CO2}}{m_{tot}}; \quad \%N_2 = \frac{m_{N2}}{m_{tot}} \tag{5.2}$$

The two operating schemes have been used to define the composition of the mixture entering the combustion chamber. The results are presented in Figure 5.2 in terms of oxygen mass fraction as a function of the adiabatic flame temperature and the EGR level or dilution percentage.
The matching between operating conditions at lab tests with CO_2 dilution and real EGR is made by targeting both adiabatic flame temperature and oxygen inlet concentration. Setting these two parameters during the experimental tests means univocally determining the corresponding EGR rate in a gas turbine, fixed the machine class and thus the dilution rate.

5.2 Effect on thermo-kinetics parameters

Once the oxidizer composition has been computed, a preliminary comparative analysis was performed aimed at gaining a general understanding of the impact on the thermo-kinetics of the combustion process. In particular, the key parameters chosen for the study are the Laminar Flame Speed (LFS) and the extinction strain rate (ESR), which have been considered critical as the primary effect of EGR is an overall reduction of reactivity. The investigated conditions are, as before, real EGR implemented on a gas turbine, compared with CO_2 and N_2 dilution cases.

5.2.1 Numerical set-up

For the present work, numerical tools have been exploited for some additional insights, with the purpose to support the experimental campaign. Cantera [102] has been employed as a powerful means for some additional

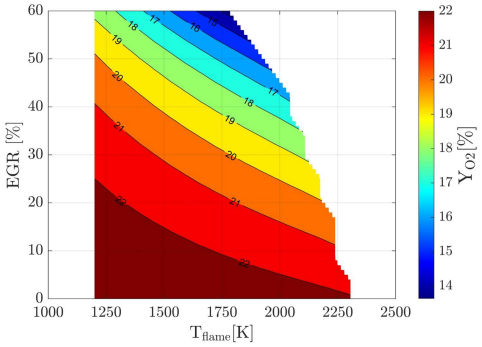

(a) Real EGR

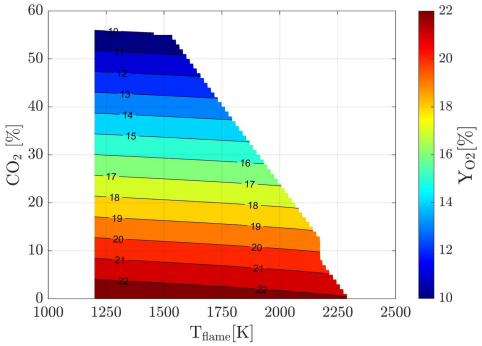

(b) CO_2 dilution

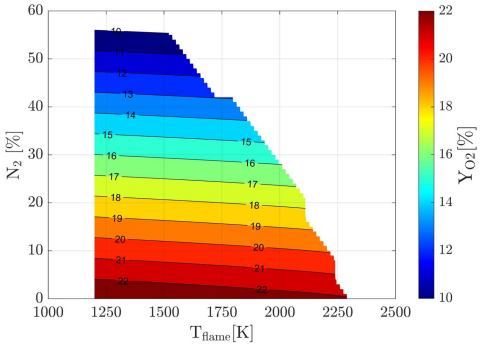

(c) N_2 dilution

Figure 5.2: Contour maps of the oxygen mass fraction in the fresh mixture for real EGR compared to approximated EGR as tested in the laboratory

	EGR		**CO_2**		**N_2**	
$\%Y_{O2}$	**$\%Y_{N2}$**	**$\%Y_{CO2}$**	**$\%Y_{N2}$**	**$\%Y_{CO2}$**	**$\%Y_{N2}$**	**$\%Y_{CO2}$**
23.3	76.7	0.0	76.7	0.0	76.7	0.0
20.0	79.7	0.3	66.4	13.6	80.0	0.0
18.7	79.5	1.8	62.4	18.9	81.3	0.0
17.7	79.7	2.6	59.1	23.2	82.3	0.0
16.6	80.1	3.3	55.5	28.0	83.4	0.0

Table 5.1: Oxidizer composition for real EGR, CO_2 and N_2 dilution

insights, but this aspect is not the main focus of the investigation. For this reason, only the key points will be discussed from a theoretical point of view.
As for the definition of the oxidizer composition reported in the previous section, pure methane is employed as fuel and detailed GRI 3.0 [103] is used as reaction mechanism. A freely propagating 1D premixed flame from the FreeFlame class in Cantera has been solved to estimate the laminar flame speed and adiabatic flame temperature. The CounterflowDiffusionFlame function has been used for the extinction strain rate, computing the highest strain rate value at which the combustion of oxidizer and fuel jets in counterflow configuration can be sustained before undergoing extinction. For all analyses, the oxidizer composition was computed with the procedure shown in the previous section.

5.2.2 Operating conditions

The analysis has been made targeting the same operating conditions that have been tested experimentally (see section 5.3).
The comparison between real EGR, CO_2 dilution and N_2 dilution cases is made matching the same inlet oxygen level, which has been selected as the main control parameter. Table 5.1 reports the oxidizer composition for the three cases, computed with the Cantera script described in the previous section. Real EGR has an intermediate composition between the other two cases, with non negligible CO_2 content, but much less than the

CO_2 dilution case.

The fuel and oxidizer mass flow rates have been kept constant (and therefore the total thermal power). Different oxygen levels have been tested, starting from $Y_{O2} = 23.2\%$ for standard air and decreasing this parameter in order to simulate higher EGR rates. Operating pressure and inlet temperature are the same as for the experiments, i.e ambient pressure and 300°C (573 K) respectively.
With constant fuel and oxidizer mass flow rates, the change in the oxidizer composition affects the adiabatic flame temperatures. The choice of keeping the thermal power constant instead of fixing T_{flame} relates to the experimental requirements of the test procedure, and the numerical analysis was therefore done under the same conditions. In particular, Figure 5.3 reports the variation of the adiabatic flame temperature for the 3 different cases as a function of the inlet oxygen mass fraction. All curves show a decreasing trend moving from standard air to lower oxygen levels, with lower values corresponding to the CO_2 dilution case, because of the high heat capacity of CO_2 with respect to nitrogen mixtures.

5.2.3 Results

Figure 5.4 reports the results of these analyses for the laminar flame speed and extinction strain rate, as a function of the inlet oxygen mass fraction.
The laminar flame speed decreases with lower inlet oxygen content moving to higher EGR rates. With CO_2 dilution, the laminar flame speed is lower with respect to real EGR and N_2 dilution, with increasing difference as the inlet oxygen content decreases. Real EGR has an intermediate composition between CO_2 and N_2 dilution cases, and indeed, the corresponding laminar flame speed curve lies between the other two, closer to pure nitrogen.

The Damköhler number (Da) is a dimensionless parameter that compares the relative importance of chemical reaction rates to transport

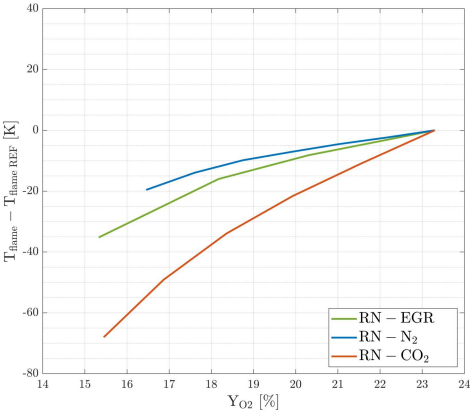

Figure 5.3: Adiabatic flame temperature with constant thermal power as a function of the inlet oxygen fraction

processes, such as flow and mixing, in combustion systems. It is defined as the ratio of the characteristic flow time (τ_{flow}) to the reaction time (τ_{reaction}):

$$\text{Da} = \frac{\tau_{\text{flow}}}{\tau_{\text{reaction}}} \tag{5.3}$$

It is used to determine whether a combustion process is controlled by reaction kinetics or by transport limitations. When $\text{Da} \gg 1$, chemical reactions occur much faster than the transport processes, leading to a flame-dominated regime where combustion is governed primarily by the availability of reactants, leading to a thin reaction zone. When $\text{Da} \ll 1$, mixing limits the combustion process, with the reaction rate controlled by how quickly reactants are transported together, as seen in diffusion flames. For $\text{Da} \approx 1$, both reaction kinetics and mixing play significant roles, resulting in complex, partially mixed conditions often observed in turbulent combustion.

Considering in first approximation that turbulence remains unaltered, the lower laminar flame velocity of the CO_2 dilution case leads to lower

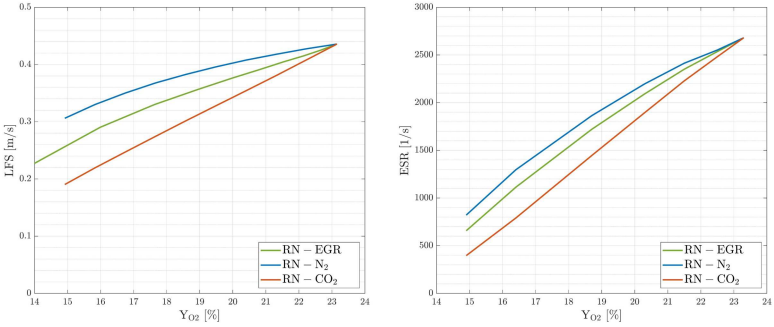

(a) Laminar flame speed *(b) Extinction strain rate*

Figure 5.4: LFS and ESR with constant thermal power as a function of the inlet oxygen fraction

Damköhler numbers, thus moving toward diffuse combustion regimes, with a thickening of the flame front [104].
Similarly, the extinction strain rate follows the same trend: it decreases with lower inlet oxygen fraction, and with CO_2 dilution flame extinction is reached for lower values of the strain rate, thus indicating a reduced combustion stability. Therefore, CO_2 dilution creates more challenging conditions for flame stability compared to N_2 dilution or real EGR, with the latter that again results in an intermediate condition.

5.3 Comparison of CO_2/N_2 dilution: experimental results

In order to evaluate experimentally the effect of replacing real EGR with CO_2 dilution, reactive tests have been performed also with nitrogen addition instead of CO_2. The comparison is made by matching different values of inlet oxygen mass fraction, diluting the combustion air with CO_2 or N_2. Total thermal power and oxidizer mass flow rates have been kept constant, as well as the the premix fuel split, set equal to 40%PMX. The oxidizer composition of the tested points is reported in Table 5.1,

together also with the corresponding case with real EGR.
This part of the discussion is focused on the differences between CO_2 and N_2 dilution to simulate EGR. Further and more detailed consideration on the effects of simulated EGR conditions on the flame behavior will be discussed in the next chapter.

5.3.1 Flame structure

Starting with the comparison in terms of steady flame structure, Figure 5.5 and Figure 5.6 show OH* chemiluminescence time averaged maps, with absolute and normalized values respectively.

With standard air as oxidizer at this fuel split (40%PMX), the flame root is well attached to the burner outlet. The reaction zone structure changes substantially when the oxygen level decreases, moving downstream and becoming widespread.
Considering first the maps with absolute intensity of Figure 5.5, a significant reduction of the OH* emission can be observed as the inlet oxygen content decreases. The reduction in the detected emission is more pronounced with CO_2 dilution than for the N_2 case. The lower adiabatic flame temperature of CO_2 dilution (see Fig 5.3) could contribute to reduced OH* signal, that is also possibly linked with the increase in optical absorption by the reactive mixture due to higher CO_2 content [90, 91]. Indeed, a lower emission value is detected with the intensified camera in the case of CO_2 dilution as a consequence of the higher absorption of mixtures with high CO_2 content, which have lower optical transmissivity.
In simulated EGR conditions both with CO_2 or N_2 dilution, the reaction zone shifts downstream and the flame lifts off more and more as the inlet oxygen content decreases. Indeed, the previous section showed how the extinction strain rate that the flame is able to resist decreases with lower oxygen content in the oxidizer. Therefore, in EGR-like conditions the flame is not able to anchor near the burner exit, where the jet velocity is high, and consequently the local strain as well, and the reaction zone shifts downstream.

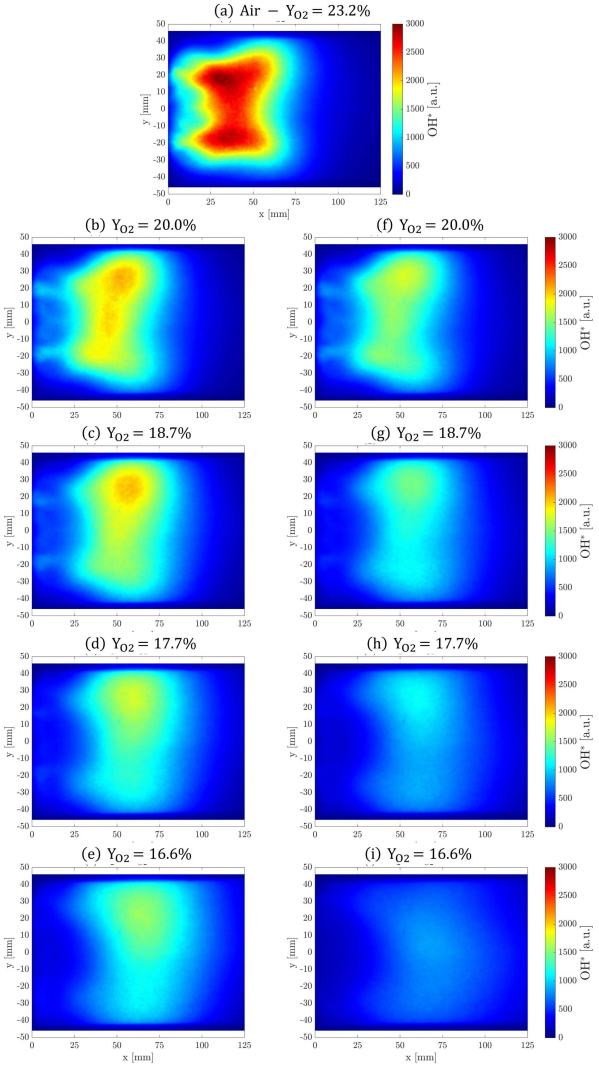

Figure 5.5: OH chemiluminescence at 40%PMX-100%NG, with different oxygen levels for N_2 (left) and CO_2 dilution (right)*

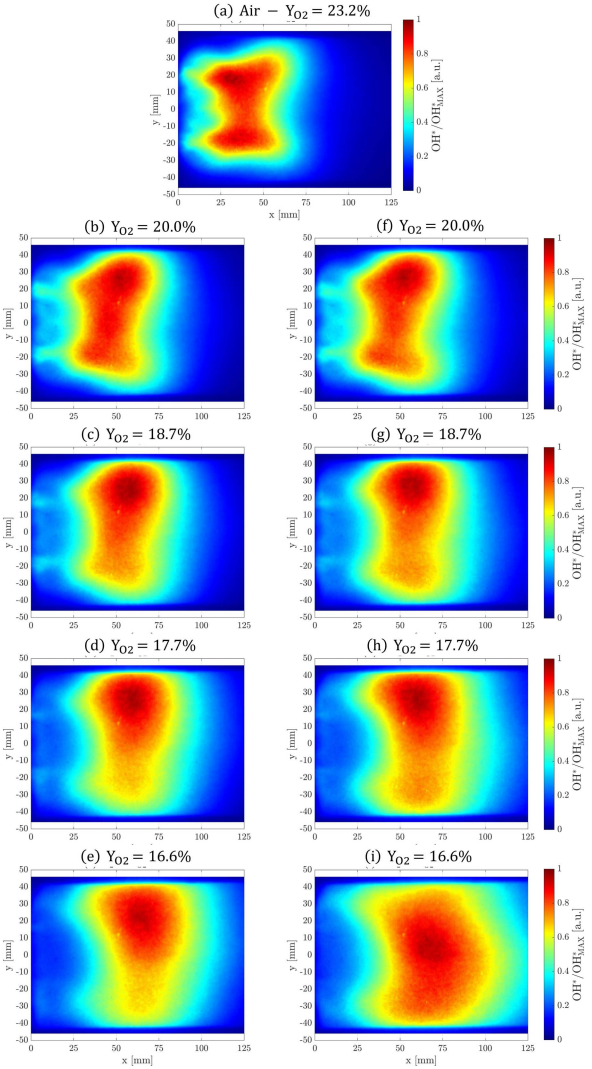

Figure 5.6: Normalized OH chemiluminescence at 40%PMX-100%NG, with different oxygen levels for N_2(left) and CO_2 dilution (right)*

A certain asymmetry of the reaction zone is observed, with the peak intensity located in the upper part of the images (line-of-sight), only slightly under standard conditions, and even more so with EGR. This is due a certain asymmetry of the pilot jets, more pronounced at this fuel split, combined with a not perfectly symmetrical flow field due to the burner manufacturing process.
The overall position of the reaction zone is almost the same for the two cases, as shown by the normalized images of Figure 5.7. The axial profiles of normalized OH* chemiluminescence have been extracted to offer a quantitative evaluation, averaging the intensity over the whole combustion chamber radius. The results are shown in Figure 5.7, confirming the trend observed from the 2D maps. The OH* peak shifts downstream as the inlet oxygen level decreases, and the corresponding position is the same for CO_2 and N_2 dilution cases at the same oxygen level.

Lowering the inlet oxygen content has also the additional effect of increasing the extension of the reaction zone, making it more diffuse. This behavior is more pronounced for the CO_2 case, as qualitatively shown by the normalized images of Figure 5.6, and more accurately in the corresponding axial profiles of Figure 5.7. Profiles are overlapping until the maximum is reached, except for the case at Y_{O2}=16.6%, and then the downstream decrease is more gradual for the case with CO_2 dilution. The thermo-kinetics study presented in the previous section showed how the laminar flame speed decreases as the oxygen fraction in the oxidizer decreases. Indeed, the reaction process with higher dilution moves toward diffuse combustion regimes. Although the presented distributions are the result of a temporal average, they highlight a decrease in OH* intensity and a broader extension of the reaction zone, confirming this behavior. A greater extension could also result from temporal oscillations of a thinner flame front; nevertheless, it is indicative of large spatial fluctuations of the flame front position, with the flame undergoing significant oscillations, as it will be highlighted with instantaneous images in the next chapter. The effect is enhanced for the CO_2 case, which has lower laminar flame speed

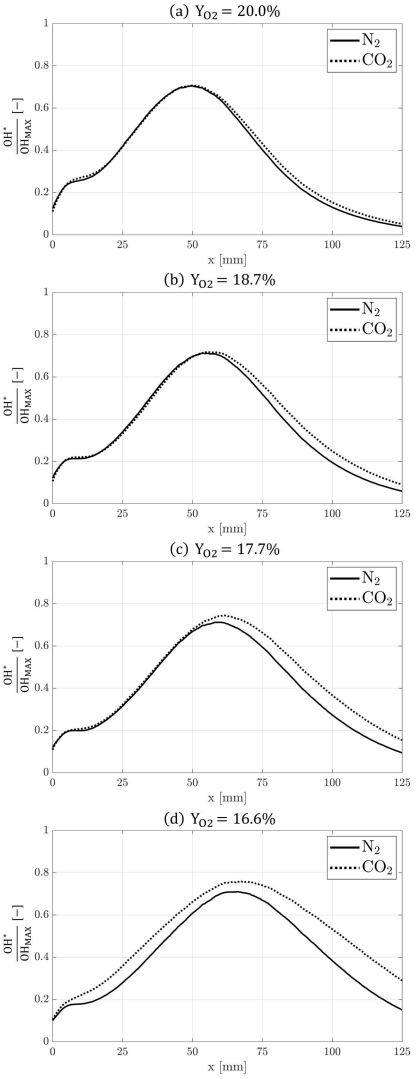

Figure 5.7: Axial profiles of radially averaged normalized OH intensity at 40%PMX-100%NG, with different oxygen levels*

at the same oxygen level than N_2 dilution. This explains the longer axial extent of the reaction zone for the CO_2 dilution case that can be observed in the normalized maps and radially averaged profiles. Differences are amplified as the inlet oxygen fraction decreases, since the discrepancy of both ESR and LFS between the two cases grows, reaching a condition where the diffuse flame covers almost the entire camera field of view (case e).

5.3.2 Pollutant emissions

During the reactive tests with CO_2 and N_2 dilution, pollutant emissions were measured, in order to assess the impact of the oxidizer composition on CO and NO_x levels. Figure 5.8 shows the results obtained for the conditions described at the beginning of this section with the mixture composition reported in Table 5.1 (CO_2 and N_2 cases).

CO emissions have an exponential trend as the inlet oxygen level decreases, but with N_2 dilution values are significantly lower than with CO_2. Recalling the chemiluminescence images of Figure 5.6, part of the CO increase with lower inlet oxygen level could also be linked with the downstream shift of the reaction zone, which doesn't allow the reaction to be completed at the probe location. The dilution strategy does not affect this aspect, as the position of the reaction zone is substantially the same between CO_2 and N_2 dilution. Therefore, higher CO levels with CO_2 dilution are not linked to the probe positioning, but probably are linked to CO_2 dissociation due to chemical equilibrium effects. Further insights on this aspect will be given in the last part of this chapter, with the support of numerical tools.
Figure 5.9 reports the relative increase in CO emissions for the two cases, obtained scaling the measured values with the following expression:

$$\Delta CO_{scaled} = \frac{CO - CO_{min}}{CO_{max} - CO_{min}} \tag{5.4}$$

It is interesting to note that the relative increase is the same for the two cases, and the values follow an exponential trend with inlet oxygen

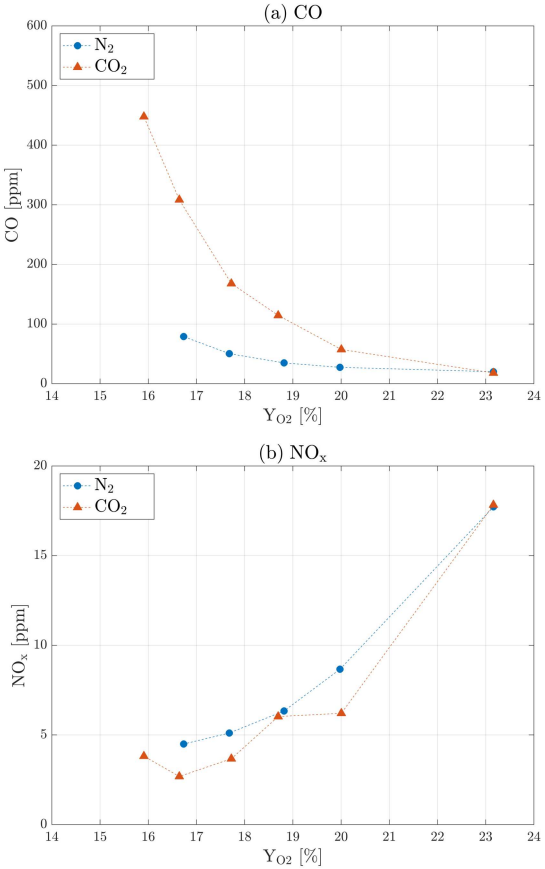

Figure 5.8: Pollutant emissions with 40%PMX and 100%NG as a function of the inlet oxygen fraction

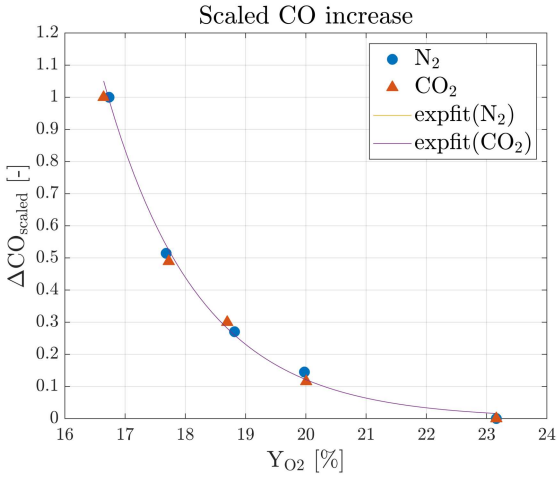

Figure 5.9: Scaled CO values at 40%PMX-100%NG for N_2 and CO_2 dilution

content. Interpolating curves have been evaluated for the experimental data, reported with solid lines in Figure 5.9, expressed as:

$$\Delta CO_{scaled} = A \cdot e^{B \cdot Y_{O2}} \tag{5.5}$$

Fitting models for the two cases practically coincide, with the same exponential coefficient $B = -0.6$. The constants A are slightly different, equal to 4.7e+04 for N_2 dilution and 3.4e+04 for CO_2 dilution.

By comparing the two cases, this simplified approach can be used to perform an approximate estimate of the CO produced from dissociation of the CO_2 present in the oxidizer, assuming that the observed difference is solely due to this effect. This allows to scale the results gained in CO_2 vitiated conditions, taking into account the CO contribution due to the CO_2 concentration.

When EGR is implemented on a gas turbine, the CO_2 concentration in the oxidizer varies with the operating conditions. Therefore, a correction expression requires resorting to iterative cycles, such as those used to

estimate the oxidant composition (see section 5.1). For this reason, the results presented in this work have not been scaled with this approach, not to further complicate the discussion of the results. While intended as a general indicator rather than a scaling factor, this estimate is crucial in shedding light on the consequences of the oxidizer composition in simulating EGR conditions. Similar considerations will be presented in the final section of this chapter, utilizing more advanced numerical tools based on chemical kinetics, complementing these results.
Moving to the NO_x emissions (Fig. 5.8b), a significant reduction can be observed as the inlet oxygen level decreases for both dilution strategies. Indeed, as the reaction zone becomes widespread and the combustion process moves toward the diffuse regime, hot rich spots where NO_x formation is high are suppressed.
Slightly higher values are recorded with N_2 dilution, which could be linked to both equilibrium effects due to the higher nitrogen concentration, and also to the higher adiabatic flame temperature, reported in Figure 5.3.

5.3.3 Dynamic behavior

During the reactive tests, strong tonal pressure oscillations were detected when the inlet oxygen content decreases from standard air conditions. Figure 5.10 reports the RMS of the amplitude of pressure oscillations measured with the PCB sensor (acquisition frequency 12.8 kHz) for the two dilution strategies, with increasing EGR going from right to left of the plot. As the inlet oxygen concentration diminishes, the amplitude of these oscillations quickly grows, reaches a maximum, and eventually decreases.
Values for both diluents are similar as long as the inlet oxygen content is higher than 19%. Below this value, with N_2 dilution the amplitude of pressure oscillations continues to increase, reaching a maximum around Y_{O2}=18%, and then decreases. With CO_2 dilution, the maximum amplitude is lower and is found for higher values of inlet oxygen content, leading to a more stable behavior for this condition. The lower laminar flame speed of the CO_2 dilution case reported in section 5.2 could be a

possible explanation, as the more distributed flame partially dampens the oscillations. A detailed study on the influence of the oxidizer composition on the dynamic flame response was performed by Rodriguez Camacho et al. [23], indicating that at extremely low oxygen levels not only the lack of oxygen but also the exact chemical composition affects the results, coherently to what observed in the present study.
Further considerations about the non-monotonic trend of pressure amplitude with inlet oxygen fraction and on the detected frequency spectrum will be done in the next section, where the dynamic behavior of the burner with CO_2 dilution is described in more detail.
Figure 5.11 reports the frequency spectrum of these pressure oscillations measured at the oxygen levels corresponding to the peaks' amplitude of Figure 5.10, and a third case with equal oxygen content. The spectrum is shown up to 600 Hz to highlight frequency variations, without losing significant information, as no peaks are detected at higher frequencies. All spectra exhibit a well-defined peak, except for case N_2-Y_{O2}=18.7%, where two adjacent peaks are visible. The peak frequency is around 300 Hz, corresponding to the resonance frequency of the test rig, observed also in other conditions with different burners. The exact peak frequency decreases with lower oxygen inlet content, and a first estimation suggests that this trend corresponds to changes in mixture composition and, consequently, in thermodynamic properties such as speed of sound.

5.4 Reactor network for emission estimation

The pollutant emissions measured during reactive tests have been exploited to tune and validate a reactor network. The purpose of this task is to provide an estimation of NO_x and CO levels when the oxidizer composition is the one obtained when EGR is implemented on a gas turbine. Experimental data have been collected for the CO_2 and N_2 dilution cases, but once the reactor network has been tuned for such conditions, it can be leveraged to explore intermediate oxidizer composition, and therefore

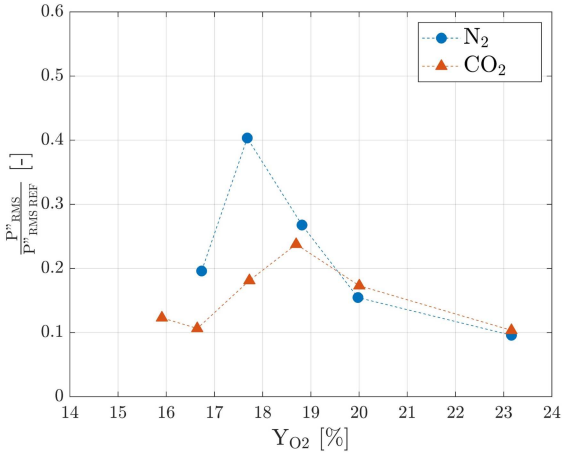

Figure 5.10: Impact of dilution species on the amplitude of pressure oscillations

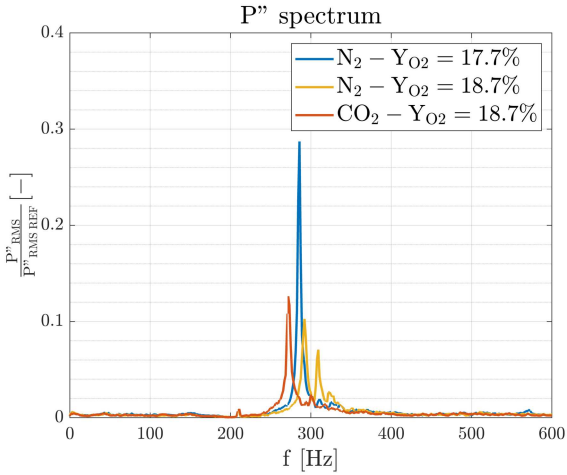

Figure 5.11: Frequency spectrum of pressure oscillations

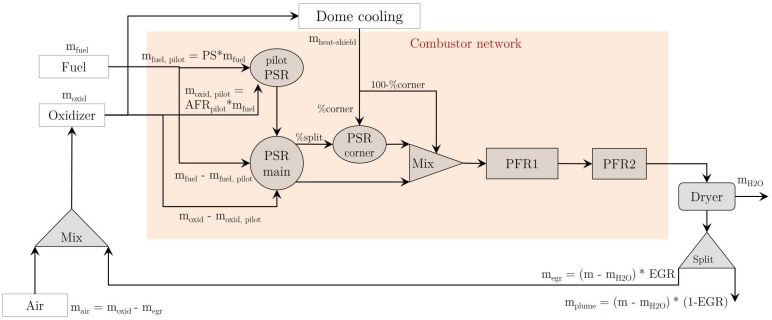

Figure 5.12: Schematic of reactor network layout for the real EGR case

the real EGR case.

5.4.1 Reactor network scheme and operating conditions

The structure adopted for the construction of the reactor network is derived from previous work carried out within the research group and not published for proprietary reasons. A detailed description of how this structure was obtained is beyond the scope of this investigation, which merely exploits this tool to explain some phenomena encountered in experimental tests.

Figure 5.12 shows the reactor network layout embedded in the EGR scheme. The combustion chamber is represented by the components inside the orange rectangle. As reported for the definition of the oxidizer composition in section 5.1, the dilution cases do not need for the closed loop.

Three distinct Perfectly Stirred Reactors (PSRs) were implemented to represent the main flame, pilot flames, and corner regions of the combustor respectively, and two Plug Flow Reactors (PFRs) were utilized to model the downstream zone.

Briefly, the PSR has zero-dimensional geometry, and assuming that the reactants undergo perfect and instantaneous mixing, it is possible to describe the evolution of the process only with reaction kinetics, without the

need to analyze transport phenomena. It is equivalent to the assumption of Da $\ll 1$.
The PFR reactor assumes 1D geometry, meaning that within the system a mean motion is realized in a given direction along which no back-mixing or diffusive transport mechanisms happen, and uniform conditions are present at each section.
The tuning parameters are the residence time for both the PSR and the the PFR. Tuning with experimental data has been done with a trial and error procedure. A possible improvement for future work is the use of an optimization algorithm, but the limited amount of data for the results presented did not require the automatization of the process.
The experimental conditions were targeted initially to calibrate the reactor network, reproducing the tested oxidizer composition obtained with CO_2 and N_2 dilution. After the reactor network was tuned for such conditions, the case of EGR was simulated, with the oxidizer composition computed with the procedure shown in section 5.1. Additionally, a different approach was adopted to simulate the CO_2 dilution case, considering the CO_2 at the inlet as inert. This was done by creating a new chemical species with the same transport and physical properties as CO_2, but chemically inert.

5.4.2 Results of the reactor modeling

Figure 5.13 reports results of the reactor network for CO and NO_x emissions.
Starting with CO, the model is calibrated to catch the two different exponential trends of the experimental data, with values close to the measured ones. When the oxidizer composition reproduces real EGR conditions, CO values are much closer to the N_2 dilution case, as the CO_2 fraction in the fresh mixture is quite low, as shown in Table 5.1. The purpose of these results is not to predict emissions in a generic case using a network of reactors, as this would require specific tuning based on factors such as flame type and combustion chamber geometry. Instead, the main goal is to understand the effect of oxidizer composition on emissions, particularly the behavior under real EGR conditions. The

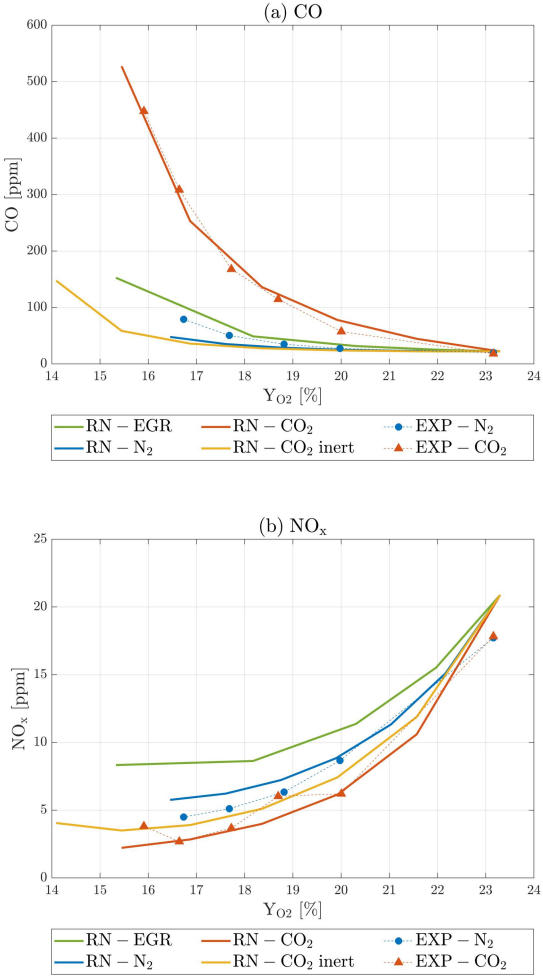

Figure 5.13: Pollutant emissions computed with the reactor network (RN) and measured experimentally (EXP) with 40%PMX and 100%NG as a function of the inlet oxygen fraction

main outcome of the analysis is that if the inlet CO_2 is considered inert, CO values drop dramatically, reaching the N_2 dilution case. This confirms the hypothesis that most of the CO is generated by the dissociation of CO_2 that is injected to lower the oxygen content in the oxidizer. The thermal effect due to higher CO_2 heat capacity has very little impact, and very high CO levels are due to equilibrium effects for high CO_2 concentration. As highlighted by the literature studies discussed in section 1.3, the dissociation of CO_2 has a significant impact on the measured emissions. The temperatures reached in the combustion chamber under these conditions are characteristic of a reactive process, but remain lower than the values that would be achieved with a higher oxygen content, which would lead to much higher NO_x levels than those observed. Therefore, the reduced oxygen concentration helps, to some extent, to limit CO_2 dissociation, which increases with temperature [52]. Nevertheless, due to the very high CO_2 concentrations in the inlet flow, the dissociation phenomenon remains important and cannot be neglected. These results indicate that testing with CO_2 to reproduce the lower oxygen content caused by EGR has a considerable impact on the measured CO emissions. Nevertheless, it can be considered a very conservative approach for a preliminary screening.

Regarding NO_x emissions, the exponential decay with lower oxygen content is correctly captured. Slightly higher values are registered in the case of N_2 dilution, that could be linked with both the higher adiabatic flame temperature, recalling Figure 5.3, but also to equilibrium effects because of the high N_2 concentration. Considering the inlet CO_2 as inert does not significantly affect NO_x emission, as CO_2 does not participate in NO_x formation paths. In this case, contrary to CO levels, the real EGR case presents the highest values. This happens because once NO_x is present in the exhaust it is recirculated to the inlet of the turbine, while this does not occur for the dilution cases, where the cycle closure is not implemented.

5.5 Concluding remarks

This chapter presented a study on the effects of the experimental strategy used to reproduce EGR conditions at lab scale, which is the addition of CO_2 to the combustion air flow in order to lower the oxygen content. This leads to significantly higher CO_2 content in the oxidizer than real, affecting the combustion process from different perspectives.
The first step of the analysis was the computation of the oxidizer composition when EGR is implemented on a real gas turbine, which depends on multiple factors. The inlet oxygen fraction was selected as the analogy parameter for the correspondence between the conditions simulated in the experimental campaign and real EGR. Numerical tools were exploited to investigate the effect of the oxidizer composition on the laminar flame speed and extinction strain rate, revealing that CO_2 dilution creates more challenging conditions for flame stability compared to real EGR.
Experimental tests were performed with a different approach to lower the oxygen content, diluting the combustion air with N_2 instead of CO_2 in order to compare the flame behavior. While the differences in terms of flame structure were limited, a dramatic impact is observed on CO emissions. With the support of numerical tools, it was possible to reveal that high CO levels are primarily generated by the dissociation of the CO_2 present in the oxidizer flow feeding the burner.
As far as emissions are concerned, testing with CO_2 dilution turned out to be a conservative strategy, but that is not the case for the dynamic behavior. For the investigated conditions, CO_2 dilution led to overall more stable conditions in terms of pressure oscillations. Stronger fluctuations arise in the case of N_2 dilution, the dependency of the oscillation amplitude from the inlet oxygen level follows a similar trend. While it is possible to roughly estimate the dependence of CO emissions on the oxidizer composition, the complexity of the dynamic behavior of the flame makes prediction very difficult under conditions other than those tested. Overall, the choice of using CO_2 dilution for conducting experimental tests, while not rigorous, can be considered a conservative and precau-

tionary approach, especially when CO emissions are concerned. The gain in terms of storage management compared to nitrogen mixtures indeed allows to explore a large number of operational points, which would otherwise require much more testing time. In the perspective of a general preliminary screening, where different burner configurations and various solutions to improve flame stability are analyzed under the same conditions, it is possible to perform relative comparisons. The derived results are still transferrable to technical cases, but it is fundamental to take into account all observed aspects in future works aiming to reproduce EGR conditions more faithfully.

Chapter 6

Effect of simulated EGR

Once the consequences of CO_2 dilution on the experimental results have been assessed, the burner characterization at simulated EGR conditions relying on CO_2 dilution has been carried out, with the results shown in this chapter. Starting with the burner fueled only with natural gas, the aim of this part of the work is to identify critical issues and understand the potential modification needed to operate in such challenging conditions. The presentation of the results starts with the variations in the velocity field and flame structure due to EGR conditions, followed by the effect on pollutant emissions. High CO emissions are one of the main drawbacks of EGR, which is why it becomes a key performance parameter. A section on the dynamic behavior is presented next, as this aspect also proved to be demanding in oxygen-depleted environment.
The main novelty of this work is the introduction of a small amount of hydrogen to improve flame stability under the challenging conditions created by EGR. Before modifying the burner architecture in order to change the fuel distribution in the primary zone, the effect of hydrogen injection has been investigated on the baseline burner configuration. The final part of this chapter covers this topic, studying the impact of addition of hydrogen to the pilot fuel line in simulated EGR conditions. Overall, as the following results will show, positive effects have been observed, and

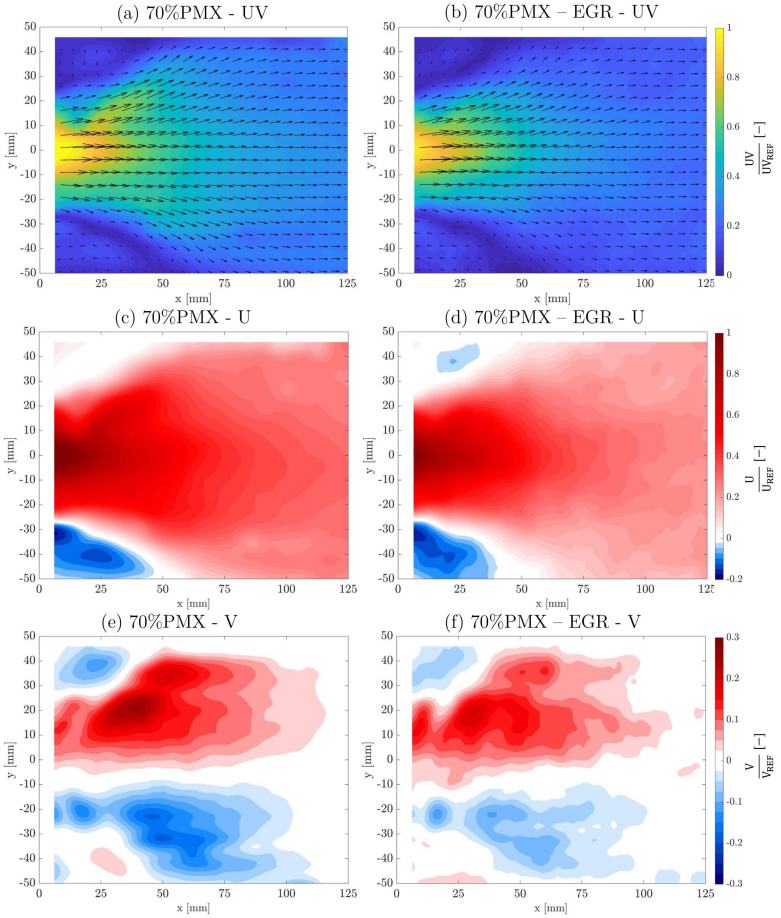

Figure 6.1: Time-averaged velocity field at 70%PMX in standard conditions (a-d-e) and with simulated EGR Y_{O2}=18.5% (b-d-f)

hydrogen has proven to be beneficial in mitigating EGR consequences.

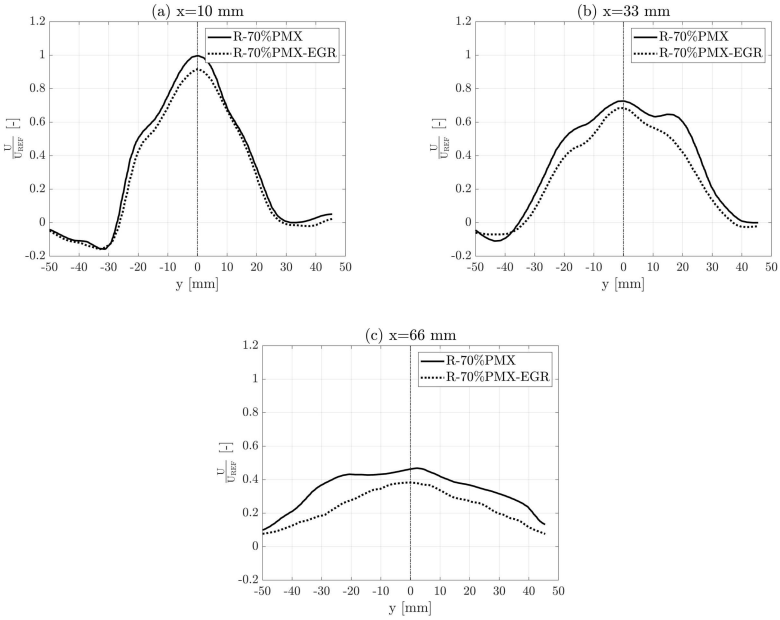

Figure 6.2: Radial profiles of axial velocity U with 70%PMX

6.1 Flow field and flame structure

Following the approach that was used for the burner characterization in standard conditions, the discussion starts from the analysis of the flow field. Figure 6.1 reports the velocity field measured with simulated EGR, compared with the corresponding case with standard air as oxidizer at the same fuel split. Tests were performed keeping the total oxidant mass flow rate constant, leading to a small decrease in the burner pressure drop for the case with CO_2 dilution.

Simulated EGR has a limited effect on the velocity-field, and only minor differences can be identified. The flow field structure maintains the jet configuration, with the same shape in terms of jet opening and size of the outer recirculation zone. Only a slight reduction in the radial velocity com-

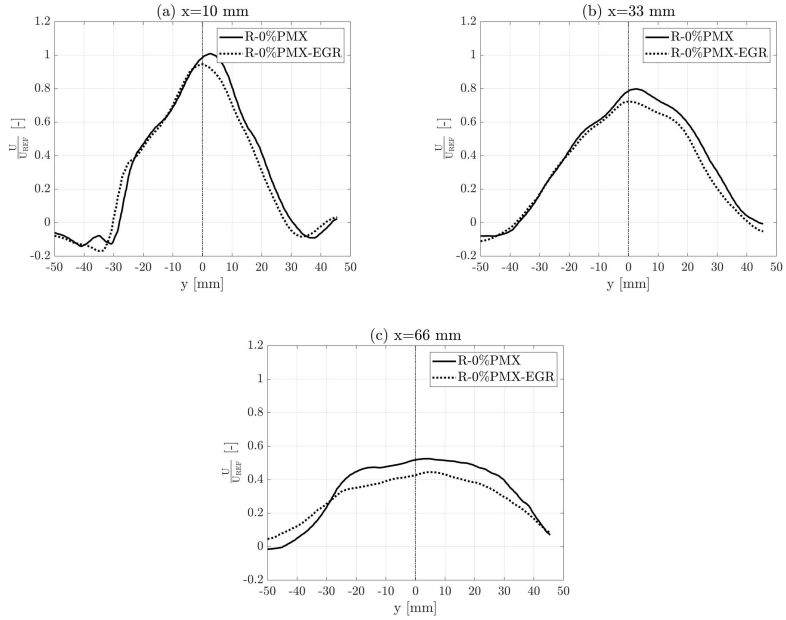

Figure 6.3: Radial profiles of axial velocity U with 0%PMX

ponents is recorded with simulated EGR, and lower velocity magnitude in the downstream region. The latter is linked to small variations in the burner pressure drop, but also to the changes in flow density due to the different combustion process that is established with lower oxygen content.

PIV measurements in simulated EGR conditions have also been performed also for the fully diffusive case. Velocity maps are not reported because also in this case the differences arising from EGR are minimal. For a quantitative evaluation of the effect of simulated EGR on the reactive flow field radial profiles of axial velocity are presented in Figures 6.3-6.2 for both fuel splits. The profiles confirm the slightly lower velocity for the cases with simulated EGR, with increasing difference moving downstream.

Overall, the flow pattern inside the combustion chamber is not substantially affected by the different oxidizer composition due to the introduction of EGR-like conditions. On the other hand, the results reported in the previous chapter showed that the structure of the reaction zone changes dramatically (see section 4.2). A different flame stabilization mechanism is therefore established in EGR conditions. In order to investigate this aspect, Figure 6.4 shows the reactive flowfield (lower half of the images) and the inverse Abel transform of OH* chemiluminescence (upper half), analogously to what was shown in Figure 4.6 with standard air.
As anticipated in the previous chapter, in EGR-like conditions the time averaged reaction zone shifts downstream and becomes widespread. These effects are linked to the decrease in both the extinction strain rate and laminar flame speed that occurs lowering the inlet oxygen content. Indeed, the flame stabilizes in a region where the local flow velocity is lower, for both fuel splits. For the 0%PMX case, the whole fuel mass flow rate is injected with the pilot jets, which are oriented in the outward direction, and indeed, the OH* peak is located near the liner walls. With 70%PMX, the maximum OH* emission is recorded along the burner axis, as the major share of natural gas is premixed with the central air jet coming out of the converging duct. The pilot jets in any case promote stabilization by anchoring the flame, in the vicinity of the boundary of the outer recirculation zone, where mixing is enhanced by the jet shear layer. In the fully diffusive case, the pilot jet velocity is very high, leading to higher jet penetration and higher local strain. As a consequence, the flame anchoring point is located at larger distance from the burner exit than in the premixed case. This also happens with standard air as oxidizer, but the effect is amplified in EGR conditions as the flame is less capable to resist extinction and becomes more sensitive. Contrary to what happens in standard conditions, with simulated EGR the time averaged flame length is increased with higher premix fuel fraction. An apparent longer OH* distribution might be produced by a spatially fluctuating narrow distribution; nevertheless, this indicates that with higher premixing level, spatial oscillations are more

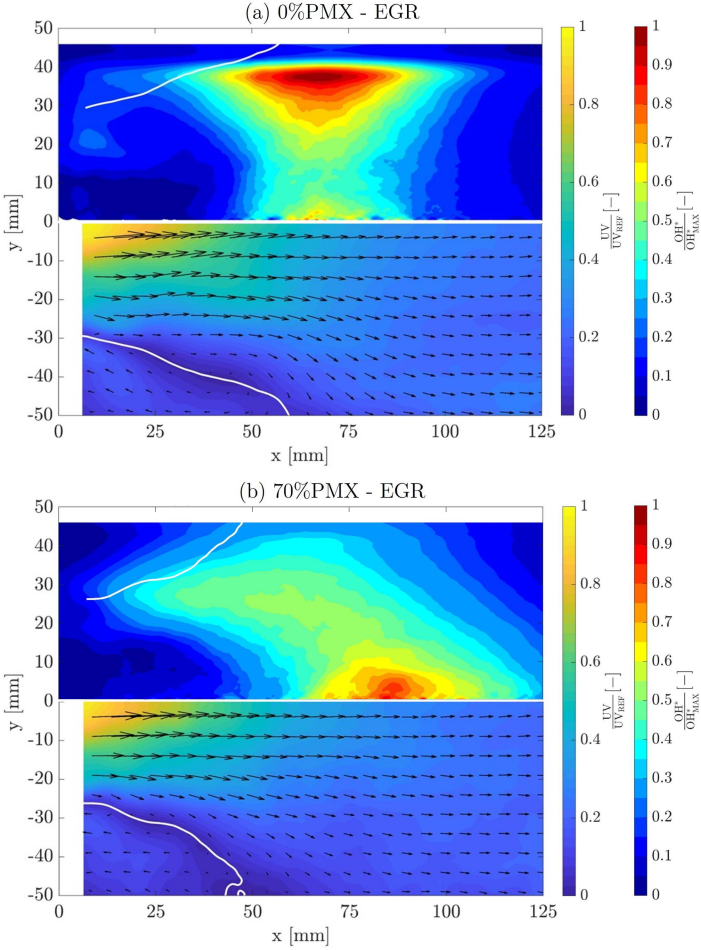

Figure 6.4: Inverse Abel of normalized time averaged OH chemiluminescence images (upper half) and time averaged UV velocity magnitude (lower half) for 0%PMX (a) and 70%PMX (b) with simulated EGR (Y_{O2}=18.5%). White lines correspond to UV=0 isolines*

pronounced, whereas with a higher pilot contribution, the reaction zone is more stably anchored. The diffusive flame seems therefore less affected by the decrease in laminar flame speed caused by the lower oxygen content.

Different EGR levels are shown in the line-of-sight OH* images of Figures 6.5-6.6, with decreasing inlet oxygen content moving from top to bottom.
Looking at the absolute OH* intensity reported in Figure 6.5, the detected emission decreases for both fuel splits with higher EGR, as observed in the previous chapter.
Trying to quantify this effect, the OH* intensity has been averaged over the whole measurement area, obtaining the values reported in Figure 6.7 as a function of the inlet oxygen content. In standard conditions, the averaged OH* value is significantly higher for the fully diffusive case (0%PMX), but reducing the inlet oxygen level this difference becomes marginal. The fully piloted case has a linear decrease, while with higher premixing lower maximum values are first balanced by the increase in the extension of the reaction zone (see normalized OH*intensity of Fig. 6.6). With further reduction of the inlet oxygen level, the averaged OH* values decrease, with a lower profile slope than for the fully diffusive case. The different trend with fuel split is not affected by the change in optical properties mentioned in the previous chapter for the CO_2 addition as both fuel splits are affected in the same way.

The normalized images of Figure 6.6 allow a better visualization of the reaction zone. For the fully diffusive case, a drastic change in the OH* distribution happens as EGR conditions are introduced. Case (e) is the same condition shown in the Abel-transformed maps of Figure 6.4, where it was observed that the flame stabilizes attached to the liner walls. For the premixed case instead, the shape of the reaction zone keeps a similar shape also in EGR conditions, only detached and elongated. It is interesting to note that for the diffusive case part of the fuel remains entrapped and reacts in the outer recirculation zone, because of the higher pilot jet

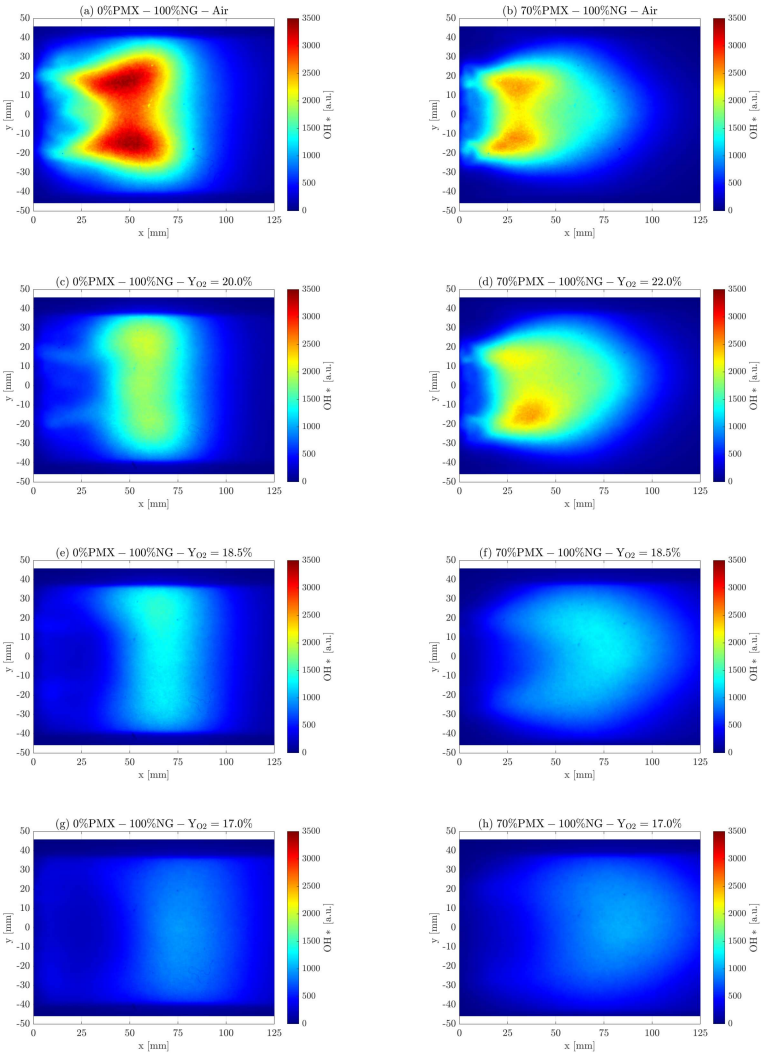

Figure 6.5: Time-averaged absolute OH intensity with simulated EGR*

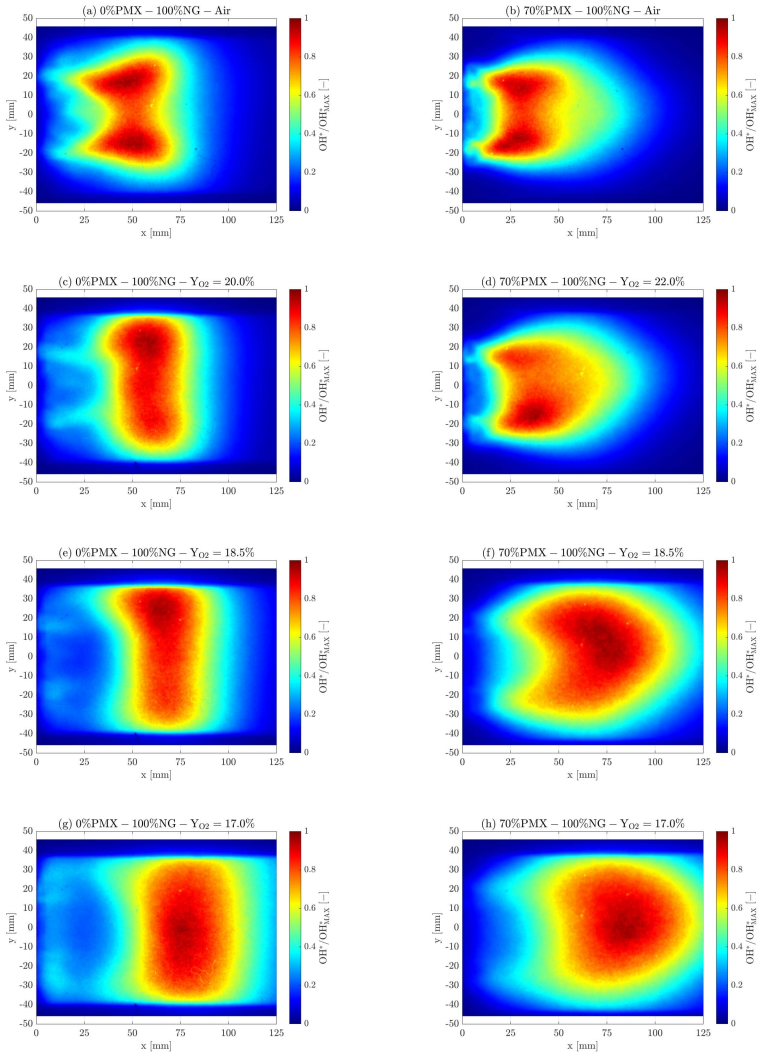

Figure 6.6: Time-averaged normalized OH intensity with simulated EGR*

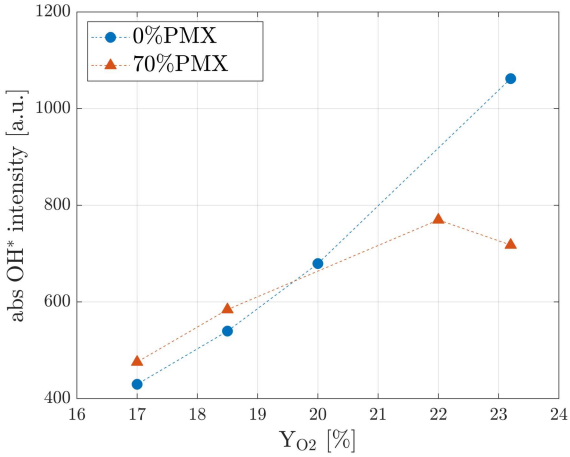

Figure 6.7: Averaged OH intensity as a function of the inlet oxygen fraction for 0%PMX and 70%PMX*

penetration. This interaction between pilot jets and outer recirculation area could be exploited to improve flame stability, and in such perspective, the effect of pilot jets orientation will be analyzed in detail in the next chapter, where different configurations are compared.

In order to quantify the flame lift-off, the axial position of the OH* peak has been evaluated. Figure 6.8 reports the distance from the burner outlet of position of the maximum of OH* intensity averaged over the radial coordinate y for the Abel deconvoluted images. The OH* distribution is time-averaged, therefore this value is not representative for the instantaneous distance of the flame base, but provides a a global indicative trend for the flame position. In standard conditions with higher premixed fuel fraction the flame is closer to the burner exit, as observed in chapter 4. In EGR conditions this trend is reversed, as the diffusive case is less affected by the decrease in laminar flame speed caused by lower oxygen levels, thanks to locally richer conditions. The overall increase in the distance of the main reaction zone from the burner exit, between standard

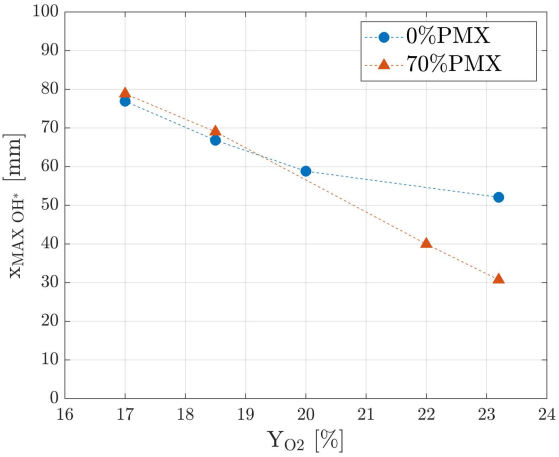

Figure 6.8: Axial position of the OH peak as a function of the inlet oxygen fraction for 0%PMX and 70%PMX*

conditions and high EGR level, is almost doubled for the more premixed case. In engine-like conditions this effect will be reduced, as the flame length decreases significantly at high pressure [2]. Nevertheless, these outcomes suggest that when the burner is operated inside a conventional gas turbine combustion chamber designed to operate without exhaust gas recirculation, the increase in flame length due to high EGR levels could be partially compensated using higher pilot fuel splits (lower %PMX). Although this phenomenon has been observed at ambient pressure, this result still provides a useful indication of flame behavior under these unconventional conditions, and should be taken into account for burner design optimization.

6.2 Emissions measurements

EGR is widely used in internal combustion engines as strategy to control NO_x emissions. As a drawback, emissions of particulate matter and unburned hydrocarbons rise because of the lower oxygen concentration

[1]. This behavior was encountered also in the context of gas turbines [7, 9], and the present results further confirm this trend.

Figure 6.9 reports NO_x and CO emission measured at different EGR levels with varying premix fuel fraction for operation with pure natural gas. Values measured in standard conditions are also reported (blue curve) to highlight the effect of EGR.
An increase in CO emission was observed in the previous chapter with CO_2 addition, and it is also encountered for different premix levels. The non-monotonic dependence on the fuel split recorded in standard conditions is also maintained, with all curves showing a minimum around 40%PMX. Increasing the EGR level shifts the profiles to higher CO values, and the amplitude of variation with fuel split is larger at low inlet oxygen levels, recalling that the presented scale is logarithmic.
At low oxygen content, CO levels are extremely high, almost two orders of magnitude higher than without EGR. The effect due to the high CO_2 concentration in the oxidizer observed in the previous chapter has to be taken into account, that leads to higher CO emissions than with oxidizer composition resulting from the implementation of EGR on a gas turbine. OH* chemiluminescence images showed how the reaction zone becomes widespread and lifted in EGR conditions. Differences in the flame structure due to different premix splits are reduced at low oxygen content, but still present. Figure 6.10 reports the radially averaged axial profile of OH* intensity for three different fuel split at Y_{O2}=16.6%. The related OH* images are the cases shown in Figure 6.5g-h and Figure 5.5i. An intermediate premix split (40%PMX) generates lower CO emissions, and indeed, the position of the OH* maximum shifts upstream, as the flame is able to stabilize closer to the burner outlet. The fully diffusive case presents a double peak, due to the reaction of part of the pilot fuel with the dome cooling air in the outer recirculation zone. This also happens for 40%PMX, but in this case, natural gas is mixed in the central main-flow jet, taking the main reaction zone closer to the burner exit. In the fully diffusive case instead, the main-flow jet is pure oxidizer and the high exit

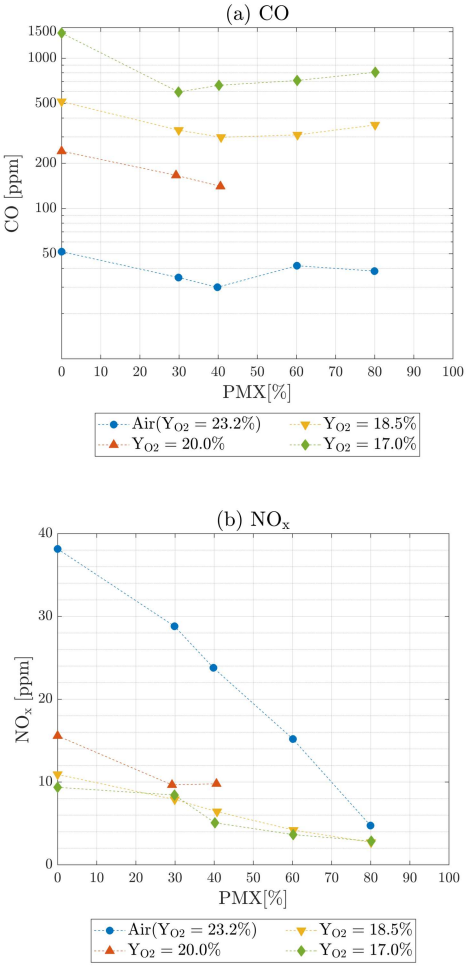

Figure 6.9: CO and NO_x emissions with 100% NG

velocity almost quenches the reaction, which is shifted downstream after a non-reactive zone with lower OH* intensity. At higher premix fraction

(70%PMX), very low OH* intensity is detected in the outer recirculation zone, as the pilot jet momentum is reduced, limiting jet penetration. These results show that the distribution of the pilot fuel in the area near the burner outlet greatly influences the stabilization process, impacting CO emissions. An optimization of the pilot injection system for these unconventional conditions could certainly support the reduction of high CO emission due to EGR.

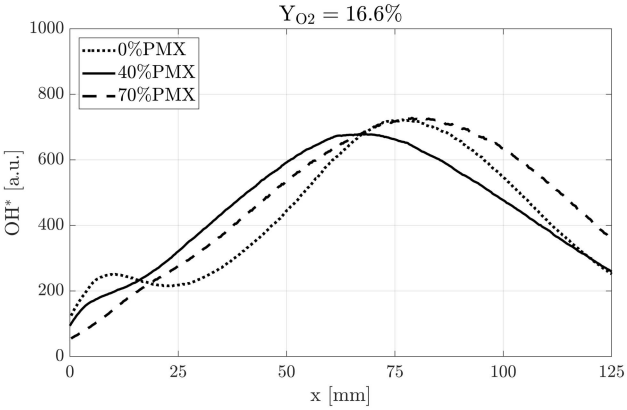

Figure 6.10: Axial profiles of radially averaged OH intensity at Y_{O2}=16.6%*

Regarding NO_x levels, Figure 6.9 shows how EGR significantly inhibit their formation. In particular, with high EGR, even with very high pilot fuel fraction (low %PMX), NO_x levels are comparable with those achieved under standard conditions with high premixing. After a significant drop of NO_x levels with the first step of oxygen reduction, a further decrease has a limited effect.

The influence of fuel split is significantly reduced in EGR conditions, with NO_x still slightly decreasing with premix fuel fraction. OH* chemiluminescence profiles of Figure 6.10 show that the maximum intensity is similar for the three fuel splits at this very low oxygen level. Recalling the trend shown in Figure 6.7 reporting averaged OH* intensity, differences

become marginal as the oxygen content decreases, similarly to what is observed on NO_x emissions, pointing out a certain correlation between the two effects.

Overall, these results allow some considerations to be made about the operability of the burner. As it is done during engine regulation with varying load, the fuel split can be leveraged to control emissions and mitigate the consequences of EGR. In standard conditions, the strong and monotonic dependence of NO_x emissions on fuel split suggest the use of high premix fractions, which are also associated to limited CO levels. In EGR conditions instead, lower premixing levels can be adopted without incurring in the detrimental NO_x increase.
In addition to exploiting the burner fuel split, the injection of hydrogen will be explored as a strategy to limit CO emissions in the last part of this chapter. This approach entails non-negligible plant complications, but it could also bring significant benefits, ultimately justifying the challenging implementation and making it worthwhile.

6.3 Dynamic behavior for operation with pure natural gas

In the previous chapter, the effect of EGR on the burner dynamic behavior was anticipated. In particular, it was observed that by lowering the inlet oxygen fraction the amplitude of pressure oscillations grows, reaches a maximum, and eventually decreases again. Figure 6.11 reports the RMS of the amplitude of pressure oscillations for three different fuel splits with pure natural gas operation, as a function of the inlet oxygen content. All tested fuel splits exhibit the behavior described above, but the oscillation amplitude increases with the fraction of fuel supplied through the premix line.
Lower premix fuel splits are more stable, since the pilot jets create locally richer conditions. In standard conditions, indeed, premixed systems are particularly subject to thermoacoustic instabilities, while diffusive flame

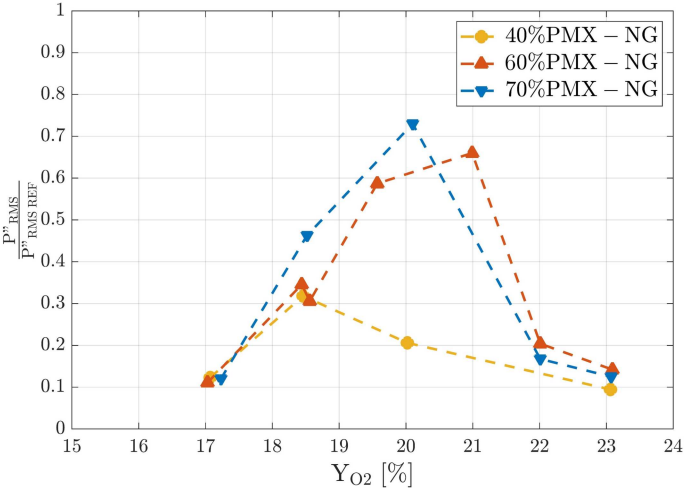

Figure 6.11: RMS of amplitude of pressure oscillation as a function of inlet oxygen fraction for different fuel splits

are intrinsically more stable, as local fluctuations of mixture composition are reduced. EGR instead, pushes the combustion process toward more challenging conditions, lowering the flame extinction strain rate, and oscillations arise also at lower premix fraction, although with reduced amplitude.

The more stable behavior of higher pilot split again suggests that under EGR conditions increasing the pilot split has a beneficial effect, and the associated increase in NO_x emission, which is a limiting factor without EGR, is marginal.

A qualitative explanation for the observed non-monotonic trend of pressure oscillations with inlet oxygen level could derive from the progressive elongation and lift-off of the flame with decreasing inlet oxygen level, as shown by time averaged images of Figure 6.6. In practical applications, the coupling between the acoustics of the combustor and the oscillations in the flame heat release rate is a critical factor in determining the

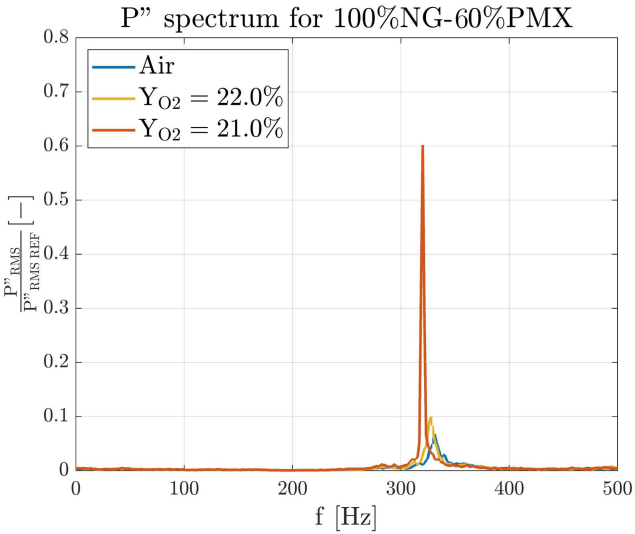

Figure 6.12: Frequency spectrum of pressure oscillation with 60%PMX for different oxygen levels

combustor's dynamic stability. The severity of this coupling is influenced by the phase relationship between these oscillations, which is in turn largely determined by the shape of the flame and its position within the combustor [105]. The coupling between heat release and pressure oscillations is altered by the variation of the flame position and length with EGR, and they result in phase only in a certain range of inlet oxygen levels. The fuel split affects the flame structure and therefore the heat release distribution, and the EGR range where constructive interference occurs consequently changes, together with the oscillations' amplitude. Recalling the differences observed with nitrogen dilution in section 5.3.3, the oxidizer composition modifies not only the flame structure but also the acoustic properties of the reactive flow, further influencing the dynamic behavior.

Figure 6.12 shows the frequency spectrum of these pressure oscillations for a fixed fuel split. The peak frequency is around 330 Hz, which corresponds

to the resonance frequency of the test rig. As discussed in chapter 5, the peak frequency decreases with lower oxygen inlet content, as a consequence of the variation in the acoustic properties of the mixture. Much higher amplitudes are reported with respect to what reported in Figure 5.11, as the premix fuel fraction in that case is lower, leading to a more stable behavior.

6.3.1 Instantaneous OH* images and further analyses of unstable behavior

High speed OH* chemiluminescence has been employed to gain a better understanding of the underlying causes of the observed oscillations, benefiting from the high spatial resolution, albeit line-of-sight, that provides detailed information on the combustion dynamics. Figure 6.13 presents instantaneous OH* images (1000 fps) captured under unstable conditions, revealing that the flame experiences significant longitudinal fluctuations. In particular, OH* images are referred to the case with higher peak amplitude in Figure 6.12. Considering the frequency spectra, one cycle at 330 Hz relates to roughly 3 ms, indeed a certain periodicity can be observed.

Also the instantaneous images correspond to a time interval equal to the intensifier gate (0.5 ms), and therefore contain a certain degree of temporal averaging. Compared to the time-averaged distribution, a globally shorter reaction zone is observed at certain instants, and while the flame base remains attached to the burner outlet, OH* intensity in the downstream region significantly varies in time. Averaging this oscillations in time generates the above presented distributed and widespread OH* maps, which are not able to show the instantaneous position and extension of the reaction zone varying over time. However, the averaged maps are considered more representative for comparisons between different cases, as they condense more robust information. In any case, it is not always entirely accurate to refer to a distributed reaction; but the term is employed in the present work referring to the temporal average of the reaction zone.

Statistic tools have been exploited to further study the dynamic behavior

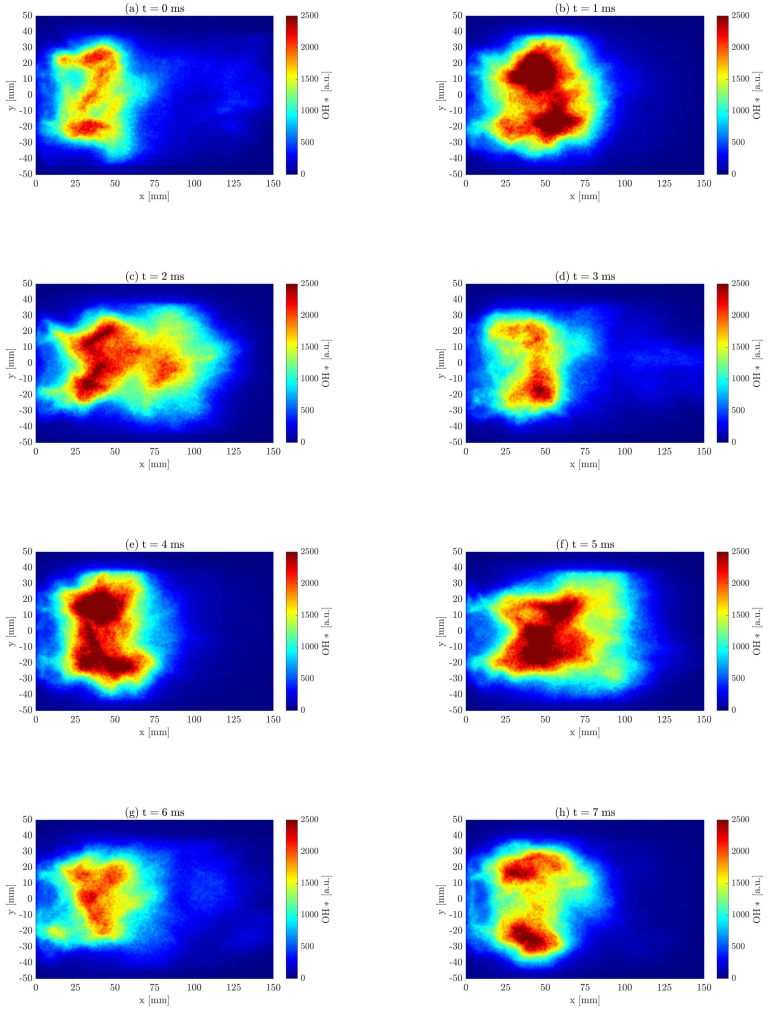

Figure 6.13: Instantaneous OH images at 60%PMX, Y_{O2}=21% and 100%NG*

and gain additional insights. In order to verify the presence of energetically coherent structures, Proper Orthogonal Decomposition (POD) of high speed OH* chemiluminescence images has been performed [106–108]. It is worth noting that chemiluminescence is a line-of-sight technique, therefore affecting the results of the POD analysis.
POD analysis is able to identify coherent modal structures and energetic modes of the flame, converting time-dependent data into orthogonal modes ordered with decreasing energy. The in-depth description of the mathematical procedure is not reported, and more details can be found in [109–111]. In summary, POD applied to OH* chemiluminescence images provides three quantities to describe the flame structure: eigenvalues, eigenvectors, and the POD modes. The POD modes constitute an orthogonal basis, extracted by decoupling the spatial and temporal contributions, determining the most energetic structures. Eigenvalues represent the energy contribution of each mode to the reconstruction of the OH* intensity distribution, while eigenvectors retain the temporal information related to each mode.

As representative condition, the procedure was applied to the case reported in the instantaneous OH* images of Fig. 6.13 (60%PMX and Y_{O2}=21%), in order to show the main outcomes. Figure 6.14 shows the energy contribution of the first 10 modes together with the cumulative (black dashed line). The first mode alone contains almost half of the total energy, which indicates the presence of coherent structures with an important energy contribution. The frequency spectrum of the first POD mode, shown in Figure 6.14, presents the same pressure oscillation peak, as the one detected with the dynamic pressure sensor for this condition, reported in Figure 6.12. A second peak at higher frequency is also present but with a significantly lower amplitude, not detected by the pressure sensor. The origin of this additional peak is presumably indicative of incomplete separation of the modes. All other modes show peaks at the same frequency, with progressively lower intensity, and the related spectra are not reported. The spatial distribution of the first POD mode

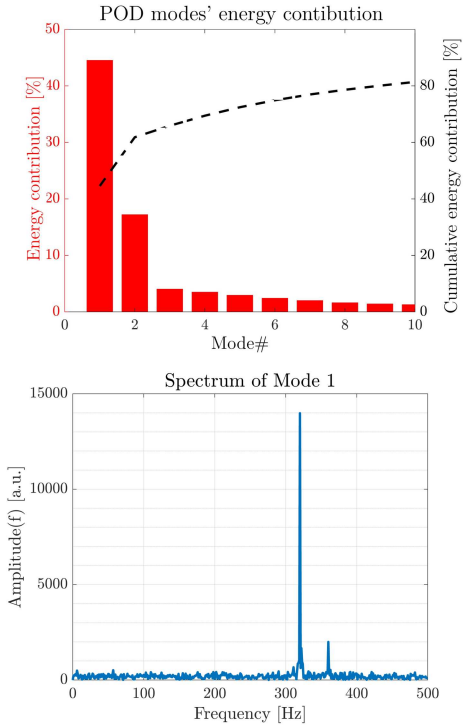

Figure 6.14: Energy contribution of the first ten POD modes and frequency spectrum of mode 1 from OH images at 60%PMX and Y_{O2}=21%*

is reported in Figure 6.15a, and it shows very defined structures. The two spots with high positive values at the flame base near the liner walls indicate that local OH* intensity (and therefore heat release) is oscillating with an energy comparable to that of the main central zone (high negative values) but in counter-phase. Recalling also the time averaged flow field of Figure 6.1, the structure of the POD first mode suggests that these thermoacoustic instabilities are associated with oscillations in the mixture composition within the outer recirculation zone, which pulsates intensely in counter-phase with the central jet region of the main flow. This

translates in a fluctuation between pilot combustion (attached/close to diffusive pilot jets) and premixed (lifted) combustion zones. Indeed, the instantaneous images in Figure 6.13 show significant movement of the flame base, which detaches from the burner exit, lifts, and subsequently reattaches. The interaction between pilot jets and the outer recirculation zone is highly influenced by flame confinement and the shape of the combustion chamber, which ultimately affects how the flow develops in the corner of the combustion chamber. The cylindrical chamber probably aggravates this behavior, because of the axisymmetric shape of the outer recirculation zone. Discontinuities encountered in the corners of a square chamber would probably partially dampen the oscillations. However, the complexity of the phenomenon makes accurate predictions challenging.

Mode two, with its two distinct zones, reveals longitudinal oscillations, where the flame extends and contracts along the axial direction, as shown in the instantaneous images. Mode 3 and 4 display well-defined structures that oppose each other, indicating they oscillate in counter-phase. This suggests a rotational movement around the axis of the flame front, a behavior also supported by ongoing numerical simulations. Unfortunately, the current test rig configuration does not allow for viewing the flame perpendicular to the burner axis, which would provide further insight into these dynamics. Lastly, in mode 5, a central region with low negative intensity is observed, in contrast to structures resembling the shape of pilot jets, suggesting that these oscillations are influenced by the interaction between the pilot flames and the central reaction zone of the premixed fuel. The dominant frequency is still the same as mode 1, and indeed this spatial distribution appears similar to an overtone of the first mode.

These results provide valuable insights into the underlying mechanisms at play when intense oscillations occur. Understanding the behavior of these oscillations can illuminate the factors that contribute to instability within the system. The primary conclusion from these findings is that the outer recirculation zone and the pilot jet region play a crucial role in the dynamic behavior of the burner, which becomes even more significant

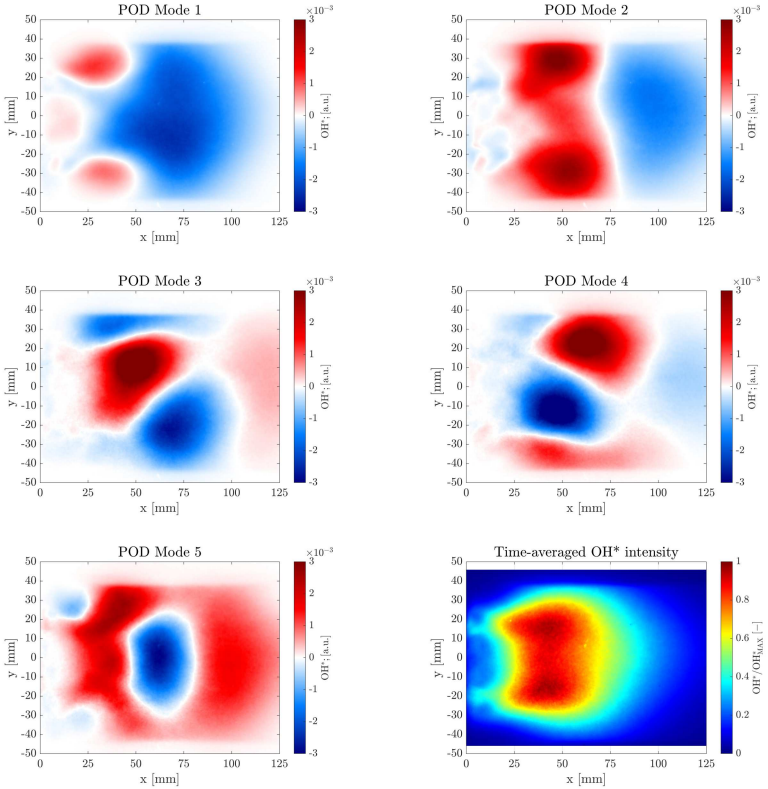

Figure 6.15: Spatial distribution of OH POD modes 1-5 and time averaged image for 60%PMX and Y_{O2}=21%*

under EGR conditions, as the system approaches the flame stability limit and is more prone to thermoacoustic fluctuations.

Concluding this section, it is worth to point out that for the experimental campaign the burner is operated in a long tubular liner, which works as a resonant tube. The exhaust gas mixes with the cooling air only at a very distant location from the burner outlet, and no diluting

air is injected inside the combustion chamber. This does not support the dampening of the oscillations that arise, while in gas turbine combustors several injections of cooling and dilution air are present, "relaxing" the acoustic boundary conditions of the burner. Nevertheless, the outcome of the study remains valuable in identifying under what conditions the flame is most prone to the onset of thermoacoustic oscillations, and the parameters to vary to mitigate this behavior.

6.4 Hydrogen addition in EGR-like conditions

The results shown so far have highlighted how EGR creates difficult conditions for stable combustion, because of the lower oxygen available to complete the fuel oxidation and the lower reaction rate. This leads to increased CO emissions and brings the burner into conditions where it is more prone to the emergence of thermoacoustic instabilities, because the flame is closer to the extinction limit, and therefore more sensitive to small variations of local conditions.
Hydrogen is well known for its high reactivity, which can be exploited to improve the flame stability in this challenging environment. The present chapter explores the effect of adding a limited amount of hydrogen through the burner pilot line with the purpose to enhance and sustain the combustion of natural gas in this oxygen-depleted environment. In particular, hydrogen has been injected both with pure pilot H_2 jets, and blended with natural gas in order to operate the burner also at lower premix fuel splits and at the same time respect the upper hydrogen limit defined by the requirement of CO_2 capture.

6.4.1 Dynamic behavior with hydrogen piloting

The previous section showed how the emergence of strong thermoacoustic instabilities is one of the main factors that is limiting achievable EGR levels for the investigated configuration, together with high CO emissions. In chapter 4, hydrogen addition was identified as beneficial in reducing the amplitude of pressure oscillations that arise at high premix fractions

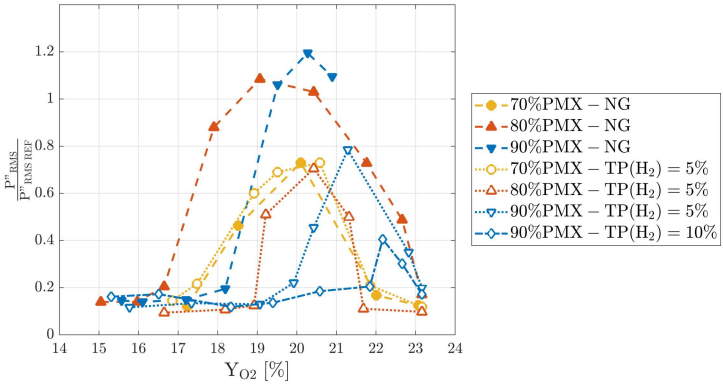

Figure 6.16: RMS of amplitude of pressure oscillation as a function of inlet oxygen fraction with hydrogen addition (dotted lines and hollow symbols) and pure natural gas (dashed lines and filled symbols) for different premixed thermal power fractions

with standard air as oxidizer. This positive effect was also encountered in EGR conditions, as detailed in the following.

Figure 6.16 presents the RMS of the recorded pressure oscillations as a function of the inlet oxygen content (increasing EGR from right to left) with different fuel splits, for conditions with and without hydrogen addition. All curves exhibit the same non-monotonic dependence with inlet oxygen level, with different positions and values of the maximum amplitude of pressure oscillations, the latter generally increasing with higher premix fuel split.

For the lower premix fraction (70% PMX), the impact of the tested hydrogen content is negligible and is not sufficient to change the flame behavior, which is already more stable than under the other conditions given the substantial pilot contribution. With higher premix split, hydrogen addition significantly dampens the oscillations. At 80%PMX, the maximum RMS of pressure oscillations is 40% lower with respect to the pure natural gas condition, and the threshold of oxygen level over which the pressure fluctuation decreases is higher, therefore enlarging the burner

operating window with EGR. The gain is even higher at 90%PMX, which for the case with only natural gas was an unstable condition in standard conditions (see section 4.5.2). In that case, the effect of simulated EGR is to dampen pressure oscillation, and the threshold oxygen level over which this happens is surprisingly higher than for cases with lower premix fuel splits. At 90%PMX, with TP(H_2)=5% the maximum amplitude value is 40% lower than the correspondent peak without hydrogen, and if the hydrogen fraction is increased to 10%, the maximum RMS value is over 70% less than for the case with natural gas. In this last condition (90%PMX-TP(H_2)=10%), pure hydrogen is injected through the pilot holes, while for the other cases it is blended with natural gas. Pure hydrogen jets prove to be very stable and only a slight increase in the oscillations amplitude can be observed as the oxygen content decreases. In addition, the range of inlet oxygen levels in which oscillations arise is very small, more narrow as the hydrogen fraction increases.
Overall, the addition of hydrogen, albeit in small amounts, has been found advantageous in reducing the intensity of thermoacoustic instabilities that arise in EGR conditions. These results will also be verified with different pilot jet configurations in the next chapter, confirming the promising outcomes.

6.4.2 Flame structure and emissions

At standard conditions, it was observed that injecting hydrogen with the pilot holes makes the reaction zone shorter and attached to the burner outlet. This can be exploited to counteract the flame lift-off due to the lower oxygen content in EGR conditions, improving flame stability. This section investigates the effect of hydrogen addition on the flame structure at EGR conditions and the consequences on pollutant emissions.
Figure 6.17 presents OH* chemiluminescence maps at low inlet oxygen content, with constant premix fraction of 50%PMX. The first map (a) is the case burning pure natural gas and moving to the bottom the hydrogen content increases. Regardless of the different hydrogen amount, the reaction zone at this very low inlet oxygen content is lifted and

widespread, but focusing on the flame base region, some differences can be detected. Higher OH* intensity is recorded in this area for the cases with hydrogen addition: traces of the pilot jets are visible near the burner exit, more intense at higher H_2 fraction (case c), meaning that hydrogen anchors the flame closer to the pilot holes. Additionally, in this last condition the length of the reaction zone is also slightly reduced. Therefore, despite the predominant effect of the very low oxygen content, which results in a diffuse reaction zone, adding a small amount of hydrogen to the pilot line blended with natural gas seems to have a positive effect on the flame anchoring zone and on reducing the overall flame length.

Looking into the implications of this variation in flame structure on CO emissions, Figure 6.18 reports the CO emissions recorded for the same operating conditions, in order to show the impact of hydrogen addition with simulated EGR. Positive effects are visible, as CO levels decrease with increasing hydrogen fraction. Part of the reduction is due to the lower amount of carbon in the fuel composition, but the hydrogen mass fraction remains very low (TP(H_2)=10% corresponds to Y_{H2}=4.3%), therefore this effect is limited. The CO reduction at this high EGR level is significant for the case with higher hydrogen amount, while the gain is limited at TP(H_2)=5%. Therefore, the positive effects observed in terms of a shorter and more attached reaction zone and are reflected in the CO emissions. In this condition, where hydrogen is blended with natural gas in the pilot line, significant differences are observed only with higher hydrogen percentages, whereas at 5% hydrogen addition, the effect is limited.

In order to explore the configuration where pure hydrogen is injected with the pilot holes, the studied conditions necessarily are characterized by higher premix fractions.

Figure 6.19 presents the OH* chemiluminescence images for three different inlet oxygen levels, starting with the case without simulated EGR on top and decreasing the inlet oxygen content moving to the bottom. The premix fuel split is 90% for all presented conditions, and the maps on the left show the cases with only natural gas, while for the right column, the hydrogen fraction of the total thermal power is kept constant at 10%

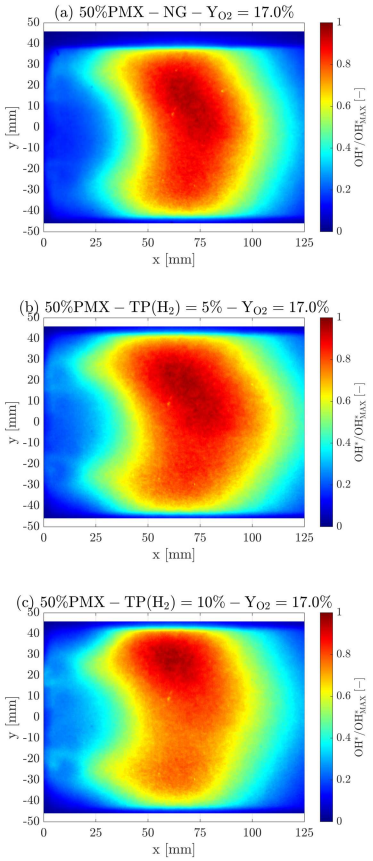

Figure 6.17: Effect of hydrogen addition on the flame structure in simulated EGR conditions

with pure hydrogen fuel jets. At this very high premix fraction with the hydrogen pilots and without EGR, a separation of the reaction zone is observed (see chapter 4, Fig. 4.11), with the natural gas flame that detaches from the diffusive hydrogen pilot flames burning attached to the burner outlet. For the case with only natural gas, this high premix

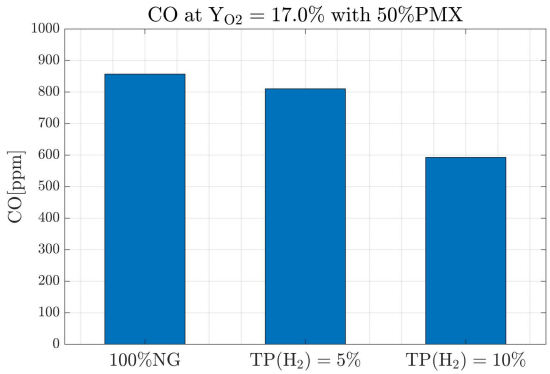

Figure 6.18: Effect of hydrogen addition on CO emissions with simulated EGR (Y_{O2}=17.0%-50%PMX)

fraction is an unstable condition also without EGR, with a very long and detached flame (case a). When EGR conditions are introduced, consistent with observations for other splits, the pure natural gas flame becomes progressively more lifted as the oxygen decreases (Fig. 6.19c-e). This also happens for the more distributed downstream portion of the OH* chemiluminosity attributed to natural gas combustion of the case with hydrogen addition. The downstream detached flame is shifted further downstream and becomes more widespread (Fig 6.19d-f) with lower inlet oxygen level. The highly reactive hydrogen pilot jets instead continue to burn well attached to the burner, providing an anchor point for the reaction. However, the interaction with the premixed natural gas reaction zone weakens and weakens as the oxygen inlet level decreases and the distance between the two increases.

Looking at the impact on CO emissions under these conditions, Figure 6.20 shows the measured CO values. The inlet oxygen level is Y_{O2}=16.6%, lower than the case shown earlier in this section for lower premix fraction (Fig. 6.18). Indeed, CO values are even higher, partly as a consequence of the higher CO_2 concentration in the oxidizer, but beacuse the flame is close to extinction in this conditions.

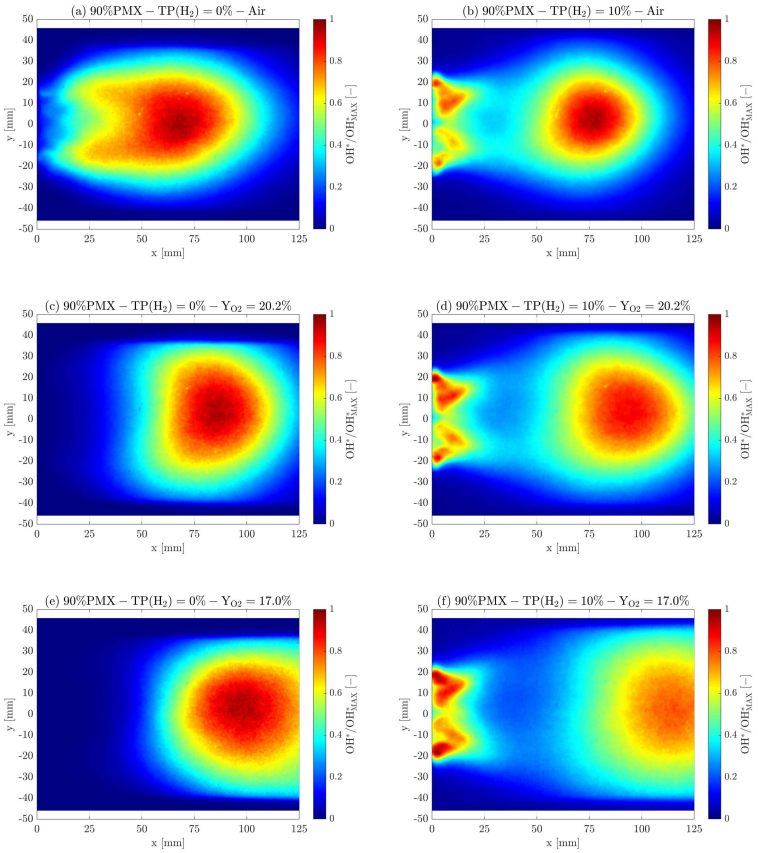

Figure 6.19: Effect of hydrogen addition on the flame structure in simulated EGR conditions

The positive effect of hydrogen addition is evident also in this case. Recalling the OH* chemiluminescence images of Figure 6.19, the hydrogen pilot flames supply hot products to the natural gas detached flame, providing a certain preheating to the incoming mixture. The locally higher temperature increases the rate of CO oxidation, consequently lowering

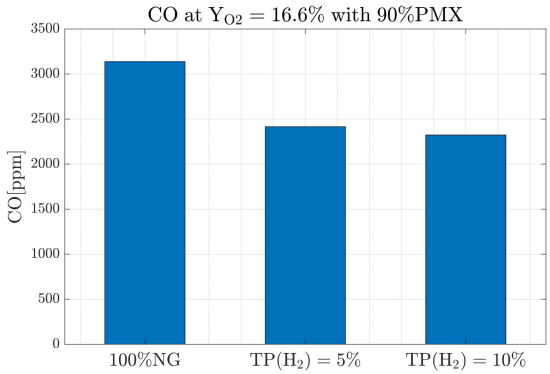

Figure 6.20: Effect of hydrogen addition on CO emissions at high premix fraction with simulated EGR (Y_{O2}=16.6%-90%PMX)

CO emissions.

The separation of the reaction zones observed under these high premix conditions suggests that the interaction between hydrogen jet flames and the natural gas premixed flame is not very strong, even in standard conditions. With simulated EGR, this aspect is amplified, with increased distances between the two flame fronts. This aspect could be improved, enhancing the interaction between the hydrogen pilot flames and premixed natural gas combustion, in order to further reduce CO emissions. A study on the pilot jet injection geometry is indeed crucial to improve the burner performance, in order to take full advantage of the dual fuel configuration under these challenging conditions. This aspect will be illustrated in the next chapter, exploring different fuel injection configurations. In particular, one of the configurations investigated was specifically designed for this purpose, with straight pilot jets with higher exit velocity in order to intercept the natural gas flame and enhance the interaction between the two flames.

With pure hydrogen pilot jets, the benefit is already significant at 5% of the thermal power, while increasing the hydrogen content further

has a limited effect, with only a very small gain. This behavior contrasts with what was observed when H_2 is blended with natural gas. OH* chemiluminescence images showed how pure hydrogen pilot flames behave differently compared to blended H_2-natural gas flames: even under conditions of low oxygen content, pure hydrogen pilot flames remain stable and well-anchored to the burner (see Fig. 6.20). This stability is maintained despite the reduced oxygen levels, in contrast to what was observed earlier in this section, where the flame with blended pilot fuel tends to become more lifted and less stable as oxygen decreases (see Fig. 6.17).

Overall, the collected results showed that with hydrogen addition the flame is able to stabilize slightly closer to the burner outlet, with positive consequences in reducing high CO levels due to EGR conditions. Hydrogen exhibits different effects depending on whether it is injected through pure jets or blended with natural gas. In the latter case, a larger amount of hydrogen is necessary to achieve noticeable benefits. The significant advantage observed with pure hydrogen jets, considering the current burner architecture that utilizes a single pilot supply line, is limited by the onset of pressure oscillations, which arise when operating with very high premix ratios. These results suggest that implementing separate injection lines for hydrogen and natural gas pilot holes would enable use of the benefits of pure hydrogen jets while simultaneously limiting the premix fraction. This approach would enable the use of smaller quantities of hydrogen, which could still have a positive impact on combustion, and at the same time limit the CO_2 reduction in the exhaust gases due to lower carbon content of the fuel. Furthermore, NO_x emissions remain low, thanks to the use of EGR, and are not a significant issue under these operating conditions. Although this innovative configuration was not explored in the present study, it represents a promising direction for future research, and offers a valuable approach for optimizing the combustion performance in dual-fuel systems.

Chapter 7

Effect of fuel injection mode

The results presented so fare have highlighted how the pilot jets play a critical role in the flame stabilization process, providing an anchoring point also at higher premix splits. This becomes even more important in the oxygen depleted environment caused by EGR, where achieving stable combustion is is more challenging. In this perspective, different configurations of the pilot jets have been tested, varying the inclination of the holes, their number and dimensions. A different injection strategy has also been tested for the premix line.

This last chapter of results covers this topic, investigating the effect of the fuel injection mode. In particular, the performance of 6 different configurations will be presented, in addition to the baseline case studied so far. This systematic screening allows the identification of the geometric parameters with the greatest influence and how they can be exploited to improve burner performance.

The different injection system geometries have been presented in detail in chapter 2.3.2, and are summarized in Table 7.1.

After a summary of the tested conditions, the performance of the new configurations will be analyzed in terms of stability limits, emissions and dynamic behavior, both with standard air as oxidizer and in EGR conditions. The effect of different fuel injection strategies on these parameters

will be analyzed with the support of OH* chemiluminescence, which allows to see variations in the reaction zone structure.
Following a first results overview, a more detailed and systematic analysis of the effect of each geometric parameter of the fuel injection system will be presented, including the description of the dynamic behavior in EGR conditions. The chapter concludes with a summary of the performance of all tested configurations.

	PLT			**PMX**	**CB**
	N [-]	**D** [mm]	**Direction**	**Position**	
B0*	N	1	3/4N Outward, 1/4N inward	Inner swirler	-
B1	N	1.2	Outward with tangential component	Outer swirler	-
B2	2N	0.7	Outward	Outer swirler	-
B4	N	0.7	Straight	Outer swirler	-
B5-PMX	N	1	Outward	Outer swirler	-
B5-CB	N	1	Outward	-	YES
B6	N	1	Outward with double angle	Outer swirler	-

Table 7.1: Investigated burner configurations.
**Baseline layout*

7.1 Operating conditions

After the detailed characterization of the burner baseline configuration, a restricted set of test points has been selected for the new geometries. Special care was put toward defining a sufficiently wide operational range for burner features comparison. At the same time, sensitivities have been conceived to maintain the comparison on equal term. In gas turbines conventional operation, once the combustor geometry is fixed, the flame temperature usually increases with load to guarantee low emissions [112]. For each configuration, the total thermal power was computed to match the same adiabatic flame temperature as standard conditions, in order to have a fair comparison. This was done to compensate small variations in the burner effective areas due to the 3D printing process, leading to slightly different oxidizer mass flow rate with the same pressure drop.

Then, varying the operating conditions, total thermal power has been kept constant for each configuration, following the approach of the previous chapter for the dual fuel configuration. Split changes between the two fuel lines at constant total thermal output have been carried out to identify the most promising operational window for each configuration.
Even though CO_2 dilution is much more convenient than using nitrogen mixtures for the oxidizer to simulate EGR, tests with EGR-like conditions are still demanding in terms of gas consumption. Indeed, only a single EGR level has been tested, sufficiently high to push the burners to operate close to the stability limit, correspondent to $Y_{O2} = 16.6\%$. This condition is referred to as "EGR" in the charts.
Data collected with the baseline configuration highlighted the beneficial effect of the injection of a small amount of hydrogen with the pilot line, both with pure jets and blended with natural gas. Following this indication, the new configurations have been tested in simulated EGR conditions only with hydrogen addition.

7.2 Overall comparison

This section presents an overview of the performance of the different configurations. The results include some considerations on the burner operability in standard conditions, in order to explore the possible improvements also for normal operation in gas turbines without EGR. More importantly, the impact of EGR conditions on the new layouts is analyzed, showing improved performance with respect to the baseline case.
It is worth reemphasizing that results were obtained on the described specific experimental test rig, with the burner installed in a tubular chamber and with the reported operating conditions. In addition to the different operating conditions in gas turbines, the long tubular liner does not fully replicate real gas turbine combustors that employ staged air injection for cooling and dilution. This difference could influence key combustion characteristics, such as flame stability, temperature distribution, and emissions. Therefore, the collected data cannot be used to describe the

burner performance when operated in gas turbines, but they provide useful indications about the effect of the main driving parameters. Aspects related to the specific combustion chamber shape, cooling air injection, and the interaction between adjacent burners in annular configuration are crucial for accurate realistic applications and will be explored numerically in more advanced stages of the research.

7.2.1 Lean blow out margin in standard conditions

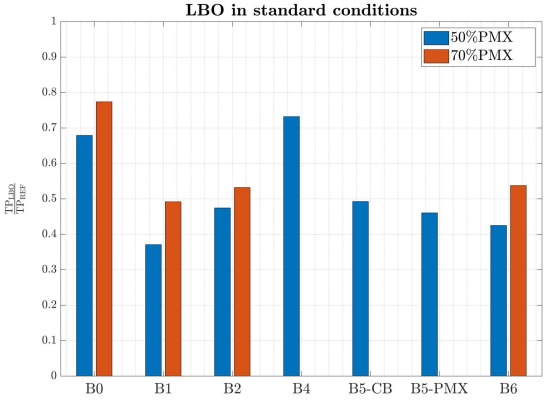

Figure 7.1: LBO limits for different burner configurations with 100%NG and standard air as oxidizer

Lean blow out tests have been performed with the same procedure as presented in chapter 4, in order to explore the stability limits of the different burner configurations for two different fuel splits. Results are reported in terms of scaled thermal power at lean blow out in Figure 7.1. All new configurations show improved lean blow out resistance with respect to the baseline case B0, except for B4, which has straight pilot jets with higher exit velocity. The leanest condition is instead reached with B1 layout, with outward swirled holes and increased total pilot exit area, therefore reduced jet velocity. Therefore, the lean blowout limit

is strongly influenced by the pilot jet velocity, as the interaction with the main flow significantly affects flame stability under lean conditions, a phenomenon that will be further explored in the following sections. As observed for the baseline configuration, and following the expected behavior, with lower premix fraction the lean blow out margin increases. This further underlines the importance of the pilot jets in the flame stabilization process. In the perspective of achieving safe operation with high EGR rates, a detailed study exploring the influence of the pilots injection system is therefore essential.

7.2.2 Unstable behavior

Another operability constraint in standard conditions was found in the outbreak of thermoacoustic instabilities, observed with the baseline configuration when the premix split exceeds a certain threshold. Hydrogen injection through the pilot line allows to shift this limit to higher premix fractions, therefore widening the burner operating window. This aspect was verified also for the new configurations, with the results reported in Figure 7.2. Results are expressed in terms of RMS of the amplitude of pressure oscillation as function of the premix thermal power fraction, comparing the case with only natural gas and the case with pilot line fed with pure hydrogen.

All configurations show a threshold value of the premix fuel split around 70-80%PMX over which the amplitude of pressure oscillations rises suddenly and significantly, except for the B5-CB case, for which this threshold could not be reached due to facility limitations [1].

Injecting hydrogen through the pilot line widens the stable region, to a slightly different extent depending on the configuration.

In general it is worth noticing that the configurations with worst lean blow out limits (B0 and B4) show instead the capability to stably reach higher premix fractions without triggering pressure oscillations. Furthermore,

[1] The fuel mass flow rate is limited by the pressure upstream of the calibrated orifice on the fuel line inside the burner. For the center-body line of B5 configuration the loss on the orifice was such that the pressure required to achieve higher flow rates exceeded the limit of the pressure regulator installed on the fuel skid in the lab.

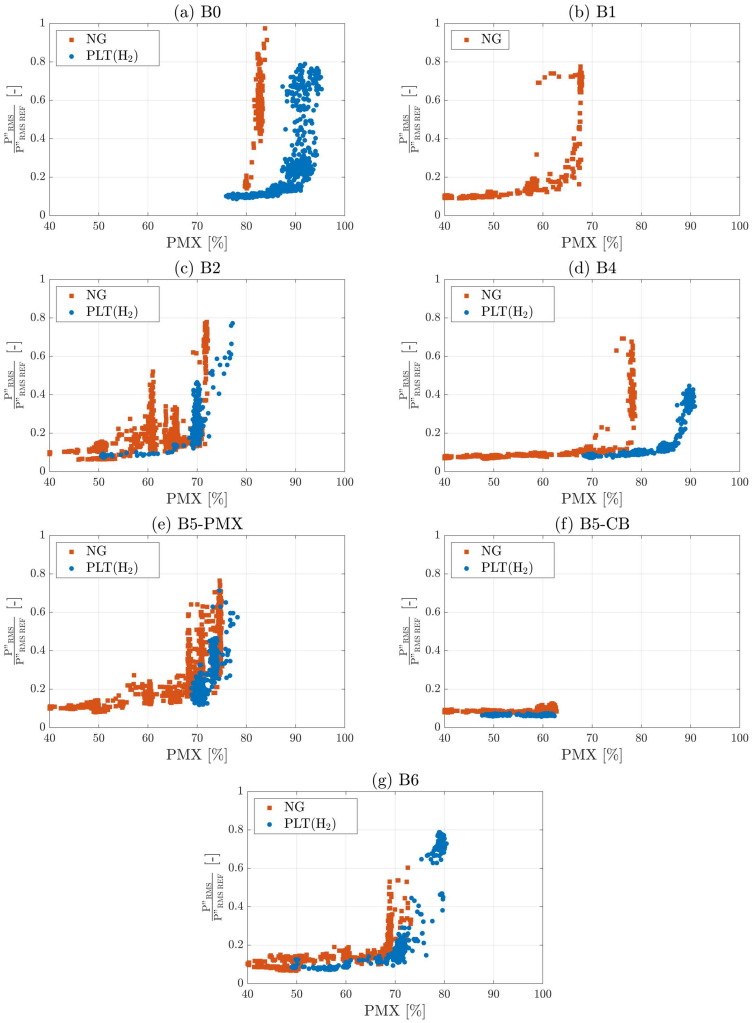

Figure 7.2: RMS of pressure oscillation amplitude with standard air as oxidizer, for the case 100%NG (NG) and with pure hydrogen injected with the pilot line (PLT(H_2))

the effect of hydrogen addition is more beneficial for those configurations. A possible interpretation of this phenomenon will be discussed later in this chapter.

7.2.3 Transient behavior with simulated EGR

Moving to EGR conditions, for the baseline configuration thermoacoustic instabilities have been detected when the oxidizer composition varies, with a non-monotonic dependence on the inlet oxygen content, as described in section 6.11. This aspect was characterized for the new layouts, recording the amplitude of pressure oscillation as the operating conditions vary in terms of premix fraction, hydrogen content and inlet oxygen level, with the results reported in Figures 7.3, 7.4 and 7.5. The red rectangles highlight the conditions with simulated EGR, following the decrease in the oxygen inlet content reported in the first plot. EGR is introduced with a relatively quick transient, not sufficient for assuming equilibrium during those mixture variations, to minimize the time during which the quartz liner was exposed to intense oscillations. Additionally, since the tested conditions were adapted to operate within the optimal range for each configuration, a fully rigorous comparison is not feasible. Nevertheless, the observed behaviors are presented to qualitatively illustrate the differences among the various configurations, while the emission values reported the next section are measured under equilibrium conditions, corresponding to the constant conditions intervals of the plots. In the following a summary of the observed trends is presented:

- – Tangential component on pilot jets with lower exit velocity and premixed fuel injected in outer swirler:
  Instabilities with standard air rises as PMX $>$ 65% with only natural gas (see Fig. 7.2b), while with hydrogen this aspect was not investigated because of problems encountered during operation, that will be described in the next sections. In simulated EGR conditions the premix fraction was kept under 60%, and no thermoacoustic instabilities have been detected. Figure 7.3 shows that the amplitude

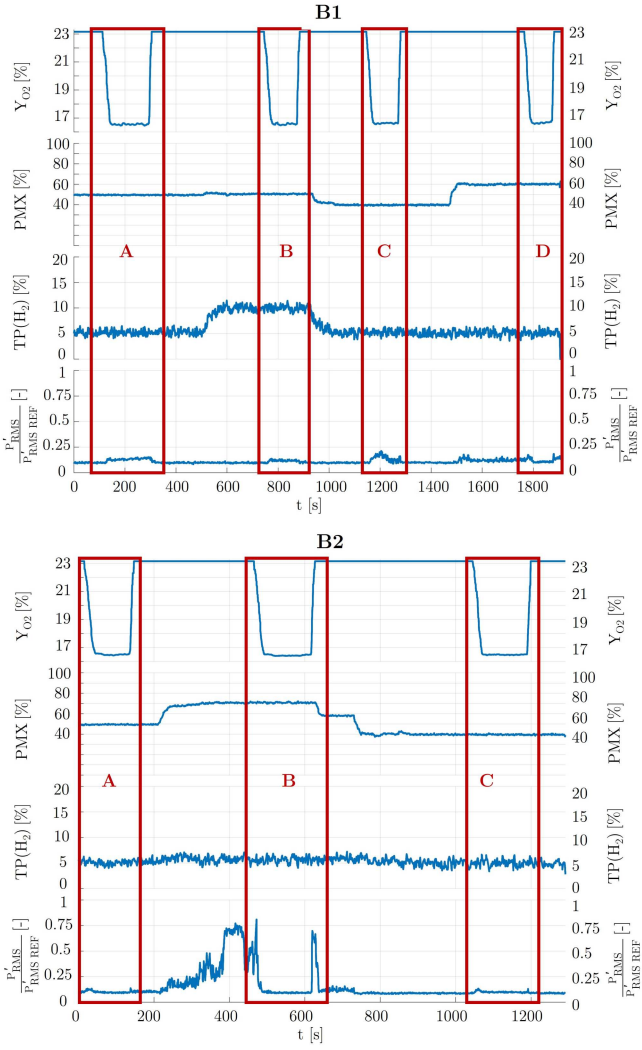

Figure 7.3: Transient behavior with simulated EGR for B1 and B2

of pressure oscillations is very low for all tested conditions, with PMX up to 60% and H_2=5-10% (points B1-a-b-c-d).

- B2 – Doubled number of holes and same geometric exit section as baseline and premixed fuel injected in outer swirler:
  With standard air and only natural gas, the amplitude of pressure oscillations start to rise as PMX > 55%, reaches a maximum and decreases again increasing the premix split up to 70%, where fluctuations rise again. With hydrogen addition, the first peak is not present, and oscillations only rise as the premix fraction exceeds 70%.
  With simulated EGR, no thermoacoustic instabilities occur with PMX up to 50% (Figure 7.3, points B2-a-c). Moving to higher premix fractions, at 70%PMX and 5%H_2, lowering the inlet oxygen content initially decreases the amplitude of pressure oscillations which were due to the high premixing, similarly to the behavior observed in the baseline configuration in the previous chapter. With further decrease first a maximum is reached, then the amplitude lowers significantly (Figure 7.3 point B2-b). Intermediate EGR conditions are therefore critical at this level of premixing for this configuration, and higher premixing was not tested.

- B4 – Straight pilot jets with double exit velocity and premixed fuel injected in outer swirler:
  With standard air and only natural gas, amplitude of pressure oscillations rises as PMX > 75%, and hydrogen pushes this limit to 85%, with a significant improvement. This configuration is the only one among the new ones that is able to reach this high premix fraction stably, similarly to the baseline case. With simulated EGR, no thermoacoustic instabilities occured with PMX up to 50% (Figure 7.4, points B4-b and B4-c). With very high premixing (90%PMX) and 10%H_2, lowering the inlet oxygen content decreases the amplitude of pressure oscillations which were due to the high premixing (Figure 7.4, points B4-a).

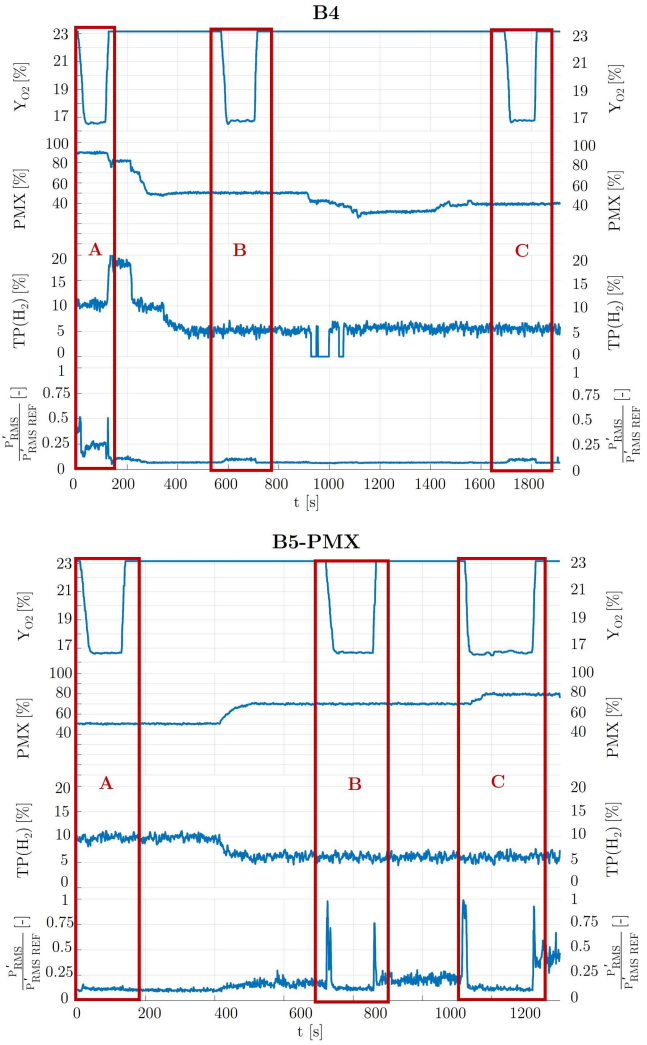

Figure 7.4: Transient behavior with simulated EGR for B4 and B5-PMX

- B5-PMX – Outwards oriented pilot jets and premixed fuel injected in outer swirler:
  With standard air and only natural gas, the amplitude of pressure oscillations rises as PMX > 65%. Hydrogen has a limited effect, only slightly enlarging the range of premix fraction with stable behavior. With simulated EGR, no thermoacoustic instabilities occurred with 50%PMX (Figure 7.4, points B5-PMX-a). Increasing the premix fraction to 70%, intermediate oxygen levels trigger strong thermoacoustic instabilities, which disappear with further decrease of Y_{O2} (Figure 7.4, points B5-PMX-b and c).

- B5-CB – Outwards oriented pilot jets and premixed fuel injected with center-body:
  With standard air, no pressure oscillations occur with PMX up to 60%, and further values where not tested for facility limitations. Also in EGR conditions, no thermoacoustic instabilities occurred for the tested conditions with PMX up to 60% and H_2=5-10% (Figure 7.5, points B5-CB a-b-c-d).

- B6 – Pilot jets oriented outward with double angle and premixed fuel injected in outer swirler:
  With standard air and only natural gas, the amplitude of pressure oscillations rises as PMX > 65%, and hydrogen pilots allow to reach 75%. With simulated EGR, no thermoacoustic instabilities occurred with PMX up to 50% (Figure 7.5, points B6 a-c). With PMX=70%, intermediate oxygen levels trigger strong thermoacoustic instabilities, which disappear with further decrease of Y_{O2} (Figure 7.5, point B6-b).

In general, higher premix fractions are always more unstable, and the configurations that show more stable behavior without EGR maintain lower oscillation amplitude also with lower oxygen content. In certain conditions, CO_2 dilution helps in dampening oscillations associated to high premix fractions.

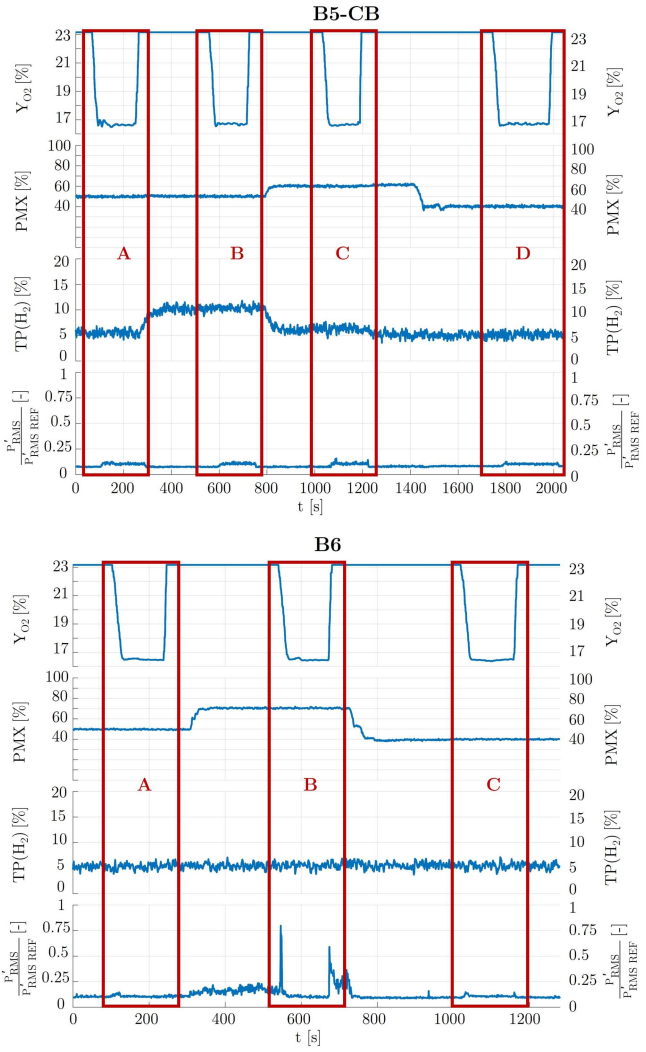

Figure 7.5: Transient behavior with simulated EGR for B5-CB and B6

7.2.4 CO and NO_x emissions

Figure 7.6 shows CO and NO_x emission measured for the different burner configurations, with only natural gas and standard air as oxidizer, varying the premix thermal power split.
As observed for the baseline case, NO_x levels decrease linearly with growing premix fraction. Diffusive pilot flames are mainly responsible for NO_x production due to local quasi-stoichiometric conditions, which, on the other hand, are crucial in the stabilization process.
The dependency of CO emission on the premix fraction is lower, but again all burner configurations exhibit the same non-monotonic trend as the baseline case. The premix fraction corresponding to minimum CO slightly varies between the different layouts, and further details will be discussed in the next sections, as for the different behavior of B1 configuration.

Moving to EGR conditions, Figure 7.7 reports CO and NO_x emissions recorded at $Y_{O2} = 16.6\%$ with constant hydrogen fraction of 5%. It is difficult to identify a trend with premix level for CO, while NO_x values remain decreasing with higher premix fraction. The beneficial effect of EGR on NO_x emissions overcomes the differences between the different layouts, and all tested configurations show very low and similar values (note the reduced scale of the plot axis), within uncertainties of the measurements.
High CO emissions are instead one of the main drawbacks of EGR, and indeed represent the major performance parameter for evaluating the burner capabilities. Contrary to what was observed for NO_x, the influence of the fuel injection mode on CO emissions is considerable and some configurations have improved performance over others. In particular, all new configurations show lower CO levels than the baseline, except B1 at low premix. The most promising layouts are B5-PMX, B2 and B6, which are able to stay under 500 ppm. Indeed varying with the pilot jets orientation and number helps in reducing CO emissions, and also the premix strategy can be improved for these unconventional operating conditions. Further insights will be detailed in the final part of this chapter, understanding the role of each geometric feature on the burner performance.

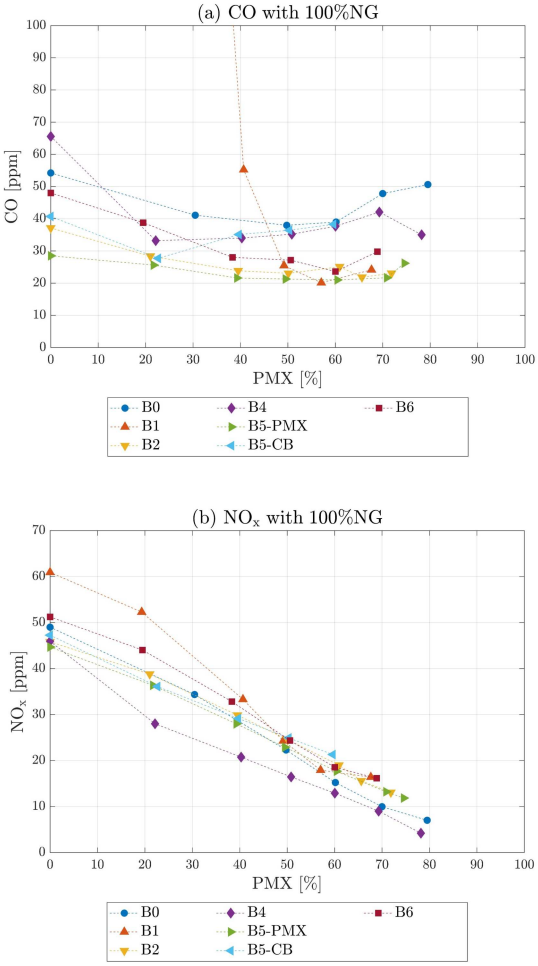

Figure 7.6: Pollutant emissions measured with standard air as oxidizer and 100%NG.
CO levels for B1 with complete scale are reported in Figure 7.15.

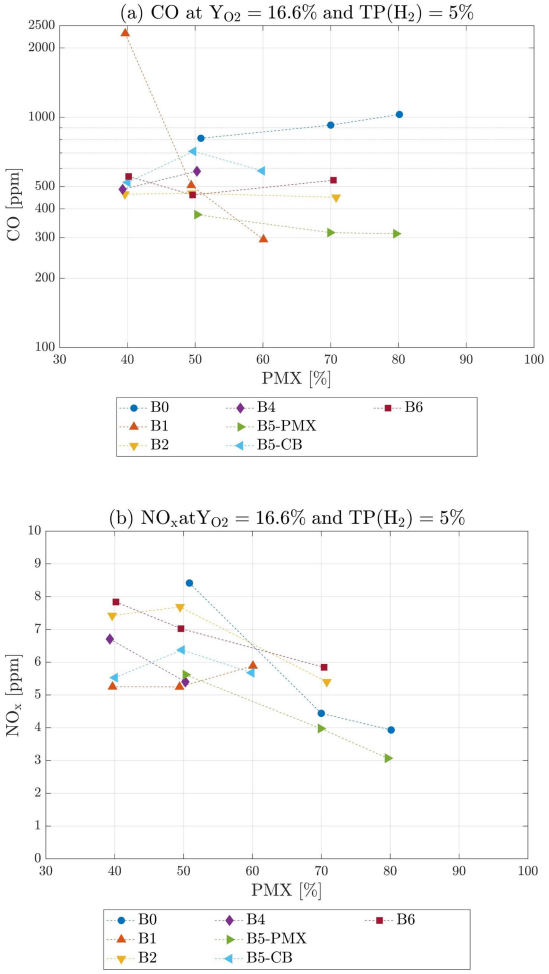

Figure 7.7: Pollutant emissions measured with 50%PMX - Y_{O2}=16.6% and TP(H_2)=5%

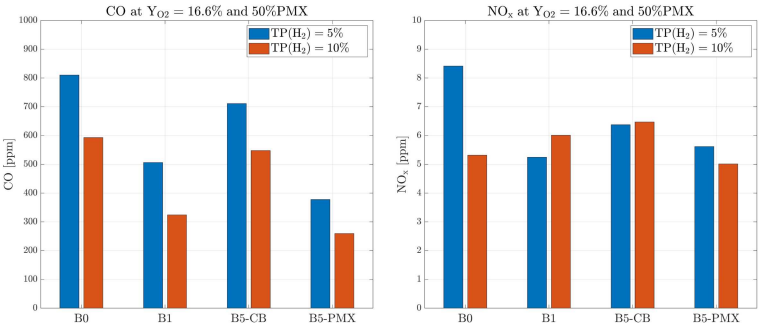

Figure 7.8: Pollutant emissions measured with 50%PMX - Y_{O2}=16.6%

The effect of the hydrogen amount has also been evaluated, even though the margin on this parameter is limited because it is desired to keep the CO_2 content in the exhaust high. Two different levels were tested, equal to 5 and 10% of the total thermal power, keeping the premix fraction constant at 50%PMX, with the results reported in Figure 7.8. Increasing the hydrogen fraction has a beneficial effect on CO emissions, which decrease for all tested configurations. The gain is quite relevant in all cases, but the reduction of carbon atoms when increasing the hydrogen fuel fraction has also to be taken into account.
NO_x levels are already very low thanks to the low inlet oxygen content, and the effect of increasing the hydrogen fraction is almost negligible, except for B0, for which NO_x decrease with higher hydrogen level.

7.2.5 Flame structure

In order to highlight the differences in flame structure among the different burner configurations, time-averaged normalized OH* chemiluminescence images are shown in Figure 7.10. The first column reports the fully diffusive case with only natural gas, while the second and third columns refer to 50%PMX and 5%H_2 with standard air as oxidizer and in simulated EGR conditions respectively.

In the fully diffusive case, the reaction zone is lifted, with different extent for each configuration. At 0%PMX, some layouts give rise to a non symmetrical reaction zone (B1-B2 and B4), probably due to small geometrical differences in the cross section of the exit holes, altering the jets' velocity. In some cases, individual jets can be distinguished near the burner exit. At higher premix, the influence of the single pilot jets is reduced, and the flame becomes approximately symmetrical. In all cases with higher premixing and doping the pilot jets with a small amount of hydrogen, the reaction zone becomes more compact, both shorter and closer to the burner axis.
The effect of simulated EGR is consistent for all tested configurations, with the reaction zone that shifts downstream and becomes widespread. In this condition, the diffuse flame structure is similar among all the configurations, but some differences can be highlighted, especially at the flame base. In particular, configuration B1 shows the flame located very close to the burner exit, and with a slightly a shorter length. This last case is a consequence of the pilot reduced jet velocity, which causes some of the fuel to be entrained in the external recirculation zone, inducing the flame to anchor closer to the burner outlet, as will be detailed in section 7.4. On the other hand, B5-PMX positions the flame further downstream compared to the other layouts, and additionally, in some cases (B0 and B4), a more pronounced curvature is visible at the flame base, anchoring near the pilot jets closer to the burner exit.

7.3 Effect of premixing strategy

After presenting the overall performance of all configurations, the analysis focuses on the effect of each individual geometric parameter.
For all new configurations, premix fuel is injected at the tip of the outer swirler, while for the baseline case the injection point is located in the inner swirler.
The B5 configuration has outward oriented pilot jets, not exactly identical to the baseline configuration but very similar, with same diameter, number

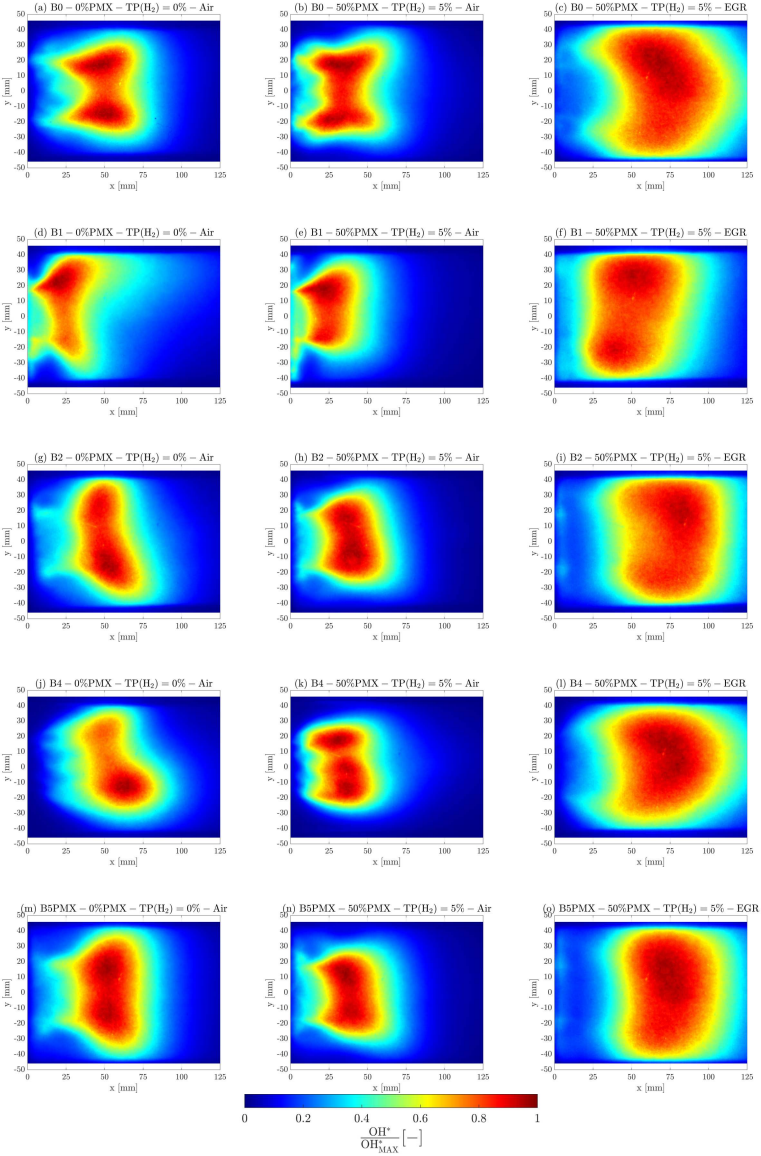
(a) B0 – 0%PMX – TP(H_2) = 0% – Air
(b) B0 – 50%PMX – TP(H_2) = 5% – Air
(c) B0 – 50%PMX – TP(H_2) = 5% – EGR
(d) B1 – 0%PMX – TP(H_2) = 0% – Air
(e) B1 – 50%PMX – TP(H_2) = 5% – Air
(f) B1 – 50%PMX – TP(H_2) = 5% – EGR
(g) B2 – 0%PMX – TP(H_2) = 0% – Air
(h) B2 – 50%PMX – TP(H_2) = 5% – Air
(i) B2 – 50%PMX – TP(H_2) = 5% – EGR
(j) B4 – 0%PMX – TP(H_2) = 0% – Air
(k) B4 – 50%PMX – TP(H_2) = 5% – Air
(l) B4 – 50%PMX – TP(H_2) = 5% – EGR
(m) B5PMX – 0%PMX – TP(H_2) = 0% – Air
(n) B5PMX – 50%PMX – TP(H_2) = 5% – Air
(o) B5PMX – 50%PMX – TP(H_2) = 5% – EGR
x [mm]
y [mm]
0 0.2 0.4 0.6 0.8 1
$\frac{OH^*}{OH^*_{MAX}}$ [–]

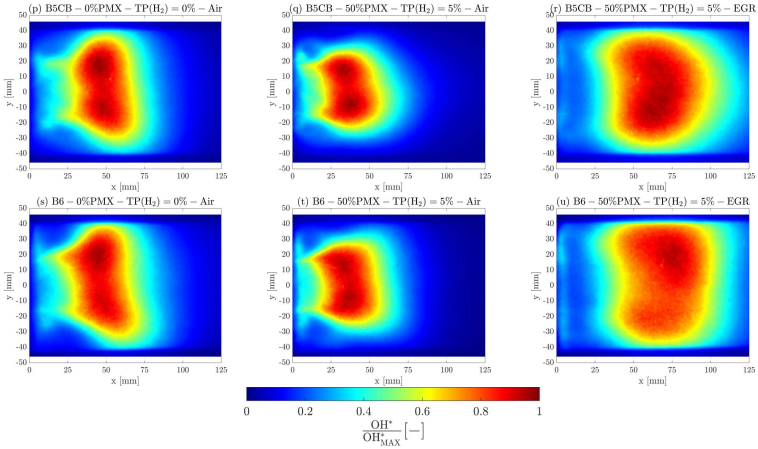

Figure 7.10: Normalized OH chemiluminescence images*

of the holes and orientation. The only difference is that for the baseline case 1/4 of the pilot jets are inward oriented and located at a slightly lower radius. Indeed, also for the fully diffusive condition the steady flame structure is not identical for B0 and B5, opening the flame more toward the chamber walls for the latter case (Fig. 7.10a-m-p).

This layout was operated also injecting the fuel with the center-body along the burner axis in configuration B5-CB. In this last case, the premixing level achieved at the burner outlet is lower compared to injecting the fuel in the swirler vanes, because of the reduced distance from injection to combustion chamber, related to short time available for mixing.

In both cases (B5-PMX and CB) the reaction zone at 50%PMX (Fig. 7.10n-q), is more compact than for the baseline case, with the contribution of the single pilot jets merged close to the burner axis. This is linked to the higher interaction with the pilot flames for the B5-PMX case, which also has positive effects on the lean blow out behavior. Indeed, all new configurations are characterized premixed fuel injected in the outer swirler, except B5-CB, and generally show improved lean blow out margin. This last aspect is improved for the center-body injection (B5-CB) as well, to

a slightly lower extent than the injection of the premixed fuel in the outer swirler. The B5-CB can be considered as intermediate condition, since premixed fuel is injected along the axis, similar to when it is injected in the inner swirler in terms of position, but lower mixture uniformity is achieved due to shorter premixing length. This last aspect indeed helps in stabilizing the flame, improving the lean blow out margin.
The oscillation amplitude increases for lower levels of the premix split compared to the baseline case for B5-PMX, and the behavior is not significantly improved even with hydrogen pilots. This aspect was not investigated for the B5-CB design for facility limitations in terms of fuel pressure. Overall, all new configurations have worse dynamic behavior compared to the baseline case, as the amplitude of pressure oscillation rises around 70%PMX, except for B4. These results indicate that injecting premixed fuel into the outer swirler leads to better resistance to lean blow out due to the increased interaction with the pilots and the external recirculation zone, but at the same time the flame is more sensitive to local equivalence ratio fluctuations at high premix fractions.
Notably, NO_x emissions in standard conditions are the same as for the baseline case for both B5 configurations, meaning that all the presented premixing strategies are effective, thanks to the high velocity of the airflow and strong turbulence created by the swirlers. CO levels are substantially lower for the B5-PMX case, because of the higher interaction between pilot and premix fuel. For the center-body configuration, the premix fraction corresponding to minimum CO is lower than for the other cases, around 20%PMX. In this configuration, lower premix is achieved, and while NO_x values are generally low, a slightly reduced dependency on the premix fraction can be seen.
Also in EGR conditions, B5-PMX has better performance than the other configurations in terms of low CO emissions, but at the same time the dynamic behavior is not ideal also in these conditions, and strong pressure oscillations occur.

7.4 Effect of pilot orientation and jet velocity

The pilot jets' orientation and velocity determines their interaction with the main flow, and consequently the mixing process. Playing on these parameters allows modifying the fuel distribution near the burner outlet, where the flame anchors, and therefore affects the stabilization process.

The pilot jets for the baseline case (B0) are 1/4 N oriented inwardly and positioned at smaller radius, 3/4 N oriented in outward direction. Configuration B6 maintains the holes number and dimension, but with axisymmetric pattern, with holes all outwardly oriented with double angle, and the same premix system as B5-PMX. It is therefore more rigorous to compare these last two configurations to isolate the effect of the pilot orientation.

Starting from the stability limits shown in Figure 7.1, the lean blow out margin is slightly improved for B6 compared to B5-PMX, as the pilot jets are more open and directed outward. For B6 layout, with double outward angle of the pilot jets, (Fig.7.10s-t-u), enhanced interaction between pilot fuel and the outer recirculation zone is present, as proven by the smears of OH* intensity at the flame base in this area for 50%PMX and 5%H_2. Indeed, improved lean blow out resistance is recorded because of the more intense recirculation of activated radicals at the flame base.

The dynamic behavior is not significantly affected by the larger outward orientation of the pilot jets, with similar trends in pressure fluctuations upon variation of the premix fraction for B5-PMX and B6 (Fig. 7.2e-g). As mentioned earlier, this aspect is affected more by the premix fuel injection mode, as it constitutes the majority of the fuel at these high premix fractions.

Regarding emissions, for both CO and NO_x levels B6 shows slightly higher values, with decreasing difference as the premix fraction increases. Indeed, the mixing process is improved as the pilot jets interact more with the oxidizer main flow. Therefore, with less outward oriented pilot jets (B5-PMX), a higher level of premixing is achieved also at lower pilot fractions,

while increasing the premix fraction this effect is reduced.
Higher CO values are recorded also in EGR conditions for B6 configuration, which has however improved performance compared to the baseline case. Looking at the steady flame structure in this condition (see Fig. 7.10o-u), differences are negligible and the reaction zone is similar.

A different orientation of the pilot jets is also present for B4 configuration, which has straight holes injecting the fuel parallel to the burner axis. In this case, the total cross section of the jets is reduced to half, therefore doubling the jet exit velocity.
Looking at the chemiluminescence images of Figure 7.10, with standard air for B4 (cases j-k), the flame is significantly lifted, especially for the fully diffusive case and stabilizes at higher distance from the burner outlet compared to the other configurations. In the fully diffusive case, despite the straight direction of the pilot jets, the reaction zone opens toward the walls of the chamber. Indeed, even though the pilot jets have high velocity, the lower mass flow rate improves the mixing with the central oxidizer jet, which instead expands outward. This effect is reduced at higher premix fraction, but the flame remains lifted. Straight pilot fuel jets intercept the main flow in a region where the premixed jet has high velocity (see PIV velocity field of Figure 4.6), and the higher fuel jet velocity causes the flame to be more lifted. This does not help the stability, as the flame is subjected to higher strain. As a consequence, flame loss is approached earlier, resulting in the worst lean blow out margin among the investigated configurations. This result also emphasizes the importance of the outer recirculation zone for the flame stabilization process. Indeed, with less outward oriented and faster jets, the interaction between the outer recirculation zone and the flame base is weaker, further worsening combustion stability.
The straight pilot jets with higher velocity of layout B4 were conceived with the purpose to enhance the interaction between the hydrogen pilot flames and the natural gas premixed reaction zone, which separate for the baseline configuration when the premix fraction exceeds 80% (see Fig.

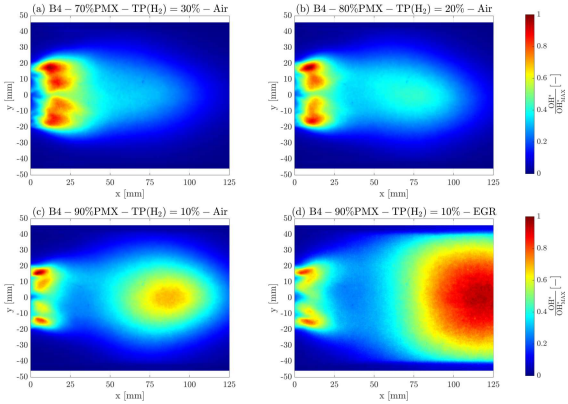

Figure 7.11: Normalized OH chemiluminescence images for B4 configuration*

6.19b). Figure 7.11 reports OH* chemiluminescence maps corresponding to B4 configuration, highlighting that this configuration shows the same behavior. It can be noted that the hydrogen pilot flames are slightly lifted because of the higher jet velocity, with the positive effect of reducing the thermal load on the burner tip. Moving to EGR conditions (d), there is no noticeable improvement on this aspect compared to what was seen for the baseline case. Indeed, CO emissions are about the same in this conditions, as reported in Figure 7.12. This behavior is probably due to the high core velocity of the main flow jet, which causes the premixed natural gas flame front to stabilize very far from the burner exit. Varying the pilot jet orientations and increasing the velocity is not sufficient to mitigate this aspect. In terms of stably achievable premixing level (see Figure 7.2), B4 reaches about the same values of the baseline configuration both with and without hydrogen addition, better than the other cases. A possible interpretation of the recurrent behavior, where improved blow out resistance corresponds to a narrower window of stable premix range, could be linked with the flame lift-off. Indeed, detaching the flame base from the burner outlet increases the strain to which the flame is subjected,

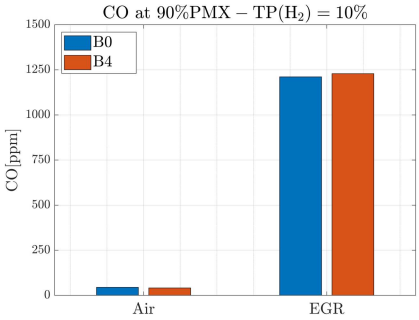

Figure 7.12: CO emissions for B0 and B4 at 90%PMX and TP(H_2)=10%

but at the same time helps in dampening fluctuations of the local main flow velocity, with the lift-off height acting as a buffer, with positive effect on the dynamic behavior.
Lower instabilities for the B4 case were observed also in EGR conditions, and at very high premix fraction, lowering the inlet oxygen content decreases the amplitude of pressure oscillations (Fig. 7.4 B4-a).
Looking at the emissions in standard conditions (see Fig. 7.6), B4 has the lowest NO_x levels, further reinforcing the concept that faster and less outward oriented pilot jets mix better with the oxidizer. Indeed, by detaching the flame from the nozzle outlet, lifted flames provide a higher premixing level in the reaction zone, with beneficial effect on NO_x emissions, especially at low premix fraction. CO levels are not significantly improved for B4 configuration, with values slightly lower than the baseline configuration. For the fully diffusive case, high CO is recorded, corresponding to the OH* image of Fig. 7.10-j. In this condition, the reaction zone is strongly lifted and asymmetric, indicating an inhomogeneous fuel distribution among the single pilot jets, causing the CO emission to rise.

B1 configuration introduces a tangential component and lowers the exit velocity of the pilot jets, because of a higher total exit cross section. Some manufacturing issues result in non-uniform exit areas among the

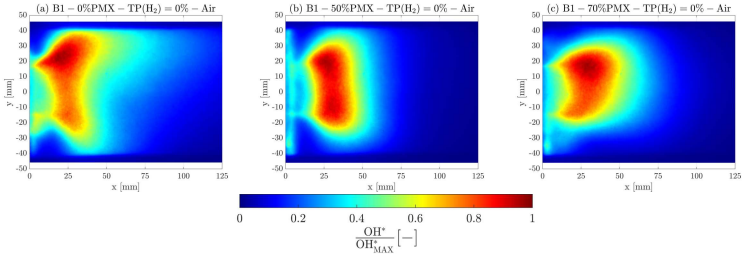

Figure 7.13: Normalized OH chemiluminescence images for B1 configuration*

holes, leading to the highly asymmetric reaction zone observed in Figure 7.10d. The same condition is also reported in Figure 7.13, along with OH* distributions at increasing premix levels for pure natural gas operation and without EGR, to highlight a problematic behavior encountered at these conditions. It can be seen that part of the reaction zone is attached to the dome, with considerable radial extension. An explanation of this behavior can be found in the low pilot jet exit velocity, which decreases with the premix fraction and causes part of the pilot fuel to remain trapped in the outer recirculation zone, reacting with the dome effusion cooling air. This leads to an important thermal load on the dome, which has been evaluated for all the investigated configurations with the temperature measurements reported in Figure 7.14. Values are measured on the dome cold side, with a thermocouple installed near the liner walls, as reported in the schematic. In general, all the configurations show a decreasing trend with higher premix fractions, because the flame closes towards the burner axis, therefore reducing the thermal load at higher radius where the thermocouple is located. B4 configuration with higher jet velocity shows the lowest thermal load on the dome, as the flame is more lifted, with negative consequences on combustion stability, confirmed by LBO measurements. Configuration B1, however, stands out with a different trend and significantly higher temperature values measured when the premix fraction exceeds a certain threshold, because of the behavior highlighted above by chemiluminescence images. Further

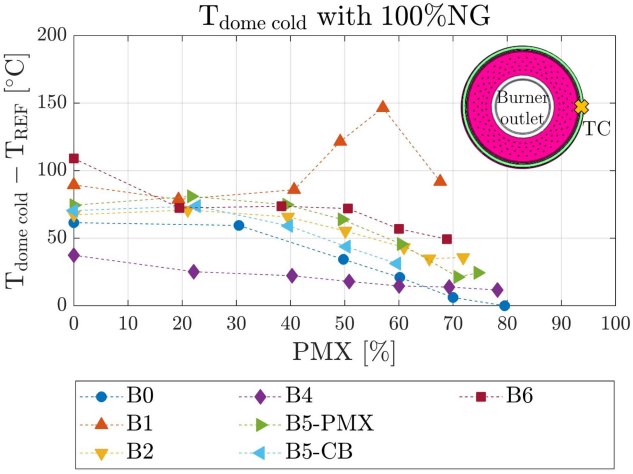

Figure 7.14: Temperature measured on the dome cold side for 100%NG and TP_{REF}

increasing the premix does not lead to an increase in the measured temperature, probably because the small differences in the holes exit cause a non-symmetrical distribution of the reaction zone, as it can be observed in Figure 7.13c, and only a single thermocouple is present. Overall no damages or alterations were detected, neither on the burner outlet or on the dome. At engine conditions such behavior would be aggravated, indeed compromising the combustor integrity, and managing this effect would require a dedicated design of the cooling system. The reduced jet penetration, causing the pilot fuel to react near the dome, beside the drawback of high dome temperature, is instead beneficial in terms of blow out resistance, and indeed, B1 is able to reach the leanest conditions without blow out among the different configurations for both premix splits. When the pilot fuel mass flow rate is decreased approaching lean blow out, the jet velocity is even lower, and the flame stabilizes attached to the dome in the low velocity area of the outer recirculation zone, where the reaction is able to sustain also in globally very lean conditions. This

very high lean blow out resistance with the flame attached to the dome further confirms the crucial role of the outer recirculation zone in the flame stabilization, discussed earlier. Indeed, also in EGR conditions the flame is able to stabilize closer to the burner outlet and the overall length is reduced compared to the other configurations (see Fig. 7.10f).
The maximum premix fraction stably achievable is lower than the baseline case with natural gas (Fig. 7.2), and has not been tested with hydrogen addition. In simulated EGR, no thermoacoustic instabilities occurred for the tested conditions with PMX up to 60%.
Also emission measurements in standard conditions show a problematic behavior at low premixing, where the influence of the pilot jets plays a greater role. NO_x values are higher than for the other configurations (see Fig. 7.6b), indicating poor mixing. The upper axis limit of Figure 7.6a is 100 ppm to be able to distinguish the behavior of the different configurations. Figure 7.15 shows the emissions of B1 compared with the baseline case, with increased scale in order to fit the very high CO values recorded for this configuration. CO emissions still show a minimum with premix fraction, but moving to lower premix levels the increase is much more pronounced than for the other configurations.
Also in EGR conditions, CO emissions strongly vary with the premix fraction: the highest and lowest recorded value among all the configurations correspond to B1 at 40%PMX and 60%PMX respectively (see Fig. 7.7a). The high resistance to blow out with standard air is accompanied by low CO levels, as far as the premix fraction is sufficiently high. In addition to the problems encountered in standard conditions with the flame attached to the dome, this wide variation in CO levels with premix level is not very attracting for the burner stable operation.
Overall, B1 performance is mainly driven by the low exit velocity of the pilot jets, which can cause uncontrolled reactive conditions involving the dome cooling air. On the other hand, the use of dedicated jets from the dome could be an interesting configuration to take advantage of some of the positive features outlined in this section, as the improved flame stability at low thermal power. This aspect opens up potential for new

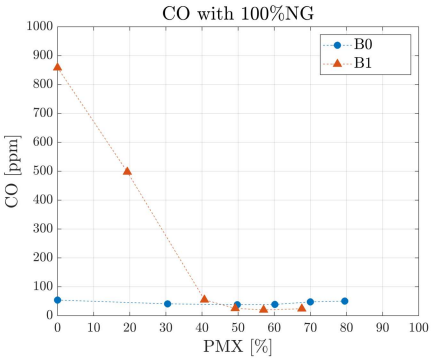

Figure 7.15: CO emissions for B0 and B1 with 100%NG and standard air

burner layouts, implying substantial modifications that must be carefully considered, and are beyond the scope of the present work.

These results emphasize the important role played by the external recirculation zone in conditioning the flame behavior. In absence of an inner recirculation zone due to the low swirl component generated by the counter-rotating swirlers, the radical transport through the outer recirculation zone becomes the fundamental flame stabilization process, as vortices that are formed in the corner of the combustion chamber provide hot products to the flame base.
In general, higher pilot jet velocity worsens the lean blow out margin because of higher local strain. The results derived for configuration B1 as described in this sub-chapter suggest that when fuel remains trapped in this external recirculation zone, the blow out resistance is improved, and this can be achieved both with higher jet orientation in outward direction (B6) or with lower jet velocity (B1). At the same time, in these conditions the flame is more prone to thermoacoustic instabilities. Indeed, varying the pilot jets modifies the fuel distribution in this area, affecting the recirculation rate and the recirculated flow composition, and consequently the fluctuations that may arise.

The structure and size of the outer recirculation zone mainly depend on the chamber geometry and the burner confining ratio, although operating conditions also have a certain influence, as seen from the velocity field measurements in the previous chapters. In gas turbine engines, this burner is generally operated in annular combustors, where the flame confinement and therefore the flow field are completely different, and interaction between adjacent burners occurs. It is difficult to predict the behavior of the flame in such a complex context, but the present outcomes suggest that exploiting greater interaction between pilot jets and the external recirculation zone could have positive implications on the burner performance.

7.5 Effect of the number pilot holes

The effect of doubling the number of pilot jets was studied with configuration B2, with premixed injection in the outer swirler. The pilot jets' exit velocity is nominally the same as for the baseline configuration, as the diameter of the holes has been reduced in order to match the same total geometric area.

The double number of jets with half the original mass flow rate makes the fuel distribution along the annulus of the burner more homogeneous, and reduces the jet penetration. The lean blow out resistance is better than the baseline configuration, but it is almost the same as for the B5-PMX case, which has the same premix system. Therefore, the specific effect of the pilot holes number is limited, and the main difference in terms of blow out margin comes from the enhanced interaction between pilot and premixed fuel that is established with the injection of the premixed fuel in the outer swirler.

Looking at the flame structure, unexpectedly, the fully diffusive case (Fig. 7.10g) is more lifted than the baseline case, and similar to B5-PMX with all jets oriented outwards. Increasing the premix fraction, B2 layout gives rise to a more compact flame (h), almost identical to B5-PMX (n), with improved stability at leaner conditions compared to the

baseline case, but more susceptible to local mixture fluctuations causing instabilities. Indeed, the dynamic behavior is worse than B0, and unstable conditions are approached for lower premix fractions, also with hydrogen addition. As previously highlighted, a high LBO margin is associated with a narrower window of stably reachable premix fractions. In this case, the effect of varying only the number of holes can be observed by comparing configuration B2 with configuration B5-PMX in terms of oscillation amplitude as function of the premix fraction (without EGR). It is noticeable that, with a higher number of holes, the dynamic behavior appears to worsen, with the emergence of a first peak around 60%PMX (Fig. 7.2c). This is slightly visible also for B1 and B4, but more intense. The emissions in standard conditions benefit from the improved mixing, with significantly lower CO and same NO_x levels than the baseline case. Lower CO is recorded also in EGR conditions, making this configuration one of the most promising, close to B5-PMX configuration. Overall, the effect of the number of holes is limited, as B2 performance is very similar to that of B5-PMX configuration.

7.6 Performance summary

All data presented in this chapter constitute an extensive data set characterizing the performance of the tested configurations. To provide a final synthesis, the variation of key performance parameters for each configuration was evaluated relative to the baseline case. Specifically, the following metrics were analyzed:

- LBO Air: Thermal power at lean blow out with standard air at 50%PMX
- P" NG Air: Stable premix limit achievable with natural gas
- P" H_2 Air: Stable premix limit achievable with pure hydrogen pilot jets
- NO_x Air: NO_x emissions under standard conditions with 100%NG averaged over different premix fractions

- CO Air: CO emissions under standard conditions with 100%NG averaged over different premix fractions
- NO_x EGR: NO_x emissions with simulated EGR at 50%PMX and TP(H_2)=5%
- CO EGR: CO emissions with simulated EGR at 50%PMX and TP(H_2)=5%

Regarding emissions in the case of EGR, all compared values were obtained under the same conditions. The values with air were measured at different fuel splits and averaged for each configuration. The tested split levels are similar across the various configurations, and averaging the values should not significantly affect the results. For pressure oscillations, an amplitude threshold was defined to evaluate stability. Although this threshold is arbitrary, it was considered a suitable approach, given the similar behavior of all burners tested. The dynamic behavior under EGR conditions is challenging to quantify due to the variations across all the different operating parameters, and thus has not been captured with a single metric. A qualitative description of the observed behavior is provided in the previous sections.
The variation of these parameters with respect to the baseline case has been scaled with the maximum variation of each quantity, to allow a better visualization of the differences, and to be able to present different aspects in a single plot. These parameters were defined based on the specific conditions investigated and the type of analysis performed, and serve primarily to offer a general indication of each configuration's behavior relative to the baseline case. Figure 7.16 shows a summary of all configurations for each parameter. This avisualization supports the identification of the most promising solutions for each aspect, highlighting the best configurations and the influence of geometric parameters. In particular, it is evident that nearly all configurations show improved performance in terms of lean blowout margin and CO emissions with EGR. The latter is the most important parameter for this application, as it represents the primary operational limit. However, the dynamic behavior is adversely

affected, with pressure oscillations at high premix ratios occurring earlier compared to the baseline configuration, both with natural gas and with the addition of hydrogen.

Figure 7.17 summarizes all performance parameters for each configuration, allowing to identify the most critical and the most promising aspects for each configuration, and providing valuable insight into where optimization efforts might be most effective. As noted earlier, it is observed that configurations with better lean blowout margins tend to exhibit worse dynamic stability.

Among the parameters analyzed, CO emissions under EGR conditions stand out as the most relevant for the target application of this research. This metric's significance is rooted in its direct impact on quantifying the low-emission goals with high EGR rates, central to the final objectives of this work. Defining a single performance indicator that encompasses all relevant parameters could provide a more nuanced understanding of configuration behavior, streamlining the comparison and selection of optimal setups. In order to do that, it would be necessary to define a weight-function for each performance parameter, reflecting their varying importance within different operational contexts. This function would allow for the synthesis of multiple performance criteria into a single composite metric, enabling a clearer assessment of each configuration's effectiveness and advancing the pathway toward practical implementation. Defining a comprehensive weighting function presents considerable challenges due to the need to account for numerous performance parameters, each influenced by a wide range of operating conditions. In order to maintain a general approach, the present study has not developed such method. Instead, it has focused on analyzing the variations of individual parameters and examining their correlation with the geometry of the injection system, yielding important and valuable insights into the flame behavior both in standard operation and under the challenging conditions caused by EGR.

Overall, some configurations demonstrate promising results, outperforming others. Among these, B5-PMX layout appears to be the most effective

solution investigated, featuring premix fuel injected into the outer swirler and axisymmetric pilot jets oriented outward at the same angle as the baseline. The B2 configuration also shows potential, with an improved pilot fuel distribution due to the increased number of holes. However, both configurations exhibit significantly worse dynamic stability limits compared to the baseline, an issue that will need to be addressed in future developments.

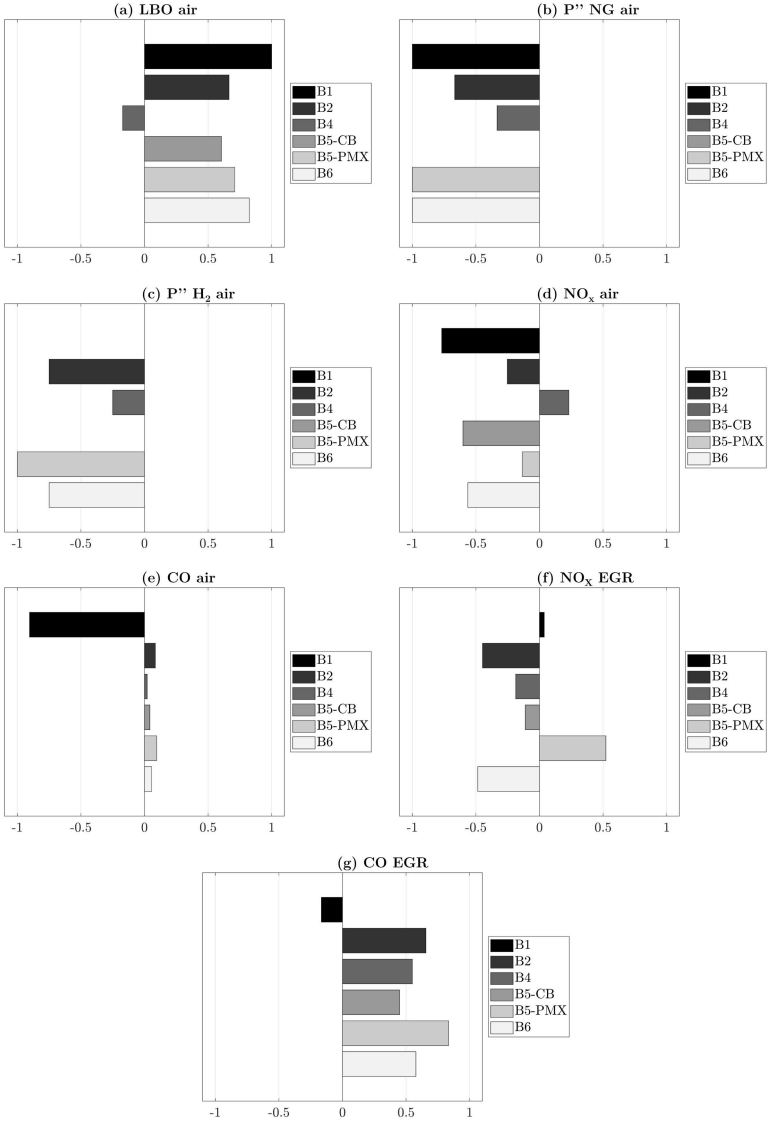

Figure 7.16: Performance summary for each parameter relative to baseline case

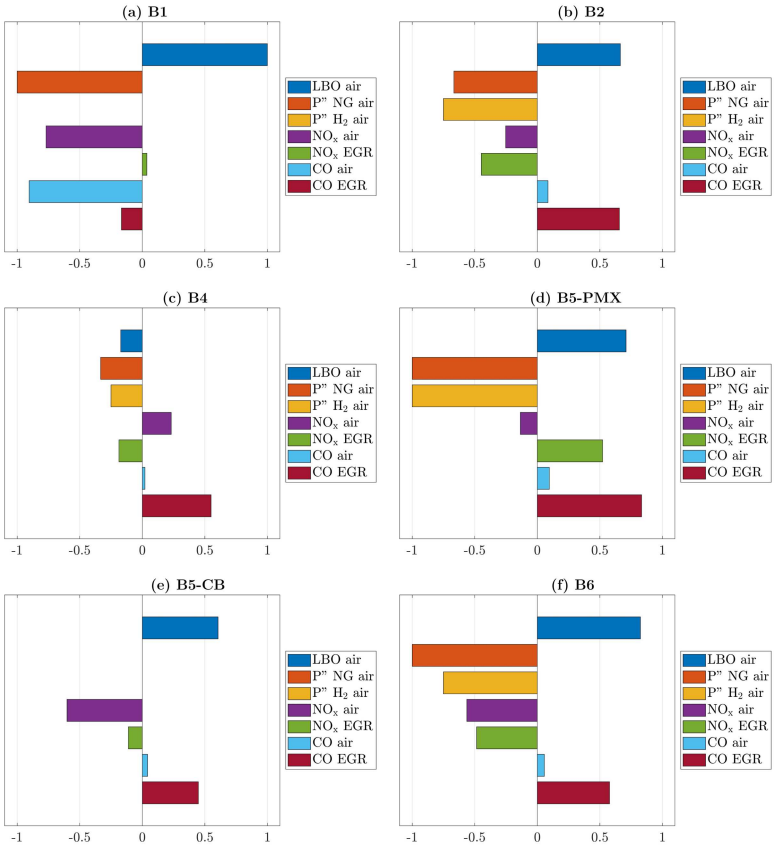

Figure 7.17: Performance summary for each configuration

Conclusions

The present work collects a large part of the activities performed during the Ph.D. project, focusing on the topic of combustion under EGR-like conditions. In this conclusive chapter, the main findings of this investigation are presented, offering a brief overview of the study, summarizing the main achievements, and discussing the potential impact of these outcomes for future work.

This study is part of a wider European research and development project framework, focused on the coupling between gas turbine power plants and carbon capture units, that can be improved through the use of high EGR rates. The studied and presented approach allows to increase the CO_2 content in the gas turbine exhaust gases, with beneficial effects on the efficiency of CCS systems. As a drawback, high EGR rates create challenging conditions in the gas turbine combustor, because of the reduced oxygen content available for combustion.
In the literature, studies on EGR application in gas turbines are relatively limited, as interest in this topic has only recently reemerged with the prospect of improving the efficiency of carbon capture systems. In addition to numerical and experimental research on more fundamental configurations, investigations on gas turbines at engine conditions have proven that, beside benefits in terms of lower NO_x emissions, oxygen depletion hinders combustion efficiency and drastically increases CO and unburned hydrocarbons, highlighting the need to advance current combustion technologies in order to improve performance under these conditions.

The present work fits in this context, with the aim to contribute to the development and optimization of gas turbines burners able to operate efficiently under unconventional conditions, such as EGR. Such a complex combustion environment, regardless of the significant improvements in terms of reliability of computational models, requires dedicated experimental investigations supporting the design process. However, testing at close to engine conditions is extremely expensive, especially when optical diagnostics is involved. Experimental tests at ambient pressure can be considered the first step of a design improvement to be placed inside the more general framework of the project, allowing exploration of multiple configurations efficiently. In particular, a well established design of an industrial burner from Baker Hughes has been tested in a single sector optical test rig at the THT Lab of the University of Florence, in conditions that reproduce the lack of oxygen caused by EGR. Optical diagnostics techniques such as Particle Image Velocimetry and OH* chemiluminescence imaging have been employed to analyze the flame behavior and understand the effects of various control parameters on the structure of the reaction zone, providing important insights into the implications for pollutant emissions and stability limits.

The investigated burner concept is an aero-derivative design, composed by a double counter-rotating swirler and a converging duct that accelerates the flow. Regarding fuel injection, the burner features two independent fuel lines: a premix system that injects natural gas in the outer swirler and diffusive pilot jets that provide stability, anchoring the combustion process. In standard operation, the fuel split between these lines is adjusted to achieve stable combustion and maintain low emissions with variable engine load. Reactive tests were conducted in a cylindrical chamber enclosed in an outer vessel with optical access, operated at ambient pressure.

The analysis begins with the characterization of the baseline configuration of the burner under conventional conditions without EGR, to understand the mechanisms of flame stabilization and the impact of the fuel split. Measurements of the reactive flow field revealed the absence of an internal recirculation zone because of the low swirl component generated by the

counter-rotating swirlers, and a jet-like flow field is established. The flame stabilizes at the boundary of the external recirculation zone, where the fuel/air mixture effectively gets into contact with hot reaction products in the turbulent shear layer between incoming fresh mixture and recirculated reaction products. Indeed, the external recirculation zone provides heat and activated radicals, which are essential for sustaining combustion stability. Even with an increased premix split, the flame remains anchored at the pilot jet locations, underscoring the critical role of the pilot fuel in maintaining stability under diverse operating conditions. Indeed, the stability margin decreases at higher premix fractions, although these conditions correspond to the lowest NO_x emissions. This trade-off highlights the complex relationship between premix levels and combustion stability, as the enhancement in mixing that leads to reduced NO_x emissions comes at the expense of flame instability.

In the fully diffusive case, the flame is lifted, and as the premix fraction increases, it moves closer to the burner exit and shortens in length. However, with further increase of the premix fraction, the reaction zone detaches again, ultimately leading to an unstable condition when the premix exceeds 80%. In these conditions, the flame becomes elongated and is subject to significant thermoacoustic oscillations, drawing the attention to the challenges associated with high premix levels in maintaining stable combustion. The CO emissions exhibit a non-monotonic relationship with fuel split, displaying a minimum value. This behavior can likely be explained by the previously mentioned dynamics of flame lift-off, which results from a combination of mixing effects and strain due to the high velocities of the main flow jet. As the flame transitions from being lifted to more anchored positions with varying premix fractions, the changes in mixing and combustion conditions contribute to this non-linear CO emission profile.

In order to improve flame stability, the injection of hydrogen has been explored with the final purpose to allow higher levels of EGR to be stably achieved. The amount of hydrogen is limited by the associated reduction of CO_2 in the exhaust gases and has been maintained at less than 10%

of the total thermal power for most part of the investigation. The effect of hydrogen addition in the pilot diffusive fuel line has been evaluated also in standard conditions, and, despite the limited amount, positive consequences were encountered in terms of improved lean blow out margin and higher premixing level stably achievable. This last aspect can be exploited to achieve very low NO_x emissions thanks to enhanced mixing reached with higher premixing levels. Adding hydrogen brings the flame closer to the burner exit, which enhances flame stability. However, this adjustment also increases the thermal load on the burner and combustion chamber dome. This aspect must be carefully considered, especially under engine-like conditions, where this behavior is exacerbated. The increased thermal load resulting from the closer proximity of the flame can lead to greater stresses on the components, potentially impacting their performance and lifespan. Therefore, it is crucial to find the optimal compromise that leverages the stability improvements associated with hydrogen without compromising the integrity of the components, ensuring reliable and efficient operation. In this regard, employing a blend of natural gas and hydrogen on the pilot line can be beneficial.

In the present investigation, EGR conditions have been reproduced by lowering the oxygen content of the oxidizer, diluting the combustion air with CO_2. This results in a high CO_2 concentration in the oxidizer, influencing combustion from various perspectives. A dedicated study was performed to assess the consequences of this experimental strategy. The oxidizer composition has been computed, using the inlet oxygen fraction as an analogy for experimental conditions when EGR is implemented in a real gas turbine. Numerical tools were employed to investigate how the oxidizer composition affects laminar flame speed and extinction strain rate, revealing that CO_2 dilution creates more challenging conditions for flame stability compared to actual EGR. Dedicated experimental tests were conducted using nitrogen to lower the oxygen content instead of CO_2 for comparison. While differences in flame structure were limited, CO emissions were significantly impacted, with high levels attributed to CO_2 dissociation due to the high concentration in the oxidizer flow feeding

the burner, confirming previous literature results. CO_2 dilution led to more stable behavior in terms of pressure oscillations, while N_2 dilution resulted in stronger fluctuations, with higher oscillation amplitude. Overall, using CO_2 dilution for experimental tests, while not fully rigorous, is a conservative approach, particularly concerning CO emissions. This method allows for convenient storage management with the given infrastructure, which can be exploited to explore a wide range of conditions while minimizing the demand of experimental testing. Therefore, it has been considered suitable for the present preliminary screening of various burner configurations and solutions.

Once the effects of CO_2 dilution on the experimental results have been evaluated, the characterization of the burner under simulated EGR conditions has been carried out. OH* chemiluminescence imaging revealed that with low oxygen content the reaction zone lifts and spreads out. This results in a major decrease in NO_x emissions, with levels dropping sharply also with a limited oxygen reduction, and showing a reduced dependence on fuel split. On the other hand, CO emissions rise significantly with simulated EGR, especially at low oxygen levels, partially because of the high CO_2 concentration in the oxidizer. A minimum is recorded at intermediate premix split, reaching conditions where the flame is able to stabilize slightly closer to the burner exit. Overall, the results confirm trends previously observed in the literature, such as lower NO_x emissions and higher CO levels. Additionally, the collected data highlight that fuel split can actively contribute to mitigating the adverse effects of EGR, in a manner similar to engine load regulation. While high premix fractions are beneficial under standard conditions for reducing NO_x emissions, lower premixing levels can be adopted in EGR conditions without resulting in a detrimental increase in NO_x emissions. Changes in dynamic behavior were observed in EGR conditions, with the onset of thermoacoustic instabilities displaying a non-monotonic dependence on oxygen levels. At elevated premix fractions, the flame is more susceptible to thermoacoustic instabilities, resulting in larger oscillation amplitudes.

One of the main novelties investigated in this work is the injection of

hydrogen, with the purpose of enhancing flame stability and supporting natural gas combustion in an oxygen-depleted environment, taking advantage of the high reactivity of hydrogen to reduce the negative effects of EGR. The beneficial effect in reducing pressure oscillation that was observed in standard conditions is also encountered at lower oxygen level, widening the burner operability window with EGR. Overall, the results indicate that the addition of hydrogen, whether blended with natural gas or injected pure, allows the flame to stabilize closer to the burner outlet. This positively impacts the reduction of high CO levels associated with EGR conditions.
In addition to hydrogen injection, the research analyzed the effect of the fuel injection mode, with particular focus on the pilot jets, which play a critical role in stabilizing the flame within the burner's primary zone. Different injection systems were tested for a total of 7 configurations including the baseline case, analyzing how variations in geometric features affect flame stability and emissions. The results highlight the critical role of the external recirculation zone in influencing the flame behavior, particularly in the absence of an inner recirculation zone due to low swirl from the counter-rotating swirlers. When fuel is retained in this zone thanks to a larger orientation of the pilot jets towards the combustor wall, the blowout resistance improves, but the flame also becomes more susceptible to thermoacoustic instabilities. Modifying the premix fuel injection point also positively affects CO emissions and lean blow out margin, at the cost of lower dynamic stability.

In conclusion, the present study remarks the importance of dedicated experimental investigations to understand the flame behavior and stabilization mechanisms, with the final purpose of enhancing the performance of modern combustion systems under unconventional and demanding operating conditions. The collected results allow for an understanding of the influence of control parameters and how they can be leveraged for effective operation with EGR. They also highlighted the positive effects of hydrogen addition and the impact of fuel injection methods, providing

valuable insights for optimizing designs to work under these conditions. In addition, interesting considerations regarding the use of CO_2 dilution to simulate EGR have been identified, which can be useful for other experimental studies aiming to conduct tests under EGR conditions. Finally, the extensive data gathered during this work could be valuable for validating numerical models, particularly when analyzing unstable phenomena such as lean blowout or non-conventional conditions involving oxidant mixtures with reduced oxygen levels. The combustion regimes resulting from the dual fuel operation into an oxygen-depleted environment are particularly challenging to predict. Thus, numerical models can greatly benefit from dedicated experimental investigations using optical diagnostics.

Within the Transition project, a restricted number of the presented burner configurations will be subjected to testing at high pressure, along with new designs optimized through CFD analysis utilizing the data gathered in this study. In parallel, numerical models will be refined and validated against experimental data obtained both at atmospheric and elevated pressures on single-sector test rigs. These validated models will not only reproduce real engine geometries and operating conditions with high fidelity, but will also serve as a fundamental tool for the exploration of innovative design solutions and operating strategies, accelerating the development of burners with improved performance. Both the experimental and numerical activities involve an increase in the complexity of the setup and simulation frameworks, aiming for a more accurate representation of the conditions experienced in real combustion systems. As a result, the research will provide deeper insights into burner performance and stability, enabling a more reliable prediction of complex phenomena such as flame stabilization, pollutant formation, and dynamic behavior under high EGR conditions. Ultimately, this approach will contribute to the development of more efficient and robust combustion technologies capable of meeting the stringent requirements of future low-emission engines.

List of Figures

List of Tables

Bibliography

[1] Zheng, Ming, Reader, Graham T., and Hawley, J.Gary. "Diesel engine exhaust gas recirculation: a review on advanced and novel concepts." *Energy Conversion and Management*, 45(6):883–900, 2004. ISSN 0196-8904. doi: 10.1016/S0196-8904(03)00194-8.

[2] Lieuwen, T., Chang, M., and Amato, A. "Stationary gas turbine combustion: Technology needs and policy considerations." *Combustion and Flame*, 160(8):1311–1314, 2013. doi: 10.1016/J.COMBUSTFLAME.2013.05.001.

[3] Li, Hailong, Ditaranto, Mario, and Berstad, David. "Technologies for increasing CO_2 concentration in exhaust gas from natural gas-fired power production with post-combustion, amine-based CO_2 capture." *Energy*, 36(2):1124–1133, 2011. ISSN 0360-5442. doi: 10.1016/j.energy.2010.11.037.

[4] IEA. World Energy Outlook 2024. Technical report, IEA, Paris, France, 2024.

[5] Vantaggiato, E., Riboldi, L., Anantharaman, R., Carcasci, C., Andreini, A., Roussanaly, S., and Ditaranto, M. "Understanding the Potential and the Challenges of a NGCC Integrated With Hydrogen-Assisted EGR and CO_2 Capture." *ASME Conference Proceedings*, 2024. doi: 10.1115/GT2024-125639.

[6] Burnes, D., Saxena, P., and Dunn, P. "Study of Using Exhaust

Gas Recirculation on a Gas Turbine for Carbon Capture." *ASME Conference Proceedings*, 2020. doi: 10.1115/GT2020-16080.

[7] Elkady, A. M., Evulet, A., Brand, A., Ursin, T. P., and Lynghjem, A. "Exhaust Gas Recirculation in DLN F-Class Gas Turbines for Post-Combustion CO_2 Capture." *ASME Conference Proceedings*, 2008. doi: 10.1115/GT2008-51152.

[8] Røkke, Petter and Hustad, Johan. "Exhaust Gas Recirculation in Gas Turbines for Reduction of CO_2 Emissions; Combustion Testing with Focus on Stability and Emissions." *International Journal of Thermodynamics*, 8:167–173, 2005. doi: 10.5541/IJOT.1034000158.

[9] Evulet, A. T., Elkady, A. M., Branda, A. R., and Chinn, D. "On the performance and operability of GE's dry low NO_x combustors utilizing exhaust gas recirculation for post-combustion carbon capture." *Energy Procedia*, 1:p. 3809–3816, 2009. doi: 10.1016/j.egypro.2009.02.182.

[10] Elkady, A., Evulet, A., Brand, A., Ursin, T., and Lynghjem, A. "Application of Exhaust Gas Recirculation in a DLN F-Class Combustion System for Postcombustion Carbon Capture." *Journal of Engineering for Gas Turbines and Power*, 131:034505, 2009. ISSN 0742-4795. doi: 10.1115/1.2982158.

[11] Li, H., Elkady, A., and Evulet, A. "Effect of Exhaust Gas Recirculation on NO_x Formation in Premixed Combustion System." *Proceeding of 47th AIAA Aerospace Sciences Meeting including the New Horizons Forum and Aerospace Exposition*, 2009. doi: 10.2514/6.2009-226.

[12] Elkady, A., Brand, A., Vandervort, C. L., and Evulet, A. "Exhaust Gas Recirculation Performance in Dry Low Emissions Combustors." *ASME Conference Proceedings*, 2011. doi: 10.1115/GT2011-46482.

[13] Burdet, A., Lachaux, T., de la Cruz Garcia, M., and Winkler, D. "Combustion Under Flue Gas Recirculation Conditions in a Gas

Turbine Lean Premix Burner." *ASME Conference Proceedings*, 2010. doi: 10.1115/GT2010-23396.

[14] Yu, B., Lee, S., and Lee, C. "Study of NO_x emission characteristics in CH_4/air non-premixed flames with exhaust gas recirculation." *Energy*, 91:119–127, 2015. doi: 10.1016/j.energy.2015.08.023.

[15] Bellas, J., Finney, K., Diego, M., Ingham, D., and Pourkashanian, M. "Experimental investigation of the impacts of selective exhaust gas recirculation on a micro gas turbine." *International Journal of Greenhouse Gas Control*, 90:102809, 2019. doi: 10.1016/j.ijggc.2019.102809.

[16] Rosec, Ž., Katrašnik, T., Žvar Baškovič, U., and Seljak, T. "Exhaust gas recirculation with highly oxygenated fuels in gas turbines." *Fuel*, 278:118285, 2020. doi: 10.1016/j.fuel.2020.118285.

[17] Konishi, Noriyuki, Kitagawa, Kuniyuki, Arai, N., and Gupta, Ashwani Kumar. "Temporally resolved two-dimensional spectroscopic study on the effect of highly preheated and low oxygen concentration air on combustion." *Journal of Engineering for Gas Turbines and Power*, 125(1):326–331, 2002. ISSN 0742-4795. doi: 10.1115/1.1520155.

[18] Kobayashi, Hideaki, Hagiwara, Hirokazu, Kaneko, Hideaki, and Ogami, Yasuhiro. "Effects of CO_2 dilution on turbulent premixed flames at high pressure and high temperature." *Proceedings of the Combustion Institute*, 31:1451–1458, 2007. ISSN 1540-7489. doi: 10.1016/j.proci.2006.07.159.

[19] Cohé, Cécile, Chauveau, Christian, Gökalp, Iskender, and Kurtuluş, Dilek Funda. "CO_2 addition and pressure effects on laminar and turbulent lean premixed CH_4 air flames." *Proceedings of the Combustion Institute*, 32(2):1803–1810, 2009. ISSN 1540-7489. doi: 10.1016/j.proci.2008.06.181.

[20] Askari, O., Vien, K., Wang, Z., Sirio, M., and Metghalchi, H. "Exhaust gas recirculation effects on flame structure and laminar burning speeds of H_2/CO/air flames at high pressures and temperatures." *Applied Energy*, 179:451–462, 2016. doi: 10.1016/j.apenergy.2016.06.118.

[21] Lipardi, A. C., Versailles, P., Watson, G. M., Bourque, G., and Bergthorson, J. M. "Experimental and numerical study on NO_x formation in CH_4–air mixtures diluted with exhaust gas components." *Combustion and Flame*, 179(C):325–337, 2017. doi: 10.1016/j.combustflame.2017.02.009.

[22] Shen, Wenkai, Xing, Chang, Liu, Haiqing, Liu, Li, Hu, Qiming, Wu, Guohua, Yang, Yujia, Wu, Shaohua, and Qiu, Penghua. "Exhaust gas recirculation effects on flame heat release rate distribution and dynamic characteristics in a micro gas turbine." *Energy*, 249:123680, 2022. ISSN 0360-5442. doi: 10.1016/j.energy.2022.123680.

[23] Rodriguez Camacho, J., Akiki, M., Blust, J., and O'Connor, J. "Effect of Inert Species on the Static and Dynamic Stability of a Piloted, Swirl-Stabilized Flame." *Journal of Engineering for Gas Turbines and Power*, 146(6):061021, 2024. ISSN 0742-4795. doi: 10.1115/1.4064048.

[24] Jiang, Yuanjie, del Alamo, Gonzalo, Gruber, Andrea, Bothien, Mirko R., Seshadri, Kalyanasundaram, and Williams, Forman A. "A skeletal mechanism for prediction of ignition delay times and laminar premixed flame velocities of hydrogen-methane mixtures under gas turbine conditions." *International Journal of Hydrogen Energy*, 44(33):18573–18585, 2019. ISSN 0360-3199. doi: 10.1016/j.ijhydene.2019.05.068.

[25] Bougrine, S., Richard, S., Nicolle, A., and Veynante, D. "Numerical study of laminar flame properties of diluted methane-hydrogen-air flames at high pressure and temperature using detailed chemistry."

Fuel and Energy Abstracts, 36:12035–12047, 2011. doi: 10.1016/j.ijhydene.2011.06.053.

[26] Beerer, D., McDonell, V., Therkelsen, P., and Cheng, R. K. "Flashback and Turbulent Flame Speed Measurements in Hydrogen/Methane Flames Stabilized by a Low-Swirl Injector at Elevated Pressures and Temperatures." *Journal of Engineering for Gas Turbines and Power*, 136(3):031502, 2013. ISSN 0742-4795. doi: 10.1115/1.4025636.

[27] Marshall, A., Lundrigan, J., Venkateswaran, P., Seitzman, J., and Lieuwen, T. "Measurements of Stretch Statistics at Flame Leading Points for High Hydrogen Content Fuels." *Journal of Engineering for Gas Turbines and Power*, 139(11):111503, 2017. ISSN 0742-4795. doi: 10.1115/1.4035819.

[28] Anderson, David N. "Effect of hydrogen injection stability and emissions of an experimental premixed prevaporized propane burner." *NASA technical report*, 1975. URL `https://api.semanticscholar.org/CorpusID:92112523`.

[29] Oztarlik, G., Selle, L., Poinsot, T., and Schuller, T. "Suppression of instabilities of swirled premixed flames with minimal secondary hydrogen injection." *Combustion and Flame*, 214:266–276, 2020. doi: 10.1016/j.combustflame.2019.12.032.

[30] Barbosa, Séverine, de La Cruz Garcia, Marta, Ducruix, Sébastien, Labegorre, Bernard, and Lacas, François. "Control of combustion instabilities by local injection of hydrogen." *Proceedings of the Combustion Institute*, 31(2):3207–3214, 2007. ISSN 1540-7489. doi: 10.1016/j.proci.2006.07.085.

[31] Cheng, R., Littlejohn, D., Strakey, P., and Sidwell, T. "Laboratory investigations of a low-swirl injector with H_2 and CH_4 at gas turbine conditions." *Proceedings of the Combustion Institute*, 32:3001–3009, 2008. doi: 10.1016/j.proci.2008.06.141.

[32] Shanbhogue, S.J., Sanusi, Y.S., Taamallah, S., Habib, M.A., Mokheimer, E.M.A., and Ghoniem, A.F. "Flame macrostructures, combustion instability and extinction strain scaling in swirl-stabilized premixed CH_4/H_2 combustion." *Combustion and Flame*, 163:494–507, 2016. ISSN 0010-2180. doi: 10.1016/j.combustflame.2015.10.026.

[33] Aguilar, J., Æsøy, E., and Dawson, J. "The influence of hydrogen on the stability of a perfectly premixed combustor." *Combustion and Flame*, 245:112323, 2022. doi: 10.1016/j.combustflame.2022.112323.

[34] Terhaar, S., Krüger, O., and Paschereit, C. "Flow Field and Flame Dynamics of Swirling Methane and Hydrogen Flames at Dry and Steam-Diluted Conditions." *Journal of Engineering for Gas Turbines and Power*, 137:041503, 2015. doi: 10.1115/1.4028392.

[35] Beita, J., Talibi, M., Sadasivuni, S., and Balachandran, R. "Thermoacoustic Instability Considerations for High Hydrogen Combustion in Lean Premixed Gas Turbine Combustors: A Review." *Hydrogen*, 2(1):33–57, 2021. ISSN 2673-4141. doi: 10.3390/hydrogen2010003.

[36] Natarajan, J., Lieuwen, T., and Seitzman, J. "Laminar flame speeds of H_2/CO mixtures: Effect of CO_2 dilution, preheat temperature, and pressure." *Combustion and Flame*, 151:104–119, 2007. doi: 10.1016/j.combustflame.2007.05.003.

[37] García-Armingol, Tatiana and Ballester, Javier. "Influence of fuel composition on chemiluminescence emission in premixed flames of $CH_4/CO_2/H_2/CO$ blends." *International Journal of Hydrogen Energy*, 39(35):20255–20265, 2014. ISSN 0360-3199. doi: 10.1016/j.ijhydene.2014.10.039.

[38] Banerjee, R., Roy, S., and Bose, P. K. "Hydrogen-egr synergy as a promising pathway to meet the pm–NO_x–bsfc trade-off contingencies

of the diesel engine: A comprehensive review." *International Journal of Hydrogen Energy*, 40(37):12824–12847, 2015.

[39] Du, Y., Yu, X., Liu, L., Li, R., Zuo, X., and Sun, Y. "Effect of addition of hydrogen and exhaust gas recirculation on characteristics of hydrogen gasoline engine." *International Journal of Hydrogen Energy*, 42(12):8288–8298, 2017.

[40] Chaichan, M. T. "Performance and emission characteristics of CIE using hydrogen, biodiesel, and massive EGR." *International Journal of Hydrogen Energy*, 43(10):5415–5435, 2018.

[41] Rodriguez Camacho, J., Le, D., Blust, J., and O'Connor, J. "Impact of Diluents on Flame Stability With Blends of Natural Gas and Hydrogen." *Journal of Engineering for Gas Turbines and Power*, 147(1):011017, 2024. ISSN 0742-4795. doi: 10.1115/1.4066246.

[42] Fackler, K., Karalus, M., Novosselov, I., Kramlich, J., and Malte, P. "Experimental and Numerical Study of NO_x Formation From the Lean Premixed Combustion of CH_4 Mixed With CO_2 and N_2." *Journal of Engineering for Gas Turbines and Power*, 133, 2011. doi: 10.1115/GT2011-45090.

[43] Halter, F., Foucher, F., Landry, L., and Mounaïm-Rousselle, C. "Effect of Dilution by Nitrogen and/or Carbon Dioxide on Methane and Iso-Octane Air Flames." *Combustion Science and Technology*, 181:813–827, 2009. doi: 10.1080/00102200902864662.

[44] Chan, Y.L., Zhu, M.M., Zhang, Z.Z., Liu, P.F., and Zhang, D.K. "The Effect of CO_2 Dilution on the Laminar Burning Velocity of Premixed Methane/Air Flames." *Energy Procedia*, 75:3048–3053, 2015. ISSN 1876-6102. doi: 10.1016/j.egypro.2015.07.621.

[45] Duva, Berk Can, Chance, Lauren Elizabeth, and Toulson, Elisa. "Dilution effect of different combustion residuals on laminar burning velocities and burned gas Markstein lengths of premixed methane/air

mixtures at elevated temperature." *Fuel*, 267:117153, 2020. ISSN 0016-2361. doi: 10.1016/j.fuel.2020.117153.

[46] Xie, Mingke, Fu, Jianqin, Zhang, Yongxiang, Shu, Jun, Ma, Yinjie, Liu, Jingping, and Zeng, Dongjian. "Numerical analysis on the effects of CO_2 dilution on the laminar burning velocity of premixed methane/air flame with elevated initial temperature and pressure." *Fuel*, 264:116858, 2020. ISSN 0016-2361. doi: 10.1016/j.fuel.2019.116858.

[47] Khalil, Ahmed E.E. and Gupta, Ashwani K. "The role of CO_2 on oxy-colorless distributed combustion." *Applied Energy*, 188:466–474, 2017. ISSN 0306-2619. doi: https://doi.org/10.1016/j.apenergy.2016.12.048.

[48] Williams, T. C., Shaddix, C. R., and and, R. W. Schefer. "Effect of Syngas Composition and CO_2-Diluted Oxygen on Performance of a Premixed Swirl-Stabilized Combustor." *Combustion Science and Technology*, 180:64–88, 2007. doi: 10.1080/00102200701487061.

[49] Kutne, P., Kapadia, B., Meier, W., and Aigner, M. "Experimental analysis of the combustion behaviour of oxyfuel flames in a gas turbine model combustor." *Proceedings of The Combustion Institute*, 33:3383–3390, 2011. doi: 10.1016/j.proci.2010.07.008.

[50] Liu, Fengsham, Guo, Hongsheng, and Smallwood, Gregory J. "The chemical effect of CO_2 replacement of N_2 in air on the burning velocity of CH_4 and H_2 premixed flames." *Combustion and Flame*, 133(4):495–497, 2003. ISSN 0010-2180. doi: 10.1016/S0010-2180(03)00019-1.

[51] Lubrano Lavadera, M., Sabia, P., Sorrentino, G., Ragucci, R., and de Joannon, M. "Experimental study of the effect of CO_2 on propane oxidation in a Jet Stirred Flow Reactor." *Fuel*, 184:876–888, 2016. ISSN 0016-2361. doi: 10.1016/j.fuel.2016.06.046.

[52] Fenning, RW and Tizard, Henry Thomas. "The dissociation of carbon dioxide at high temperatures." *Proceedings of the Royal Society of London. Series A, Containing Papers of a Mathematical and Physical Character*, 115:318–333, 1927.

[53] Wilberforce, Tabbi, Olabi, A.G., Sayed, Enas Taha, Elsaid, Khaled, and Abdelkareem, Mohammad Ali. "Progress in carbon capture technologies." *Science of The Total Environment*, 761:143203, 2021. ISSN 0048-9697. doi: 10.1016/j.scitotenv.2020.143203.

[54] Babazzi, G. *Experimental investigation of novel gas turbine combustor concepts operating with CO_2 vitiated air.* PhD thesis, Universià degli Studi di Firenze, 2022.

[55] Kline, S. J. and McClintock, F. A. "Describing Uncertainties in Single-Sample Experiments." *Mechanical Engineering*, 75:3–8, 1953.

[56] Konnov, Alexander A., Mohammad, Akram, Kishore, Velamati Ratna, Kim, Nam Il, Prathap, Chockalingam, and Kumar, Sudarshan. "A comprehensive review of measurements and data analysis of laminar burning velocities for various fuel+air mixtures." *Progress in Energy and Combustion Science*, 68:197–267, 2018. ISSN 0360-1285. doi: 10.1016/j.pecs.2018.05.003.

[57] Romano, S., Cerutti, M., Riccio, G., Andreini, A., and Romano, C. "Effect of Natural Gas Composition on Low NO_x Burners Operation in Heavy Duty Gas Turbine." *Journal of Engineering for Gas Turbines and Power*, 141(11):114501, 2019. ISSN 0742-4795. doi: 10.1115/1.4044870.

[58] Joshi, N. D., Epstein, M. J., Durlak, S., Marakovits, S., and Sabla, P. E. "Development of a Fuel Air Premixer for Aero-Derivative Dry Low Emissions Combustors." *ASME Conference Proceedings*, 1994. doi: 10.1115/94-GT-253.

[59] Leonard, G. and Stegmaier, J. "Development of an aeroderivative gas turbine DLE combustion system." *Diesel and Gas Turbine*

Worldwide; (United States), 25, 1993. ISSN 0278-5994. URL `https://www.osti.gov/biblio/5690414`.

[60] Innocenti, A., Andreini, A., Facchini, B., Cerutti, M., Ceccherini, G., and Riccio, G. "Design Improvement Survey for NO_x Emissions Reduction of a Heavy-Duty Gas Turbine Partially Premixed Fuel Nozzle Operating With Natural Gas: Numerical Assessment." *Journal of Engineering for Gas Turbines and Power*, 138(1):011501, 2015. ISSN 0742-4795. doi: 10.1115/1.4031144.

[61] Andreini, A., Facchini, B., Innocenti, A., and Cerutti, M. "Numerical Analysis of a Low NO_x Partially Premixed Burner for Industrial Gas Turbine Applications." *Energy Procedia*, 45:1382–1391, 2014. doi: 10.1016/j.egypro.2014.01.145.

[62] Raffel, Markus, Kähler, Christian J., Willert, Christian E., Wereley, Steven T., Scarano, Fulvio, and Kompenhans, Jürgen. *Particle Image Velocimetry: A Practical Guide*. Springer, 3rd edition, 2018. ISBN 978-3-319-68851-0. doi: 10.1007/978-3-319-68852-7.

[63] Atkins, M. D. *Application of Thermo-Fluidic Measurement Techniques*. Butterworth-Heinemann, 2016. doi: 10.1016/B978-0-12-809731-1.00005-8.

[64] Willert, C. E. and Gharib, M. "Digital Particle Image Velocimetry." *Experiments In Fluids*, 10(4):181–193, 1991.

[65] Dantec Dynamics. *FlowManager software and Introduction to PIV Instrumentation*. 2000.

[66] Eckbreth, A. C. *Laser Diagnostics for Combustion Temperature and Species*. CRC Press, 1996. doi: 10.1201/9781003077251.

[67] Linne, M. A. *Spectroscopic measurement: an introduction to the fundamentals*. Academic Press, 2002. ISBN 9780080517537.

[68] Hollas, J. M. *Modern Spectroscopy*. John Wiley & Sons Ltd, 2004. doi: 10.1016/0022-2860(87)85092-5.

[69] Rolf, M. and Lauer, W. *Determination of the Heat Release Distribution in Turbulent Flames by Chemiluminescence Imaging*. PhD thesis, Technischen Universität München, 2011.

[70] Gaydon, A. *The Spectroscopy of Flames*. Springer Netherlands, 2012. ISBN 9789400957206.

[71] Liu, Y., Tan, J., Wan, M., Zhang, L., and Yao, X. "Quantitative Measurement of OH* and CH* Chemiluminescence in Jet Diffusion Flames." *ACS Omega*, 2020. doi: 10.1021/acsomega.0c01093.

[72] Guethe, F., Stankovic, D., Genin, F., Syed, K., and Winkler, D. "Flue Gas Recirculation of the Alstom Sequential Gas Turbine Combustor Tested at High Pressure." *ASME Conference Proceedings*, 2011. doi: 10.1115/GT2011-45379.

[73] Kathrotia, T., Riedel, U., and Warnatz, J. "A Numerical Study on the Relation of OH*, CH*, and C_2* Chemiluminescence and Heat Release in Premixed Methane Flames." *Proceedings of 4th European Combustion Meeting*, 2009.

[74] Kathrotia, Trupti, Fikri, M., Bozkurt, M., Hartmann, M., Riedel, Uwe, and Schulz, C. "Study of the H+O+M reaction forming OH: Kinetics of OH chemiluminescence in hydrogen combustion systems." *Combustion and Flame*, 157(7):1261–1273, 2010. ISSN 0010-2180. doi: 10.1016/j.combustflame.2010.04.003.

[75] Luque, J. and Crosley, D. R. "Transition probabilities and electronic transition moments of the A–X and D–X progressions systems of nitric oxide." *The Journal of Chemical Physics*, 111(16):7405, 1999. ISSN 0021-9606. doi: 10.1063/1.480064.

[76] Kalal, M. and Nugent, K. "Abel inversion using fast Fourier transforms." *Applied optics*, 27:1956–9, 1988. doi: 10.1364/AO.27.001956.

[77] De Leo, M., Saveliev, A., Kennedy, L., and Zelepouga, S. "OH and CH luminescence in opposed flow methane oxy-flames." *Combustion*

and Flame, 149:435–447, 2007. doi: 10.1016/j.combustflame.2007.01.008.

[78] Liu, Y., Tan, J., Wang, H., and Lv, L. "Characterization of heat release rate by OH* and CH* chemiluminescence." *Acta Astronautica*, 154:44–51, 2019. doi: 10.1016/j.actaastro.2018.10.022.

[79] Bedard, M., Fuller, T., Sardeshmukh, S., and Anderson, W. "Chemiluminescence as a diagnostic in studying combustion instability in a practical combustor." *Combustion and Flame*, 213:211–225, 2020. doi: 10.1016/j.combustflame.2019.11.039.

[80] Lee, Jong Guen and Santavicca, Domenic. "Experimental diagnostics for the study of combustion instabilities in lean premixed combustors." *Journal of Propulsion and Power*, 19:735–750, 2003.

[81] Ayoola, B. O., Kaminski, C. F., Balachandran, R., Mastorakos, E., and Frank, J. H. "Spatially resolved heat release rate measurements in turbulent premixed flames." *Combustion and Flame*, 144(1), 2006. ISSN 0010-2180. doi: 10.1016/j.combustflame.2005.06.005.

[82] Nori, V. and Seitzman, J. "Chemiluminescence Measurements and Modeling in Syngas, Methane and Jet-A Fueled Combustors." *Collection of Technical Papers - 45th AIAA Aerospace Sciences Meeting*, 8, 2007. doi: 10.2514/6.2007-466.

[83] Hardalupas, Y. and Orain, M. "Local measurements of the time-dependent heat release rate and equivalence ratio using chemiluminescent emission from a flame." *Combustion and Flame*, 139:188–207, 2004. doi: 10.1016/j.combustflame.2004.08.003.

[84] Lauer, M. and Sattelmayer, T. "On the adequacy of chemiluminescence as a measure for heat release in turbulent flames with mixture gradients." *Journal of Engineering for Gas Turbines and Power*, 132(6):061502, 2010. ISSN 0742-4795. doi: 10.1115/1.4000126.

[85] Samaniego, Jean Michel, Egolfopoulos, Fokion N., and Bowman, C. Tom. "CO_2* Chemiluminescence in Premixed Flames." *Combustion Science and Technology*, 109:183–203, 1995.

[86] Kopp, M., Brower, M., Mathieu, O., Petersen, E., and Güthe, F. "CO_2* chemiluminescence study at low and elevated pressures." *Applied Physics B*, 107, 2012. doi: 10.1007/s00340-012-5051-4.

[87] Hossain, Akter and Nakamura, Yuji. "A numerical study on the ability to predict the heat release rate using CH* chemiluminescence in non-sooting counterflow diffusion flames." *Combustion and Flame*, 161(1):162–172, 2014. ISSN 0010-2180. doi: 10.1016/j.combustflame.2013.08.021.

[88] Guiberti, T. F., Durox, D., and Schuller, T. "Flame chemiluminescence from CO_2- and N2-diluted laminar CH_4/air premixed flames." *Combustion and Flame*, 181:110–122, 2017. ISSN 0010-2180. doi: 10.1016/j.combustflame.2017.01.032.

[89] Oh, S., Park, Y., Seon, G., Hwang, W., and Do, H. "Impacts of N_2 and CO_2 diluent gas composition on flame emission spectroscopy for fuel concentration measurements in flames." *International Journal of Heat and Mass Transfer*, 149:119174, 2020. doi: 10.1016/j.ijheatmasstransfer.2019.119174.

[90] Jeffries, J., Schulz, C., Mattison, D., Oehlschlaeger, M., Bessler, W., Lee, T., Davidson, D., and Hanson, R. "UV absorption of CO_2 for temperature diagnostics of hydrocarbon combustion applications." *Proceedings of the Combustion Institute*, 30:1591–1599, 2013. doi: 10.1016/j.proci.2004.08.009.

[91] Joutsenoja, T., D'Anna, A., D'Alessio, A., and Nazzaro, M. I. "Ultraviolet absorption spectra of carbon dioxide and oxygen at elevated temperatures." *Applied Spectroscopy*, 55(2):130–135, 2001. doi: 10.1366/0003702011951650.

[92] Reyes, M., Tinaut, F., Gimenez, B., and Pastor, J. "Effect of hydrogen addition on the OH* and CH* chemiluminescence emissions of premixed combustion of methane-air mixtures." *International Journal of Hydrogen Energy*, 43, 2018. doi: 10.1016/j.ijhydene.2018.09.005.

[93] Pretzier, Georg. "A New Method for Numerical Abel-Inversion." *Zeitschrift für Naturforschung A*, 46(7):639–641, 1991. doi: 10.1515/zna-1991-0715.

[94] Lefebvre, A. and Ballal, D. *Gas Turbine Combustion: Alternative Fuels and Emissions, Third Edition*. Taylor & Francis, 2010. ISBN 9781420086041.

[95] HORIBA. *PG350 Portable Gas Analyzer Manual*, 2012.

[96] Breer, B., Rajagopalan, H., Godbold, C., Johnson, H., Emerson, B., Acharya, V., Sun, W., Noble, D., and Lieuwen, T. "Numerical investigation of NO_x production from premixed hydrogen/methane fuel blends." *Combustion and Flame*, 255:112920, 2023. ISSN 0010-2180. doi: 10.1016/j.combustflame.2023.112920.

[97] Garan, Niclas, Dybe, Simeon, Paschereit, Christian Oliver, and Djordjevic, Neda. "Consistent emission correction factors applicable to novel energy carriers and conversion concepts." *Fuel*, 341:127658, 2023. ISSN 0016-2361. doi: 10.1016/j.fuel.2023.127658.

[98] Syred, N. and Beér, J.M. "Combustion in swirling flows: A review." *Combustion and Flame*, 23(2):143–201, 1974. ISSN 0010-2180. doi: 10.1016/0010-2180(74)90057-1.

[99] Ebi, D., Bombach, R., and Jansohn, P. "Swirl flame boundary layer flashback at elevated pressure: Modes of propagation and effect of hydrogen addition." *Proceedings of the Combustion Institute*, 2020. doi: 10.1016/j.proci.2020.06.305.

[100] Guethe, F., Guyot, D., Singla, G., Noiray, N., and Schuermans, B. "Chemiluminescence as diagnostic tool in the development of gas turbines." *Applied Physics B: Lasers and Optics*, 107(3):619–636, 2012. ISSN 09462171. doi: 10.1007/s00340-012-4984-y.

[101] Galeotti, S., Picchi, A., Becchi, R., Lemmi, G., Meloni, R., Babazzi, G., Giannini, N., Facchini, B., and Andreini, A. "Experimental Study on Stability Enhancement of a Natural Gas GT Burner With Hydrogen Flame Piloting Operated With Simulated Exhaust Gas Recirculation." *ASME Conference Proceedings*, 2024. doi: 10.1115/GT2024-128732.

[102] Goodwin, David G., Moffat, Harry K., Schoegl, Ingmar, Speth, Raymond L., and Weber, Bryan W. Cantera: An object-oriented software toolkit for chemical kinetics, thermodynamics, and transport processes. `https://www.cantera.org`, 2023. Version 2.5.1.

[103] Gregory P. Smith, Michael Frenklach Nigel W. Moriarty Boris Eiteneer Mikhail Goldenberg C. Thomas Bowman Ronald K. Hanson Soonho Song William C. Gardiner Jr. Vitali V. Lissianski David M. Golden and Qin, Zhiwei. Gri-mech 3.0. `http://www.me.berkeley.edu/gri_mech/`.

[104] Kuo, K. K. *Principles of Combustion*. Wiley, 1986.

[105] O'Connor, J. "Understanding the role of flow dynamics in thermoacoustic combustion instability." *Proceedings of the Combustion Institute*, 39(4):4583–4610, 2023. ISSN 1540-7489. doi: 10.1016/j.proci.2022.07.115.

[106] Bizon, K., Continillo, G., Mancaruso, E., Merola, S., and Vaglieco, B. "Pod-based analysis of combustion images in optically accessible engines." *Combustion and Flame*, 157(4):632–640, 2010.

[107] Giorgi, M G. De, Fontanarosa, D., Ficarella, A., and Pescini, E. "Effects on performance, combustion and pollutants of water emulsi-

fied fuel in an aeroengine combustor." *Applied Energy*, 260:114263, 2020. ISSN 0306-2619. doi: 10.1016/j.apenergy.2019.114263.

[108] Mehdi, G., Bonuso, S., and De Giorgi, M. G. "Identification of flow structures in a closed chamber in the presence of a needle plasma actuator." *Physics of Fluids*, 34(12):127118, 2022. ISSN 1070-6631. doi: 10.1063/5.0127117.

[109] Sirovich, L. "Turbulence and the dynamics of coherent structures. I - Coherent structures. II - Symmetries and transformations. III - Dynamics and scaling." *Quarterly of Applied Mathematics*, 45, 1987. doi: 10.1090/qam/910463.

[110] Kypraiou, A.M., Dowling, A., Mastorakos, E., and Karimi, N. "Proper Orthogonal Decomposition Analysis of a Turbulent Swirling Self-Excited Premixed Flame." *Proceedings of 53rd AIAA Aerospace Sciences Meeting*, 2015. doi: 10.2514/6.2015-0425.

[111] Lumley, J. L. "The Structure of Inhomogeneous Turbulent Flows." *Atmospheric Turbulence and Radio Wave Propagation, Nauka*, 1967.

[112] Cerutti, M., Riccio, G., Andreini, A., Becchi, R., Facchini, B., and Picchi, A. "Experimental and Numerical Investigations of Novel Natural Gas Low NO_x Burners for Heavy Duty Gas Turbine." *ASME Conference Proceedings*, 2018. doi: 10.1115/GT2018-76670.